ISSN 1580-2949
UDK 669+666+678+53 MTAEC9, 44(5)233–292(2010)

| MATER. TEHNOL. | LETNIK VOLUME 44 | ŠTEV. NO. 5 | STR. P. 233–292 | LJUBLJANA SLOVENIJA | SEP.–OCT. 2010 |
|---|---|---|---|---|---|

# VSEBINA – CONTENTS

## *IZVIRNI ZNANSTVENI ČLANKI – ORIGINAL SCIENTIFIC ARTICLES*



## *STROKOVNI ČLANKI – PROFESSIONAL ARTICLES*

UDK 669.1:669.046-547:546.711
Original scientific article/Izvirni znanstveni članek

ISSN 1580-2949
MTAEC9, 44(5)235(2010)

# SELECTIVE OXIDATION OF MANGANESE IN MOLTEN PIG IRON

## SELEKTIVNA OKSIDACIJA MANGANA V STALJENEM GRODLJU

**Derviš Pihura[1], Mirsada Oruč[1], Jakob Lamut[2]**

[1]University of Zenica, Metallurgical institute "Kemal Kapetanović", Travnička c. 7, 72000 Zenica, B&H
[2]University of Ljubljana, FNT, Department for materials and metallurgy, Aškerčeva c. 12, 1000 Ljubljana, Slovenia
dervis.pihura@gmail.com

*Prejem rokopisa – received: 2008-09-22; sprejem za objavo – accepted for publication: 2010-03-15*

An examination of the process of selective oxidation for molten pig iron indicates the possibility of lowering the content of unwanted or harmful elements. This process makes it possible to achieve the optimum Mn content in pig iron (hot metal) without any oxidation of the other elements present, such as carbon, etc. Several variants of oxygen blowing with the addition of a slag-forming component were checked. The final element content in the hot metal depends on the initial Mn content, the oxygen blowing and on the added slag components. The lowering of the Mn content in the hot metal to the limit solves the problems of converter processing, lowers the slag quantity, increases the yield of steel by more 4 % and improves the steel-making process.

Key words: selective oxidation, hot metal, high manganese content

Analiza procesa selektivne oksidacije tekočega grodlja daje možnost, da odstranimo neželene in škodljive elemente. Proces omogoča, da dosežemo optimalno vsebnost mangana v surovem grodlju (vroča kovina) brez oksidacije drugih elementov, ogljika in drugih. Preizkušenih je bilo več variant vpihovanja kisika z dodatki za tvorbo žlindre. Končna vsebnost mangana v grodlju je odvisna od začetne vsebnosti, vpihovanja kisika in od dodatkov za žlindranje. Zmanjšanje vsebnosti mangana do meje rešuje probleme konvertorskega procesiranja, zmanjša količino žlindre, poveča izkoristek jekla za več od 4 % in izboljša proces izdelave jekla.

Ključne besede: selektivna oksidacija, grodelj, visoka vsebnost mangana

## 1 INTRODUCTION

Only in some countries metallurgists face the problem of a large content of manganese in molten pig iron (hot metal) of above 4.00 % [1,2,3,4,5]. The higher Mn content in hot metal during the oxidation, i.e., during steel-making, influences the formation of slag and causes serious problems for the technology. For this reason, the reaction between manganese and oxygen in hot metal is still being investigated. There are particular problems with hot metal that has a manganese content above 1 %. The process of manganese oxidation was investigated from the points of view of the reaction mechanism, the thermodynamics and the kinetics, and different conclusions were proposed. The majority of investigations were performed on hot metal with a low manganese content, below 1.00 %. Only rarely was the object of the examination some hot metal with a high manganese content, higher than 4 %, as the initial content. Only on the basis of investigations with a high manganese iron can the present misunderstandings and confusion about results be solved, with the condition that the effect of the method of introducing the oxygen into the hot metal on the evolution of reactions is also considered.

During the processing of hot metal with a high manganese content to steel, a large quantity of slag is obtained that decreases the yield and increases the splashing [5,6]. So far, no process for the selective oxidation of manganese from hot metal before pouring into a steel-making furnace was developed and attempts to decrease the manganese content in hot metal were not successful. In fact in Austria, steel-makers gave up on the use of iron ore with a high content of manganese [1,5]. In Russia and Bulgaria trials of the oxidation of manganese were not successful and it was only possible to produce FeMn from slag with a high percentage of MnO [3,4,7]. The treated hot metal had a low carbon content and was not suitable for the making of steel with less than 2.00 % of manganese.

New technical solutions and equipment for the processing of hot metal in a ladle offer the possibility of decreasing some harmful or unwanted elements with selective oxidation [6,7,8] before tapping the hot metal into the steel furnace. In this work we ordered the problem of lowering the manganese content, combining the introduction of oxygen with the use of an appropriate slag. Specifically, the influence of the addition of slag-forming oxides, especially $SiO_2$, was investigated. The performed experiments indicate that it was possible to decrease the manganese content in the hot metal from 4.00 % or more to below 1.00 at 1773 K.

In this article the metallurgical and technological aspects of the selective oxidation of manganese with oxygen and slag formation on a pilot-plant scale are presented that offer the possibility of applications on an industrial scale.

## 2 METALLUGICAL CHARACTERISTICS OF SELECTIVE OXIDATION

Selective oxidation has to be carried out only with a sufficient supply of oxygen as well as with a slag that is rich in $Fe_xO$. The multi-reaction equilibrium of the selective oxidation of manganese can be deduced using a suitable method; however, a more reliable method of calculation is based on the equilibrium principle and a change of the Gibbs' free energy of the formation of oxides ($\Delta G^o$) for different reactions. It is important to calculate the conditions for the selective oxidation of manganese with no change in the initial carbon content and with the minimal oxidation of silicon. For the three elements carbon, silicon and manganese, three equations can be written showing a mutual equilibrium between any of two, with only two independent equations. The equilibria for the systems Mn-C and Mn-Si are solved with numerical iteration.

It is assumed that the change of the manganese content for low and higher initial contents does not have corresponding changes in the decreasing part of the curves in **Figure 1**, especially for the case of the Mn–humpback [3,9]. The changes in the manganese content at the lower part of the curves at 1873 K do not occur below the of Mn–humpback in melts without carbon content and for hot metal melts with 4.00 % or more C at 1573 K [1]. This strengthens the importance of clarifying the mechanism of the reactions in the systems Mn–$\{O_2\}$ and Mn–$Fe_xO$.

It is assumed that the mechanism of the reactions of selective oxidation of manganese with oxygen in the presence of $Fe_xO$ slag components occurs as shown in **Figure 2**. It is important that in the processing the continuity of the reactions fields is maintained: 1 – initial reactions (1st field), 2 – transition reactions (2nd field) and 3 – stable reactions (3rd field). It is further concluded that oxygen blown into the field of the initial reactions (mark 1) can react with iron, silicon, manganese and carbon. On the base of the $\Delta G^o - T$ dependences it is possible to expect that at 1573 K only the manganese is oxidised. It is assumed that the oxidation of carbon is damped because of the influence of a ferro-static pressure deep into the melt. In the second field (number 2 in **Figure 2**), the formed $Fe_xO$ is reduced with silicon. It is assumed that additional reactions occur in the third field of permanent reactions (number 3). The process of selective oxidation of manganese is achieved with a transition through all three fields in **Figure 2**, only.

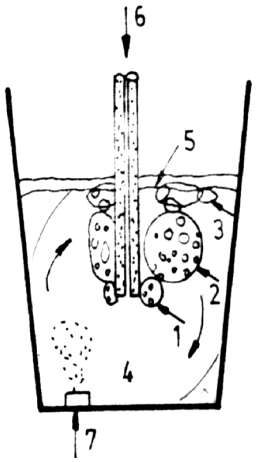


**Figure 2:** Mechanism of reaction blowing oxygen and slag components 1. initial reactions.; 2. transition reactions; 3. permanent reactions; 4. hot metal; 5. slag; 6. oxygen; 7. argon

**Slika 2:** Mehanizem reakcijskega vpihovanja kisika in komponente žlindre. 1 – začetne reakcije, 2 – prehodne reakcije, 3 – permanentne reakcije, 4 – tekoči grodelj, 5 – žlindra, 6 – kisik, 7 – argon

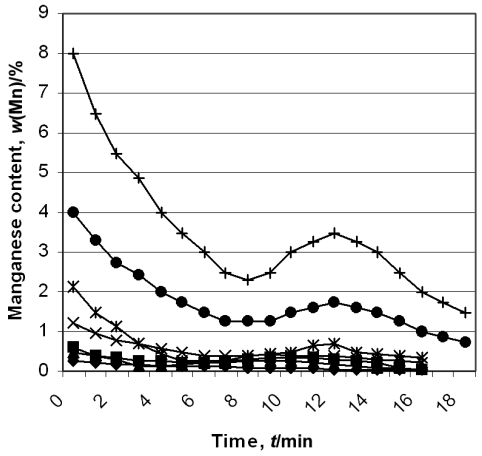


**Figure 1:** Change of the different initial Mn content during the oxidation process: (•) 0.20 % Mn; (Δ) 0.40 % Mn; (□) 0.5 % Mn; (x) 1.2 % Mn; (x) 2.0 % Mn; (•) 4.00 % Mn; 4. (+) 8.00 % Mn

**Slika 1:** Sprememba različne začetne vsebnosti mangana med procesom oksidacije: (•) 0.2 % Mn; (Δ) 0.4 % Mn, (□)0.5 % Mn, (x) 1.2 % Mn, (x) 2.0 % Mn, (•) 4.0 % Mn, (+) 8.0 % Mn

The $e_i^j$ values for the temperature of 1573 K are calculated by applying two approaches: from the obtained data or from values for 1873 K, considering the difference in temperature.

The calculation of the free energy $\Delta G^o$ at different stages of the manganese's selective oxidation leads to a

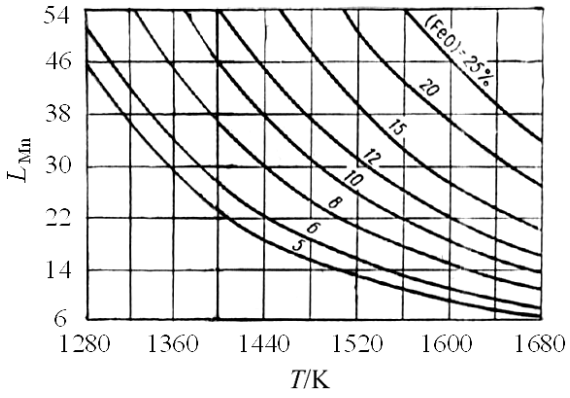


**Figure 3:** Dependence of the coeficient of manganese distribution $L_{Mn} = w(Mn)/w[Mn]$ of melt temperature and the (FeO) content in the slag

**Slika 3:** Odvisnost koeficienta porazdelitve mangana $L_{Mn} = w(Mn)/w[Mn]$ od temperature taline in vsebnosti FeO v žlindri

different equilibrium situation. The possibility of prior silicon oxidation at 1573 K, thus, before the oxidation of manganese and carbon, is dependent on other influencing factors; firstly, of the slag composition. The equilibrium between the silicon and the manganese is reached at the beginning of the oxidation process and both elements are oxidized in parallel in preference to the carbon until the ternary equilibrium silicon, manganese and carbon is achieved. The content of carbon has to remain constant at the initial level or changed insignificantly. Thus, the final equilibrium composition of the hot metal depends not only upon the temperature and the initial composition, but also upon the activity of the oxides $a_{SiO2}$ and $a_{MnO}$.

## 3 THE OXIDATION OF MANGANESE, THE PRINCIPLE AND THE EXPERIMENTAL PROCEDURE

The solution to the problem of a high manganese content of about 4.00 % in the hot metal produced in Zenica could be found by considering the system Fe-Mn-Si-C-O at 1573–1673 K for $\Delta G^o - T$ dependences that offer the possibility of irreversible reactions. In this temperature range it is possible to achieve the value for the $w$[Mn]/$w$[C] ratio of 0.10, which allows the successful selective oxidation of manganese. The measure of the rate of accelerated reactions of manganese oxidation, which determines the degree of reaction, is the mass transport coefficient ($k_{Mn}$). A significant decrease in the content of one element ($X_1$) by a sufficient decrease of the second ($X_2$) can be achieved on the condition of $k_{X1} > k_{X2}$ and for the ratio of the distribution coefficient $L_{X1} > L_{X2}$. The most important is the distribution of elements, and especially manganese, between the hot metal and the slag ($L_{Mn} = w$[Mn]/$w$(Mn)) (**Figure 3**).

The experiments were performed in the ladle with a porous plug with a charge of hot metal with the composition in mass fractions: (4.03 ± 0.25) % C, (3.80 ± 0.52) % Mn and (0.56 ± 0.10) % Si. The oxidation was carried out with oxygen blowing and the addition of 6 % of $Fe_xO$ for the slag formation. The experiments were performed in three variants of the lance blowing of oxygen: 1. on the slag surface, 2. in the hot metal and 3. in the metal being rinsed with argon. The temperature of the hot metal was, in all cases, 1573 K.

For the existence of all three reactions fields, only the role of $Fe_xO$ as an oxidation intensifier and the control of the oxidation of silicon with the present component $SiO_2$ were assumed. If all the reaction fields are reduced to one field of permanent reaction, it would be difficult, or even impossible, to control the selective oxidation of iron, silicon, manganese, carbon, etc. The decrease of manganese content to the equilibrium value excludes it from the oxidation process and the content of manganese at the start of the oxidation of carbon and iron is considered as critical $[Mn]_c$.

## 4 EXPERIMENTAL RESULTS

The obtained experimental results show that the most successful manganese oxidation process occurs during the blowing of oxygen with parallel argon rinsing (variant 3) without the oxidation of carbon, and acceptable kinetics of silicon oxidation. Data on the oxidised quantity of manganese and the losses of silicon and carbon are presented in **Figures 4 and 5**. It is obvious that already after 7.5 min. of oxidation in the variant 3, the final manganese content of 0.10 % Mn was achieved with the oxidation rate of $v_{Mn}$ = 0.39 % Mn/per min, which is higher than that quoted rate of $v_{Mn}$ = 0.35 % Mn/per min [3]. With the variant 2, the final manganese content was <1.00 %. The slag with the optimal characteristics was obtained with the largest additions of $Fe_xO$ and $SiO_2$. In spite of the large oxygen supply, the average free oxygen content in the hot metal is (3 ± 2) µg/g.

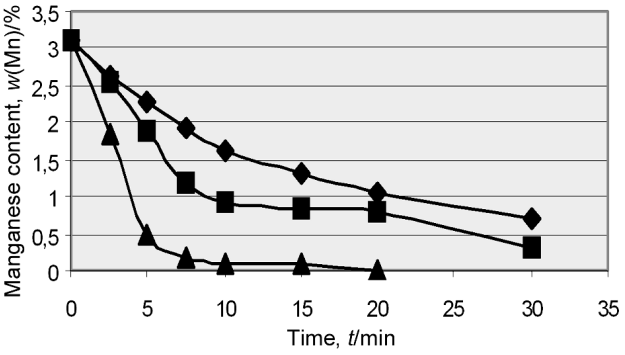


**Figure 4:** Oxidation of manganese at 1573 K for variants: 1. (◊) blowing on melt surface; 2. (□) blowing in melt; 3. (Δ) blowing in melt and rinsing through a porous plug

**Slika 4:** Oksidacija mangana pri 1573 K za variante: (◊) vpihovanje na površino taline, (□) vpihovanje v talino, (Δ) vpihovanje v talino in izpiranje z argonom skozi porozen čep

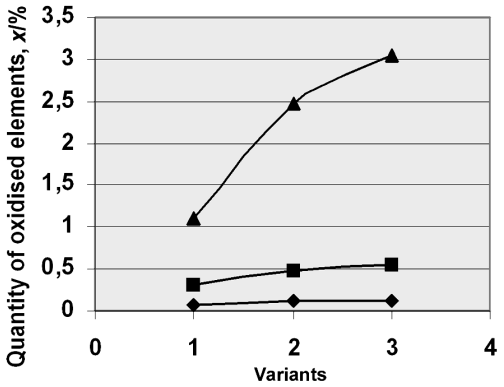


**Figure 5:** Average oxidised elements quantity of carbon (◊), silicon (□) and manganese (Δ) during oxidation for variants: 1 – blowing to surface; 2 – blowing into melt; 3 – blowing into melt with argon rinsing

**Slika 5:** Povprečna količine oksidiranih elementov ogljika (◊), silicija (□) in mangana (Δ) med oksidacijo mangana za variante: 1 – vpihovanje na površino, 2 – vpihovanje v talino in 3 – vpihovanje v talino z izpiranjem z argonom

In the hot metal at 1573 K, the oxidation of manganese alone is connected to the effect of the high carbon content and to interaction parameters with a value different to that at 1873 K. The composition and activity of slag formed with lance oxygen blowing on the melt top, in the melt, as well as for argon rinsing are different for the same slag addition. For instance, the activities $a_{MnO}$ and $a_{FeO}$ at 1573 K are for oxygen top blowing, 0.234 and of 0.642, into melt blowing, 0.395 and of 0.464, and blowing with argon rinsing, 0.474 and of 0.459.

## 5 CONCLUSIONS

1. On the basis of the thermodynamics, kinetics, mechanism and mass transfer conditions as well as the effect of slag addition it was concluded that it was possible to ensure the selective oxidation of manganese in hot metal without significantly affecting the content of the other elements.
2. Through the pilot-plant oxidation of only manganese at 1573 K it was possible to determine suitable values of the technological and metallurgical parameters to achieve an optimal decrease for the high initial manganese content in the hot metal.
3. Considering the influence of oxygen and $Fe_xO$ for the checked oxidation variants, it is obvious that the optimal mechanism of selective oxidation of the manganese is connected with the kinetics of the supply of oxygen. The decrease of the manganese content is only achieved if the selective oxidation occurs in three reaction fields.
4. During the oxidation of manganese, other elements are maintained at the initial contents or are minimally oxidised, as carbon, or silicon, depending on the $SiO_2$ in the slag.
5. The obtained results of the manganese oxidation do not lead to a secondary increase in the content of manganese in the hot metal.
6. From the environmental point of view, of all the checked variants, the variant 3 is the most acceptable, as in the processing no brown fumes are produced.

## 6 REFERENCES

[1] Pihura D.: Pregled procesa oksidacije Si, Mn, P i S (Survey of the process of oxidation of Si, Mn, P and S); Metalurški institut, Zenica, 1989

[2] Lamut J, Pihura D, Selektivna oksidacija mangana (Selective oxidation of manganese), Project, Slovenia – BiH, 2004

[3] Kvitko, M. F., Afanasjev, S.G., Kislorodno-konvertorni proces (The oxigen convertor proces) Moskva, Metallurgija, 1974

[4] Malčeva, N., Kacareva, I., Savov, P., Rudodobiv i metalurgija (**1969**) 5, 23

[5] Kammerhofer Van E, Dobrowsky F et al., BHM, 113 (**1986**), 444–449

[6] Ohkotskij, V. B. et al., Steel in USSR 20 (**1990**) 7, 317/20

[7] Vincent D. i Makin S.B., A New Concept in Liquid Metal Treatment ISID Ltd, 1999

[8] Deo B, Boom R. Fundamentals of Steelmaking Metallurgy, London 1993

[9] Koch K et al. Stahl u. Eisen 104 (**1984**), 767

UDK 620.193:669.14.018.8
Original scientific article/Izvirni znanstveni članek

ISSN 1580-2949
MTAEC9, 44(5)239(2010)

# THE CORROSION BEHAVIOUR OF FERRITIC STAINLESS STEELS IN ALKALINE SOLUTIONS

## KOROZIJSKO VEDENJE FERITNIH NERJAVNIH JEKEL V ALKALNIH RAZTOPINAH

**Aleksandra Kocijan**

Institute of Metals and Technology, Lepi pot 11, 1000 Ljubljana, Slovenia
aleksandra.kocijan@imt.si

*Prejem rokopisa – received: 2010-03-11; sprejem za objavo – accepted for publication: 2010-04-07*

The corrosion resistances of X6Cr17 and X2CrTi17 ferritic stainless steels and cold-rolled, low-carbon steel, as well as circular and transversal welds of X6Cr17 ferritic stainless steel, were investigated in a non-phosphate detergent with a solution pH of 10.5 and at a temperature of 60 °C. The second investigated solution contained the non-phosphate detergent and sodium perborate tetrahydrate at pH 11 and was at a temperature of 90 °C. The potentiodynamic measurements showed that the corrosion resistance decreased from X2CrTi17 and X6Cr17 to the welded specimens and the cold-rolled, low-carbon steel in non-phosphate detergent at the lower temperature. At the elevated temperature and with the addition of sodium perborate tetrahydrate the corrosion stability of all the investigated materials decreased significantly.

Keywords: ferritic stainless steel, potentiodynamic, alkaline solution, corrosion

Preučevali smo korozijsko odpornost vzorcev X6Cr17, X2CrTi17 feritnih nerjavnih jekel, hladno valjanega malooglji čnega jekla in krožnega ter prečnega zvara X6Cr17 feritnega nerjavnega jekla v raztopini nefosfatnega detergenta pri pH 10,5 in temperaturi 60 °C. Druga preiskovana raztopina je vsebovala nefosfatni detergent in natrijev perborat tetrahidrat pri pH 11 in temperaturi 90 °C. Rezultati potenciodinamskih meritev so pokazali, da sta korozijsko najbolj obstojna materiala X2CrTi17 in X6Cr17, manj pa obe vrsti zvarov in hladno valjano malooglji čno jeklo. Pri povišani temperaturi in z dodatkom natrijevega perborata tetrahidrata se je korozijska odpornost vseh petih vzorcev izrazito zmanjšala.

Ključne besede: feritna nerjavna jekla, potenciodinamske, alkalna raztopina, korozija

## 1 INTRODUCTION

Ferritic steels with about 17 % Cr (e.g., X6Cr17, AISI 430, and EN 1.4016) are of interest as they are some of the most widely used stainless engineering materials and offer an attractive alternative to the more expensive austenitic stainless-steel grades.[1] X6Cr17 is a ferritic, straight chromium, non-hardenable grade, combining good corrosion resistance and formability characteristics with useful mechanical properties.[1] It has a good resistance to a wide variety of corrosive media, including nitric acid and some organic acids. It attains its maximum corrosion resistance in the highly polished or buffed condition. In general, its resistance to pitting and crevice corrosion resistance is close to that of the steel grade 304.[2] The stress-corrosion cracking resistance of Grade X6Cr17 is very high, as it is for all ferritic grades.[3,4] Typical applications for the X6Cr17 grade include the linings for dish washers, refrigerator-cabinet panels, automotive trim, lashing wire, element supports, stove trim rings, fasteners and chimney liners.[1]

The ferritic stainless steel X2CrTi17 stabilised with titanium has a very good resistance to intergranular corrosion.[5] Furthermore, titanium also binds sulphur and leads to improved pitting corrosion. All ferritic stainless steels are also resistant to stress-corrosion cracking and have a good corrosion resistance to mineral acids, cold dilute organic acids and cold oxidizing and alkaline salt solutions, to atmospheric corrosion, to high-temperature oxidation and to hot water.[5] Stabilisation with titanium results in a good toughness and ductility for the welds. The corrosion resistance of the welds is similar to that of the base metal. The typical applications of this grade are in domestic appliances, such as the tubs and drums of washing machines.

The aim of the present study was to evaluate the corrosion resistance of X2CrTi17 and X6Cr17 ferritic stainless steels as well as circular and transversal welds of X6Cr17 ferritic stainless steel in alkaline solutions using potentiodynamic measurements in order to establish an appropriate substitution of X2CrTi17 with X6Cr17 for washing machines. A cold-rolled, low-carbon steel was also investigated.

## 2 EXPERIMENTAL

The nominal values of the chemical composition of the investigated materials are shown in **Table 1**.

The experiments were carried out in two solutions. The first solution consisted of 10 g/L 2508 SDC IEC non-phosphate detergent, allowed for use in the international standard "ISO 6330:2000 Domestic Washing and Drying Procedures for Textile Testing" and contains fluorescent brightening agents, with a pH of 10.5 at a temperature of 60 °C.

**Table 1:** The nominal values of chemical composition of X6Cr17, X2CrTi17 ferritic stainless steels and cold rolled low-carbon steel (*w*/%)
**Tabela 1:** Nominalne vrednosti kemijske sestave X6Cr17, X2CrTi17 feritnih nerjavnih jekel in hladno valjanega malooglјičnega jekla (*w*/%)

| | C | Si | Mn | Cr | S | P | N | Ti |
|---|---|---|---|---|---|---|---|---|
| X6Cr17 | 0.12 max | 1.00 max | 1.00 max | 14–18 | 0.03 max | 0.040 max | – | – |
| X2CrTi17 | 0.025 max | 0.50 max | 0.50 max | 16–18 | 0.015 max | 0.040 max | 0.015 max | 0.35 max |
| DC01 EN10130 | 0.12 max | – | 0.60 max | – | 0.045 max | 0.045 max | – | – |

The second solution was prepared by the dissolution of 8 g of 2508 SDC IEC non-phosphate detergent and 2 g of sodium perborate tetrahydrate per litre of $H_2O$ at pH 11 and a temperature of 90 °C. Sodium perborate tetrahydrate is a reagent allowed in the international standards "ISO 105 C06, C08 and C09" and "ISO 6330: 2000". It acts as a bleaching agent and is incorporated into the latest standards to replicate modern commercial laundry products.

The test specimens were cut into discs of 15 mm diameter. The specimens were then embedded in a Teflon PAR holder and employed as a working electrode. The reference electrode was a saturated calomel electrode (SCE, 0.242 V vs. SHE) and the counter electrode was a high-purity graphite rod. All the potentials described in the text are stated with respect to SCE.

The potentiodynamic measurements were recorded using an EG&G PAR PC-controlled potentiostat/galvanostat Model 263 with M252 and Softcorr computer programs. For the potentiodynamic measurements the specimens were immersed in the solution 1 hour prior to the measurement in order to stabilize the surface at the open-circuit potential. The potentiodynamic curves were recorded starting from a potential that was 250 mV more negative than the open-circuit potential. The potential was then increased using a scan rate of 1 mV $s^{-1}$, until the transpassive region was reached.

## 3 RESULTS AND DISCUSSION

The corrosion-current density ($i_{corr}$) and the potential at zero current ($E(I = 0)$) values were calculated from linear polarization measurements and Tafel plots using the equation:

$$R_p = \beta_a \beta_c / (2.3\ I_{corr}\ (\beta_a + \beta_c))$$

The corrosion current, $I_{corr}$, is calculated from $R_p$, the least-squares slope, and the Tafel constants, $\beta_a$ and $\beta_c$, of the 100 mV decade$^{-1}$. The value of $E(I = 0)$ is calculated from the least-squares intercept.

The potentiodynamic behaviours of the investigated materials in two testing solutions are shown in **Figures 1 and 2**, accompanied by calculated values of the corrosion rates, the corrosion-current densities ($i_{corr}$), the potentials at zero current ($E(I = 0)$) and the polarisation resistances ($R_p$) (**Tables 2 and 3**). The differences in the alloys' composition affected the polarisation and the passivation behaviours of the tested materials.

**Figure 1** compares the potentiodynamic polarisation curves for the X6Cr17 and X2CrTi17 ferritic stainless steels and the cold-rolled, low-carbon steel as well as circular and transversal welds of X6Cr17 ferritic stainless steel in the phosphate detergent at 60 °C. After 1 h of stabilization at the open-circuit potential, the $E(I = 0)$ for X6Cr17 in the non-phosphate detergent at 60 °C was approximately –0.15 V. Following the Tafel region, the alloy exhibited a semi-passive behaviour with three active-passive transition zones. The breakdown potential ($E_b$) for the X6Cr17 was approximately 0.75 V. For the case of X2CrTi17, the $E(I = 0)$ was approximately equal to –0.24 V. The range of passivation was similar to that for the X6Cr17 specimen without the active-passive

**Table 2:** Calculated values of corrosion rates ($v_{corr}$), corrosion current densities ($i_{corr}$), potentials at zero current ($E(I = 0)$) and polarisation resistances ($R_p$) for X6Cr17, X2CrTi17 ferritic stainless steels and cold rolled low-carbon steel as well as circular and transversal welds of X6Cr17 ferritic stainless steel in non phosphate detergent at 60 °C.
**Tabela 2:** Izračunane vrednosti korozijske hitrosti, gostote korozijskega toka, potenciala pri ničelnem toku in polarizacijske upornosti za vzorce X6Cr17, X2CrTi17 feritnih nerjavnih jekel hladno valjanega malooglјičnega jekla in krožnega ter prečnega zvara X6Cr17 feritnega nerjavnega jekla v raztopini nefosfatnega detergenta pri 60 °C

| Sample | $v_{corr}$ / (mm/year) | $E(I = 0)$ /mV | $i_{corr}$ / (μA/cm$^2$) | $R_p$ /kΩ |
|---|---|---|---|---|
| X6Cr17 | 0.0013 | −151.3 | 0.120 | 277.0 |
| X6Cr17 (circular weld) | 0.036 | −242.1 | 3.282 | 13.16 |
| X6Cr17 (transversal weld) | 0.015 | −281.5 | 1.399 | 27.26 |
| DC01 EN10130 | 0.059 | −340.5 | 6.132 | 5.382 |
| X2CrTi17 | 0.0013 | −240.8 | 0.116 | 310.5 |

**Table 3:** Calculated values of corrosion rates, corrosion current densities ($i_{corr}$), potentials at zero current ($E(I = 0)$) and polarisation resistances ($R_p$) for X6Cr17, X2CrTi17 ferritic stainless steels and cold rolled low-carbon steel as well as circular and transversal welds of X6Cr17 ferritic stainless steel in non phosphate detergent with the addition of sodium perborate tetrahydrate at 90 °C.
**Tabela 3:** Izračunane vrednosti korozijske hitrosti, gostote korozijskega toka, potenciala pri ničelnem toku in polarizacijske upornosti za vzorce X6Cr17, X2CrTi17 feritnih nerjavnih jekel hladno valjanega malooglјičnega jekla in krožnega ter prečnega zvara X6Cr17 feritnega nerjavnega jekla v raztopini nefosfatnega detergenta z dodatkom natrijevega perborata tetrahidrata pri 90 °C

| Sample | $v_{corr}$ / (mm/year) | $E(I = 0)$ /mV | $i_{corr}$ / (μA/cm$^2$) | $R_p$ /kΩ |
|---|---|---|---|---|
| X6Cr17 | 0.059 | −21.62 | 5.442 | 6.063 |
| X6Cr17 (circular weld) | 0.411 | −40.08 | 37.77 | 1.137 |
| X6Cr17 (transversal weld) | 0.351 | −78.87 | 32.22 | 0.781 |
| DC01 EN10130 | 8.167 | −434.4 | 847.4 | 0.0565 |
| X2CrTi17 | 0.049 | −4.851 | 4.568 | 7.700 |

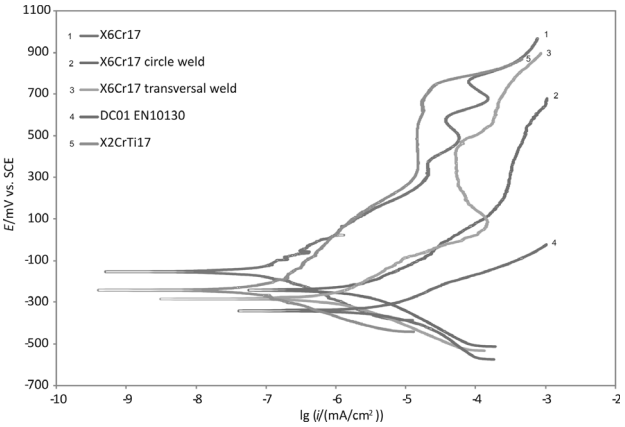


**Figure 1:** Potentiodynamic polarisation curves for X6Cr17, X2CrTi17 ferritic stainless steels and cold rolled low-carbon steel as well as circular and transversal welds of X6Cr17 ferritic stainless steel in non phosphate detergent at 60 °C.

**Slika 1:** Potenciodinamske krivulje vzorcev X6Cr17, X2CrTi17 feritnih nerjavnih jekel hladno valjanega malooglji čnega jekla in krožnega ter prečnega zvara X6Cr17 feritnega nerjavnega jekla v raztopini nefosfatnega detergenta pri 60 °C

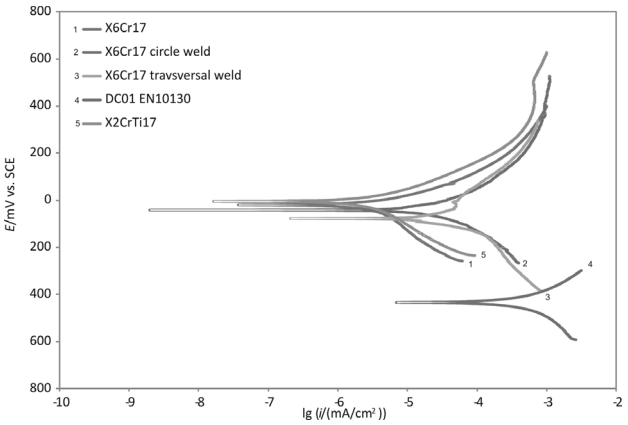


**Figure 2:** Potentiodynamic polarisation curves for X6Cr17, X2CrTi17 ferritic stainless steels and cold rolled low-carbon steel as well as circular and transversal welds of X6Cr17 ferritic stainless steel in non phosphate detergent with the addition of sodium perborate tetrahydrate at 90 °C.

**Slika 2:** Potenciodinamske krivulje vzorcev X6Cr17, X2CrTi17 feritnih nerjavnih jekel hladno valjanega malooglji čnega jekla in krožnega ter prečnega zvara X6Cr17 feritnega nerjavnega jekla v raztopini nefosfatnega detergenta z dodatkom natrijevega perborata tetrahidrata pri 90 °C

transition zones and an $E_b$ of 0.75 V. The corrosion-current densities in the passive range had lower values for the X2CrTi17 specimen. The $E(I = 0)$ values for the circular and transversal welds of X6Cr17 ferritic stainless steel in the non-phosphate detergent at 60 °C were –0.24 V and –0.28 V, respectively. The corrosion-current densities for both welded specimens increased significantly in comparison to the non-welded sample. The cold-rolled, low-carbon steel was the least corrosion resistant of all the investigated samples, with an $E(I = 0)$ value of –0.34 V and a corrosion-current density of 6 μA/cm$^2$. The calculation of the polarisation resistance ($R_p$) showed that the corrosion stability of the X2CrTi17 specimen was the greatest of all the tested materials, with an $R_p$ value of approximately 300 kΩ. The second most stable specimen was the steel X6Cr17 with an $R_p$ value of approximately 280 kΩ. The welded specimens and the cold-rolled, low-carbon steel exhibited a significant decrease in $R_p$ values, indicating a lower corrosion resistance of these specimens compared to the steels X6Cr17 and X2CrTi17 (**Table 2**).

In **Figure 2** the potentiodynamic polarisation curves for the X6Cr17 and X2CrTi17 ferritic stainless steels, and the cold-rolled, low-carbon steel, circular and transversal welds of X6Cr17 ferritic stainless steel in the non-phosphate detergent with the addition of sodium perborate tetrahydrate at 90 °C are shown. The corrosion resistance of all the investigated samples decreased considerably, compared to the results in the non-phosphate detergent at lower temperatures. The steels X2CrTi17 and X6Cr17 exhibited improved corrosion characteristics compared to the other three samples, although the difference with the welded specimens was not so pronounced as in the first solution due to the aggressiveness of the second solution (**Table 3**). The corrosion stability of the cold-rolled, low-carbon steel decreased a great deal with the addition of sodium perborate tetrahydrate and the higher temperature (**Table 3**).

## 4 CONCLUSION

The present electrochemical study was conducted in order to determine the corrosion performance of different ferritic stainless steels in a specific alkaline environment; the influence of welding and the chemical composition of the selected materials on the corrosion characteristics was evaluated, also.

The potentiodynamic measurements were performed with the investigated steels and welds in a non-phosphate detergent at 60 °C and with the addition of sodium perborate tetrahydrate at 90 °C. The results showed the superior corrosion stability of the X2CrTi17 and X6Cr17 ferritic stainless steels in comparison to the welded X6Cr17 ferritic stainless steel and the cold-rolled, low-carbon steel at the lower temperature. The corrosion resistance of all the investigated materials decreased significantly at the elevated temperature and with the addition of sodium perborate tetrahydrate. The X2CrTi17 and X6Cr17 ferritic stainless steels showed comparable electrochemical characteristics, while the corrosion stability of the circular and transversal welds of the X6Cr17 ferritic stainless steel was similar. The resistance of the cold-rolled, low-carbon steel to corrosion in the alkaline solution was significantly diminished in comparison with the other investigated materials.

The results of the present study indicate that the electrochemical characteristics of the X6Cr17 and

X2CrTi17 ferritic stainless steels in alkaline media at elevated temperatures are similar. This allows the substitution of X2CrTi17 with X6Cr17 ferritic stainless steel in the fabrication of washing machines.

## 5 REFERENCES

[1] B. Marian, C. Aurel, Metalurgia International, 13 (**2008**) 6, 55–59

[2] I. Tikhovskiy, D. Raabe, F. Roters, Materials Science and Engineering a-Structural Materials Properties Microstructure and Processing, 488 (**2008**)1–2, 482–490

[3] I. Tikhovskiy, D. Raabe, F. Roters, Scripta Materialia, 54 (**2006**) 8, 1537–1542

[4] F. Grešovnik, Mater. Tehnol. 34 (**2000**) 5, 289–293

[5] J. Charles, J.-D. Mithieux, P.-O. Santacreu, L. Peguet, Rev. Met. 3, (**2009**) 124–139

UDK 621.771.28:621.791
Original scientific article/Izvirni znanstveni članek

ISSN 1580-2949
MTAEC9, 44(5)243(2010)

# NUMERICAL DESIGN OF A HOT-STRETCH-REDUCING PROCESS FOR WELDED TUBES

## NUMERIČNO NAČRTOVANJE VROČE RAZTEZNE REDUKCIJE VARJENIH CEVI

**Stoja Rešković[1], Rade Križanić[1], Franc Vodopivec[2]**

[1]University Zagreb, Faculty of Metallurgy, Aleja narodnih heroja 3, 44103 Sisak, Croatia
[2]Institute of metals and Technology, Lepi pot 11, 1000 Ljubljana, Slovenia
reskovic@simet.hr

*Prejem rokopisa – received: 2009-12-21; sprejem za objavo – accepted for publication: 2010-05-18*

During stretch reducing, steel is submitted to complex stressing and straining processes. This paper gives a ***theoretical model*** of a heat-stretch-reducing process for the relation between the tube diameter and the wall thickness. The design is verified by a determination of the number of revolutions of rolls with every caliber for specific tubes on an industrial mill. The control of the rolled-tube dimensions confirmed the accuracy of the design.

Key words: hot-stretch reducing, welded tubes, numerical model of design, calibrate, coefficient of plastic extension of the steel

Pri raztezni redukciji je jeklo izpostavljeno kompleksni napetostni in deformacijski obremenitvi. V članku je predstavljen teoretičen model procesa vroče raztezne redukcije za razmerje med premerom cevi in debelino njene stene. Načrt je preverjen z določitvijo števila vrtljajev valjev na industrijski valjarni za vsak kaliber za določene dimenzije cevi. Kontrola dimenzij cevi je potrdila natančnost izračuna.

Ključne besede: vroča raztezna redukcija, varjene cevi, numerično načrtovanje, kalibracija, koeficient plastičnega iztezanja

## 1 INTRODUCTION

With the technology of stretch reducing, previously manufactured tubes are transformed in several passes into tubes with a selected diameter and wall thickness.[1,2,3] In the processing, the tube is submitted to strong compression and tensile stresses during the reduction of the diameter and the decrease of the tube wall with stretching and tensile stressing. Both the types of stressing are mutually dependent, complex and very high.[2,3] The extent of stretching is defined by the coefficient of plastic extension and it is regulated by the number of revolutions of the rolls during every pass.[4] This coefficient is the ratio of the reduction of the tube diameter and wall, and the ratio of the compression and tensile stresses in the tube. The number of passes depends, on the one hand, on the required reductions of the tube diameter and the wall, and on the other hand, on the lowering of the temperature from the first to the last reduction pass. The quality of the processed steel is of great importance, since it determines the temperature range of the processing. For this reason, theoretically, the number of passes of the stretch-reducing mill depends on the total size of the reduction and the decrease of the temperature in all the reducing passes.

The model design of the stretch-reducing parameters, mainly reductions, stretchings, and temperature, is relatively complex and depends on several mutually related parameters. The improper selection of the stretch-reducing parameters leads to deviations between the planned and the obtained tube dimensions and the failure of the tubes' walls and a non-uniform deformation over the tube length may also occur.[5] In comparison to other processes of tube rolling, stretch reducing has some advantages, probably the most important is that it enables the manufacturing of several finished tubes from the same initial tube diameter and wall thickness.[2,9] Also, better accuracy is achieved for the final tube diameter and the wall thickness. And finally, for stretch reducing no internal tool is necessary and welded tubes can be processed without prior removal of the welded beard, while the quality of the tube surface is improved. The technology of stretch reducing is very specific and the number of rolling mills is relatively low. Accordingly, the number of references related to the process is also small. In this work, a ***theoretical model*** of the design of the hot-stretch reducing of tubes is presented, which was used to establish the number and the form of the passes for the industrial rolling of tubes of final diameters in the range ¾ inch to 3 inch from an initial tube of 4 inch.

## 2 THE PROCESS OF STRETCH REDUCING

The stretch-reducing mill consists of a line of several passes–stands, and as example in Figure 1 a three-stands rolling mill is shown.[3] The number of rolls per caliber is two up to four, with an optimum of three, and any caliber can have an individual drive or all the calibers can have a shared drive. All the calibers have an oval, and only the last one has a circular shape. The rolls are inclined at

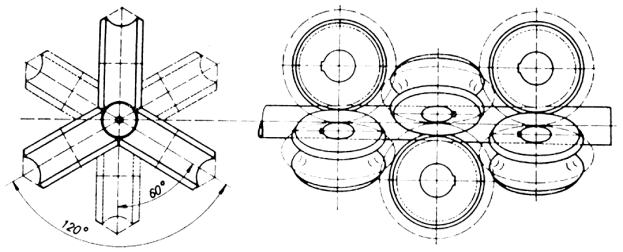


**Figure 1:** Flow chart of a three-calibers stretch-reducing rolling mill (3)
**Slika 1:** Pretočna shema trikalibrne raztezne valjarne

120° and the passes at 60° (**Figure 1**). The number of passes depends on the tube dimensions and the maximum reduction of the tube diameter and wall thickness. To lower the processing temperature and make possible the use of a greater number of passes in the prescribed temperature range, the intercaliber distance must be as small as possible.[2,3,4]

A schematic of the work of the stretch-reducing mill is shown in **Figure 2**. No change of the wall thickness occurs in the first pass, while the reduction of the diameter is 3 % to 5 %. The friction coefficient is negative and has the role of driving the processed tube. In the following two to three passes the diameter reduction is 12 %, the coefficient of plastic extension is below 0.5 and the tube-wall thickness is increased. In the middle passes the diameter reduction is up to 12 %, the extension coefficient is 0.75 and the reduction of the tube diameter and the wall thickness is achieved. In the last two passes the accuracy of the final product is ensured with a diameter reduction of 3 % to 1.5 % and with a constant wall thickness The rate of the processed tube increases from pass to pass.[4,5]

The number of passes, the dimensions of the reduction rolls and the rate of the roll revolutions are given. The calculation model is based on two basic laws: the law of the constancy of the pass rate and of the constancy of volume. When designing the successions of passes on the continuous processing line it is necessary to consider that on the same time, the tube is in several passes. To maintain the continuity of the processing, the same volume of material has to pass through every processing pass. If this continuity is not respected, the movement of the tube may be affected and by greater differences, disturbances or even breaking of the rolling may occur.[2,5,6]

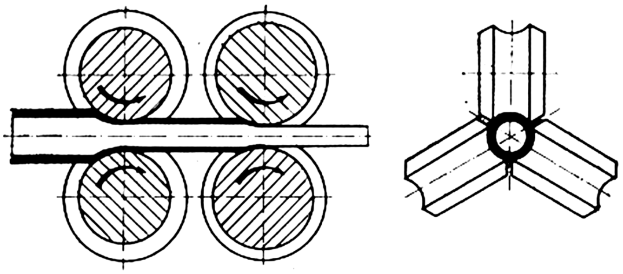

**Figure 2:** Scheme of the work of the stretch reducing mill[2]
**Slika 2:** Shema delovanja raztezne valjarne

The as-welded tube enters the stretch-reducing mill with an initial outside tube diameter of $d_0$ and a tube-wall thickness of $s_0$, which are reduced to the final dimensions of $d_n$ and $s_n$ in a determined number of passes. For the decrease of the tube wall to the required thickness, in relation to the initial, a sufficient tensile stressing ($\sigma_v$) is required[2,6,7] it is necessary that for the part of the processed tube between two following passes. For this reason, the rotation rate of the following rolls is greater than that of the precedent, thus ($n_n > \ldots > n_2 > n_1$). The increase in the rotational rate in every pass depends on the reduction of tube diameter and the wall thickness in the pass.

For the simplified design model of the process passes of the tubes, the stretch-reducing equations (1) to (6) are used. For the number of passes n the relations (1) and (2) must be fulfilled, such that:

$$v_{1(1)} = v_{1(2)} = \ldots = v_{1(n)} = const \tag{1}$$

or

$$A_1 \cdot v_{1(1)} = A_2 \cdot v_{1(2)} = \ldots = A_v \cdot v_{1(n)} = C \tag{2}$$

where $C$ is the rolling constant, $v_1$ is the tube exit rate from the pass and $A$ is the area of the tube section

The circumferential velocity of the rolls is:

$$v_0 = D \cdot \pi \cdot n \tag{3}$$

Because of acceleration, the tube rate $v_1$ is greater during the pass exit than the circumferential rolls' velocity. For a simplification of the calculation of the passes, the difference is generally neglected and it is assumed that $v_i = v_o$. On the basis of this supposition, the constant $C$ is calculated from equation (4):

$$A_1 \cdot D_1 \cdot v_{1(1)} = A_2 \cdot D_2 \cdot v_{1(2)} = \ldots = A_n \cdot D_n \cdot v_{1(n)} = C \tag{4}$$

where $D$ is the rolls' working diameter inside the pass and n is the revolution rate of the rolls.

The calculation is necessary for every new dimension of tube manufactured. After every calculation, the working diameter of the rolls is deduced with relation to the first or the final pass and the rolling constant is determined.[7,9] The number of revolutions for the other rolls is then calculated according to equation (5):

$$N = \frac{C}{A \cdot D} \tag{5}$$

On the basis of the constant $C$ the working diameters of all the rolls are calculated using equation (6):

$$D = \frac{C}{A \cdot N} \tag{6}$$

The rolls' diameter is a variable only in the projects of a new rolling mill. For mills in operation, the rolls' diameter depends on the diameter of the rolls for standardised types of mill stands.

The explained calculation is very much simplified and it could be applied only for checking in cases when

the mill constant is determined with a detailed calculation in which the compression stresses generated by the simultaneous reduction of tube diameter and of tube wall with tensile stresses are considered.

For a detailed calculation it is necessary to first determine the elements of the deformation zone. The reduction of the area is determined for the transverse tube section in every pass opening caliber (reduction of diameter), and the rate of the rolls' revolution (the reduction of the tube wall with elongation). The relation of both reductions depends on the coefficient of the plastic extension, which also represents the relation of the compression and tensile stresses.

## 3 ELEMENTS OF THE DEFORMATION ZONE

For the calculation of the reduction and the rate in the deformation zone the elements of this zone need to be determined according to **Figure 3**. The zone is defined by the angle of contact $\alpha$, the neutral angle $\gamma$, the gripping length between the surface of the rolls and the tube as well as the tube diameter and the wall thickness.

With the stretch reducing of the tubes, the deformation zone consists of two parts. In the first part with the compression stresses the tube diameter is decreased, and in the second part with the tensile stresses the wall thickness is decreased. Both parts are connected at the neutral angle $\gamma$. The total length of the deformation zone $l_d$ from the gripping point to the exit of the tube represents the line of contact between the rolls and the processed tube. The neutral angle $\gamma$ is calculated with the equation:

$$\gamma = \frac{\alpha}{2} \cdot \left(1 - \frac{\alpha}{2\beta}\right) \tag{7}$$

The angle of contact $\alpha$ is calculated from:

$$\alpha = \arccos\left(1 - \frac{\Delta d}{R}\right) \tag{8}$$

and

$$R = \frac{D_w - 2b}{2} \tag{9}$$

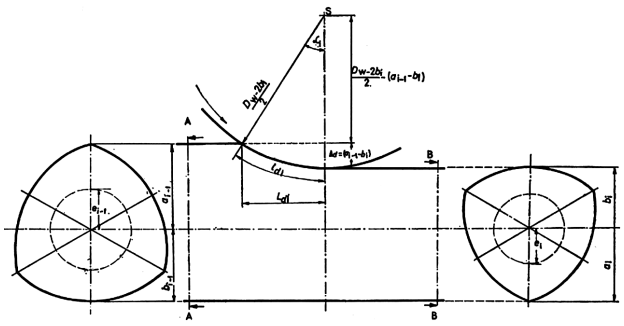

**Figure 3:** Elements of the deformation zone (10)
**Slika 3:** Elementi zone deformacije

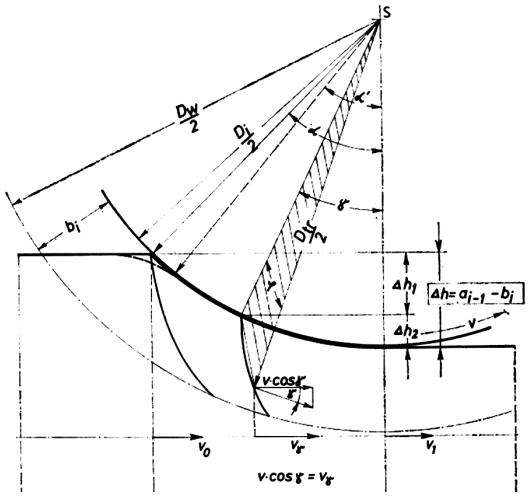


**Figure 4:** Tube and roll rates and point of the neutral angle in the deformation zone
**Slika 4:** Hitrost cevi in valjev na točki nevtralnega kota deformacijske zone

With the parameters $\Delta d$, $D_w$ and $b$ showed in **Figure 3**.[10]

The friction angle $\beta$ depends on the temperature $T_i$, the rolls type $m_1$, the rolling rate $m_2$ and the type of the steel processes $m_3$, and it is calculated from equation (12):

$$\beta = \arctan \mu \tag{10}$$

$$\mu = m_1 \cdot m_2 \cdot m_3 \cdot (1.05 - 0.005 \cdot T_i) \tag{11}$$

**Figure 4** shows that the neutral angle $\gamma$ determines the point where the tube rate in the rolling direction is equal to the horizontal component of the circumferential roll velocity on the transport radius ($v_\gamma = v \cos \gamma$), the point where the tube rate at the exit of the deformation zone ($v_1$) becomes greater than the circumferential roll velocity on the transport line.[6,10]

According to this analysis $v_1 > v_\gamma > v_0$ and with the dependence of the observation point, in the deformation zone the relative positive and negative motion occurs with respect to the roll circumferential velocity.

## 4 ROLLING RATE

To achieve the reduction of the tube diameter and wall thickness it is necessary to establish the proper relation of the rates in all the phases of the stretch reducing. The proper relation of the rates ensures the continuous processing of the changes of the diameter and the wall tube section area. As for other continuous rolling processes, the law of constant volume must be respected. For different points of the deformation zone, this law is given by the relations (12) and (13):

a) At the exit of the deformation zone

$$A_1 \cdot v_{1(1)} = A_2 \cdot v_{1(2)} = \ldots = A_n \cdot v_{1(n)} \tag{12}$$

The law of constant volume requires that in the first pass the initial rate is smaller than the pass exit rate. The

pass exit rate is increased with the decrease of the section of the tube wall until the rolling is ended.

At the neutral point of the deformation zone

$$A_{\gamma(1)} \cdot v_{\gamma(1)} = A_{\gamma(2)} \cdot v_{\gamma(2)} = \ldots = A_{\gamma(n)} \cdot v_{\gamma(n)} \quad (13)$$

The distribution of the rates and their relative place in the deformation zone for the tube rolling in a three-rolls oval pass is shown in **Figure 4**. The tube rate is equal to the horizontal component of the circumferential roll velocity and the tube rate at the exit of the deformation zone is greater than the circumferential roll velocity on the transport radius. For an angle lower than $\gamma$, a relatively positive tube motion occurs (the zone of overtaking), while, for the angle lower than $\gamma$ a relatively negative motion of the tube occurs (the tube straggling zone), **Figure 5**.

The overtaking, i.e., the difference in the roll circumferential velocity and the tube exit rate, is given in equations (14), (15) and (16).

$$s_i = \frac{v_{1(i)} - v_{\mathrm{tr}(i)}}{v_{\mathrm{tr}(i)}} \quad (14)$$

$$s_i = \frac{\frac{A_{\gamma(i)}}{\mathrm{A}_{(i)}} v_{\mathrm{tr}(i)} \cos\gamma_{(i)} - v_{\mathrm{tr}(i)}}{v_{\mathrm{tr}(i)}} \quad (15)$$

$$s_i/\% = \left( \frac{A_{\gamma(i)}}{\mathrm{A}_{(i)}} \cos\gamma_{(i)} - 1 \right) \quad (16)$$

The tube exit rate from the pass deformation zone according to equations (7) and (8) and with respect to the neutral angle (**Figure 4**) is calculated according to equations (17), (18) and (19).

$$v_i = \frac{A_{\gamma(i)} v_{\gamma(i)}}{\mathrm{A}_{(i)}} \quad (17)$$

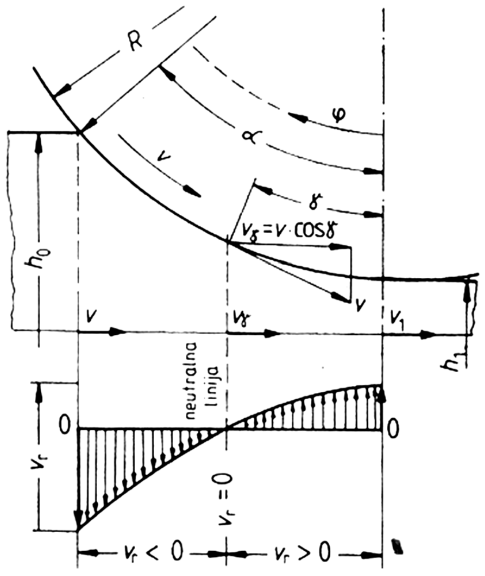


**Figure 5:** Processing rates in the deformation zone (10)
**Slika 5:** Hitrosti preoblikovanja v coni deformacije (10)

$$v_{\gamma(i)} = v_{\mathrm{tr}(i)} \cos\gamma_{(i)} \quad (18)$$

$$v_{1(i)} = \frac{A_{\gamma(i)}}{\mathrm{A}_{(i)}} v_{\mathrm{tr}(i)} \cos\gamma_{(i)} \quad (19)$$

The tube exit rate is deduced from the mill constant $C$ in equation (4) according to equation (20).

$$v_{1(i)} = \frac{C}{\mathrm{A}_{(i)}} \quad (20)$$

The number of revolutions of the rolls is calculated on the basis of the transport radius and the circumferential velocity in this radius from equation (21).

$$N_i = \frac{v_{\mathrm{tr}(i)}}{D_{\mathrm{tr}(i)}\pi} 60 \quad (21)$$

The number of revolutions of the rolls for every pass in the stretch-reducing mill $N_i$, depends on the initial rate, thus the number of revolutions of the first pass $n_1$; it depends on the number of revolutions for every caliber and it is calculated using equations (22) and (23).

$$n_i = n_1 N_i \quad (22)$$

With a multiplication of the number of stands with the number of revolutions of the first pass the number of revolution is obtained for every pass.

$$N_i = \frac{A_{\gamma(1)} D_{\mathrm{tr}(1)} \cos\gamma_{(1)}}{A_{\gamma(i)} D_{\mathrm{tr}(i)} \cos\gamma_{(i)}} \quad (23)$$

The number of revolutions of the first pass depends on the tube entering rate, i.e., the rate of tube welding.

## 5 DETERMINATION OF THE SECTION AREA OF THE TUBE DURING THE STRETCH-REDUCING PROCESS

By continuous rolling of the tubes on the stretch-reducing mill the mutual relation of the rates is defined as the change of the area of the tube section in the deformation zone.[11,12] The base equation for the calculation of the section area is:

$$A_i = \pi \cdot s_i (d_{sri} - s_i) \quad (24)$$

As the tubes are rolled with three rolls oval calibers, the calculation of the section area is complex, especially if the point in the deformation zone is also considered. With standard processing, the reduction diameter is equal for all the passes with the exception of the first and the two last passes. The average relative reduction diameter without elongation is in the range of 3 % to 5 %, and in the range 7 % to 12 % if the elongation s is also considered. With practical technology, the diameter reduction is given by the dimension of the caliber of pass size[6,7] (**Figure 6**).

The basic caliber dimensions are the width $a$ and the height $b$ (**Figure 6**). With relation to the previous, in the following stand the caliber is changed for an angle of 120° and the width ($a_{i-1}$) becomes the height with the size

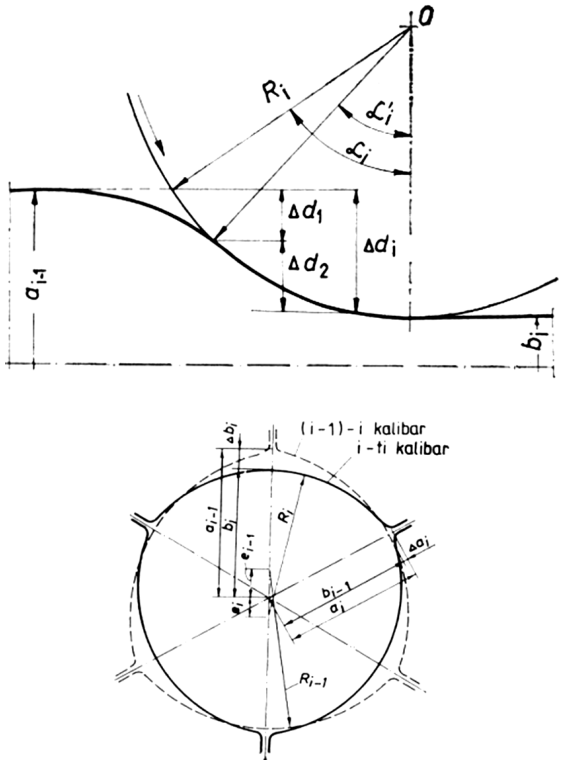


**Figure 6:** a) reduction of tube diameter, b) dimensions of the three rolls caliber
**Slika 6:** a) redukcija premera cevi, b) dimenzije kalibra s tremi valji

decreased by the reduction in this pass ($\Delta b_i$) (**Figure 6**). Simple equations for the calculations of the change of diameter $\Delta d_i$ and wall thickness $s_i$ are the relations (25) and (26).

$$\Delta d_i = a_{i-1} - b_1 \tag{25}$$

$$s_i = s_{i-1} - \frac{s_{i-1} - s_i}{d_{i-1} - d_i}(d_{i-1} - d_\gamma) \tag{26}$$

The average outside tube diameter $d_{sri}$ is determined by the dependence of the dimensions of the three-rolls oval caliber according to **Figure 6** by applying equation (27):

$$d_{sri} = \frac{2.865 \cdot b_i^2 - 0.365 \cdot a_i^2 - 0.5 \cdot b_i \cdot a_i}{2b_i - a_i} \tag{27}$$

According to[2,6,8] it is possible to determine the tube dimensions accurately. The tube section outside the deformation zone is calculated using equations (28) and (29).

$$A_i = 3\left[R_i^2 \rho_1 - (R_1 - s_1)^2 \rho_{(2)i}\right] - \frac{3e_i}{2}\sqrt{3}\left[R_1 \cos \upsilon_{(1)i} - (R_i - s_i)\cos \upsilon_{(2)i}\right] \tag{28}$$

$$d_{sri} = \frac{A_i}{s_i \pi} + s_i \tag{29}$$

At the neutral angle of the deformation zone, the outside tube diameter is:

$$d_{sri} = 2\sqrt{\frac{A_{i(\gamma)}}{\pi}} \tag{30}$$

The area of the section of the tube wall in the neutral position of the deformation zone is:

$$A_{1(\gamma)} = s_{i(\gamma)} \pi (d_{i(\gamma)} - s_{i(\gamma)}) \tag{31}$$

The area of the tube at the exit from the deformation zone is:

$$A_{i(k)} = 3\left(R_i^2 \arcsin \frac{a_i\sqrt{3}}{2R_i} - \frac{a_i e_i \sqrt{3}}{2}\right) \tag{32}$$

## 6 TUBE-WALL-STRETCHING REDUCTION

For proper stretch reducing of the tubes it is of basic importance to know the maximum allowed changes of the tube-wall thickness and diameter. The tube reduction from the initial to the end size is defined by the maximum deformation and stressing of the material at the processing temperature for every phase of the processing.[2,9,11]

The wall reduction is defined by the coefficient of plastic elongation. The maximum value of this coefficient determines the limit value of the reduction of the wall thickness. On the other hand, the maximum wall reduction thickness also depends on the maximum drawing force and on the material deformation resistance at the processing temperature. For this reason, it is necessary to determine, for every phase of stretch reducing, the maximum value of the coefficient of plastic extension to prevent the tube tearing. Theoretically, the maximum value of the coefficient of plastic extension is 1, while the practical value is in the range 0.1 to 1. The coefficient is calculated for the design of the passes for every step of the processing and the related changes to the tube diameter and the wall thickness. The calculation is performed by assuming that the deformation is uniform over the whole tube section and that the elongation is equal for all the passes.[2,6,8]

With the analysis of the coefficient of plastic elongation, it is necessary to consider the following:

a) the coefficient for the total elongation (average per pass) $z_u$ makes it possible to determine the total elongation of the tube. From the physical point of view, $z_u$ exists only for ideal cases, when the coefficient of plastic extension is equal for all the passes and it is equal to $z_u$. This cannot be achieved during practical processing, as, in the first and in the last stands of the processing line the possibility of drawing with the rolls is limited and $z_i < z_u$. For this reason, the elongation is greater in the middle caliber than $z_u$.
b) In theory, the initial and the end extension coefficients exist; however, the values of both are not clearly defined and as the average elongation coefficient the arithmetical value of both coefficients is calculated:

$$z_{i_{sr}} = \frac{z_{i-1} + z_i}{2} \tag{33}$$

This value is then used to calculate the decrease of wall thickness. Theoretically, the value of the coefficient of extension could be between 0.0 and 1.0.

For $z_{teor} < 0.5$ the wall thickness is increased and the diameter reduction of 3 % to 5 % is achieved. The increase of thickness of the tube wall is necessary to obtain in the following pass a homogenous decrease of tube diameter and to maintain, in a safe range, the material stressing.

For $z_{teor} = 0.5$ the wall thickness is unchanged and practice shows that it remains unchanged also for $z$ = 0.55

For $z_{teor., max} = 1.0$ in parallel, the tube diameter in and the wall thickness are decreased. It cannot be achieved in practice because it leads to tearing of the rolled tube. The maximum practically used extension coefficient is of $z$ = 0.7 to 0.8.

Theoretically, the coefficient is the ratio of axial stress and the deformation resistance of the material, such that:

$$z = \frac{\sigma_i}{k_f} \tag{34}$$

The analytical dependence of the stress and deformation is given by the equations:

$$\frac{\sigma_r - \sigma_{sr}}{\varepsilon_r} = \frac{\sigma_1 - \sigma_{sr}}{\varepsilon_1} = \frac{\sigma_t - \sigma_{sr}}{\varepsilon_t} \tag{35}$$

$$(\sigma_r - \sigma_{sr}):(\sigma_1 - \sigma_{sr}):(\sigma_t - \sigma_{sr}) = \varepsilon_r:\varepsilon_1:\varepsilon_t \tag{36}$$

The average stress also depends on the type of the processed material. In equation (37) the dependence upon the deformation resistance $k_f$ is:

$$\sigma_{sr} = \frac{1}{3}\cdot(2\cdot\sigma_1 - k_f) = \frac{1}{3}\cdot(\sigma_r + \sigma_1 + \sigma_t) \tag{37}$$

On the other hand, the stress depends also on the relation of the wall thickness and the tube diameter:

$$\sigma_{sr} = \sigma\cdot\left(\frac{s}{d}\right)_{sr} \tag{38}$$

$$k_f = \sigma_1 - \sigma_t \tag{39}$$

$$\frac{\sigma_{r_{sr}}}{\sigma_{t_{sr}}} = \left(\frac{s}{d}\right)_{sr} = \upsilon_{sr} \tag{40}$$

The solution of equations (35) and (36) given in equation (41) is obtained by applying the equations (34), (37), (38), (39) and (41):

$$\frac{2\cdot z\cdot(\upsilon-1)+(1-2\cdot\upsilon)}{\varepsilon_r} = \frac{z\cdot(\upsilon-1)+(1+\upsilon)}{\varepsilon_1} = \frac{z\cdot(\upsilon-1)+(2-\upsilon)}{\varepsilon_t} \tag{41}$$

Equation (41) is the basis for equation (42), which is used for the calculation of the plastic extension by stretch reducing the tubes:

$$z = \frac{\varepsilon_1\cdot(2-\upsilon)+\varepsilon_t(1+\upsilon)}{(\varepsilon_1 - \varepsilon_t)\cdot(1-\upsilon)} \tag{42}$$

The coefficient "$\upsilon$" obtained from (40) cannot be used in practice, and it is corrected by considering the uniform tube deformation "$T$" deduced from equation (43).

$$T = \frac{\upsilon_{sr}}{1-\upsilon_{sr}} \tag{43}$$

Applying the corrected value "$T$", the relation for the average coefficient of plastic extension is calculated from equation (44).

$$z_{sr} = \frac{\varepsilon_1\cdot(2-T)+\varepsilon_t(1+T)}{(\varepsilon_1 - \varepsilon_t)\cdot(1-T)} \tag{44}$$

The values for the coefficient $z_{isr}$ obtained from equation (42) are appropriate to those obtained from equation (44). However, the calculation is simpler by applying equation (42), and this equation is recommended for use in practice. The values of "$z_{isr}$" calculated from the equations (42) and (44) differ only in the second decimal[2].

The coefficient "$T$" calculated from equation (43) is reliable for the relation $(s/d)_{sr}$ in the range from 0.27 to 0.275. If the relation differs from this range and it is not constant during the processing, the correction of the coefficient "$T$" becomes necessary. For this reason, an additional coefficient "$k$" is used that considers the effect of the diameter reduction on the thickness reduction. For the three rolls the caliber the coefficient "$k$" is calculated from equation (45).

$$k_i = \frac{1}{1+0.70\delta_i^2} \tag{45}$$

Finally, for the coefficient "$T$" the following equation is obtained:

$$T = \left[\frac{0.868\cdot\upsilon_{sr} + 0.264\cdot\upsilon_{sr}^2}{1-\upsilon_{sr}}\right]^{\frac{1}{1+0.70\delta_i^2}} \tag{46}$$

From equations (46) and (44) the average value of the coefficient of extension is calculated and used for the determination of the tube-wall reduction in the $i$-pass.

In equation (44) the logarithmic values for the axial, tangential and radial deformations are included, which are calculated from equations (47), (48) and (49).

a) $\varepsilon_{1i}$ – lg of axial deformation from equation (47).

$$\varepsilon_{1i} = \left[\frac{s_{(i-1)}\cdot d_{(i-1)} - s_{(i-1)}}{s_i\cdot(d_{(i)} - s_{(i)})}\right] \tag{47}$$

b) $\varepsilon_{ti}$ – lg of tangential deformation from equation (38).

$$\varepsilon_{ti} = \ln \frac{d_i - s_i}{d_{(i-1)} - s_{(i-1)}} \quad (48)$$

c) $\varepsilon_{ri}$ – lg of radial deformation from equation (49).

$$\varepsilon_{ri} = l \frac{s_i}{s_{(i-1)}} \quad (49)$$

The diameter reduction "$\delta_i$" per pass in equations (45 and 46) is calculated from equations (50):

$$\delta_i = \frac{d_{(i-1)} - d_i}{d_{(i-1)}} \quad (50)$$

From equation (43) the coefficient "$T$" is deduced for the case when:

a) $v_{sr} \Rightarrow$ for thin tube wall as (51)

$$T \approx v_{sr} \quad (51)$$

b) $v_{sr} \Rightarrow$ for the full section of the rolled tube according to (52)

$$T \approx 2 \cdot v_{sr} \quad (52)$$

The parameters affecting the maximum value of the coefficient of plastic extension are[2,7]:

- the material plasticity at the processing temperature considering the strain hardening in the deformation zone and the softening between the rolling passes that depends on a given tube rate on the distance between the rolling stands,
- the diameter reduction,
- the total previous deformation,
- the rolling rate,
- the uniformity of the temperature over the tube length.

## 7 VERIFICATION OF THE CALCULATION

The calculation was verified on an industrial stretch-reducing mill with 18 three-rolls passes. The possibility to change the number of revolutions (minimum and maximum for every pass) of the mill are shown in **Figure 7**.

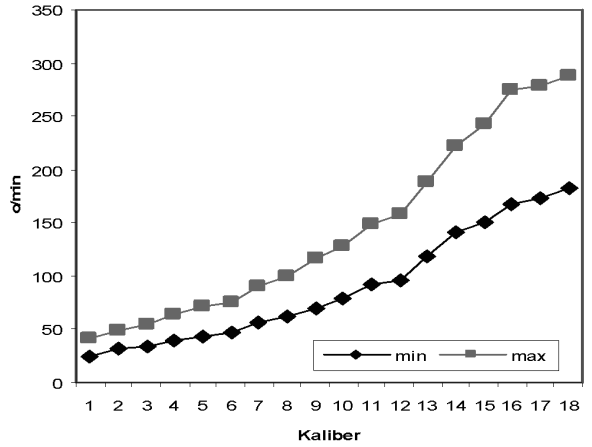


**Figure 7:** Maximum and minimum number of revolutions at the industrial stretch-reducing mill

**Slika 7:** Največje in najmanjše število vrtljajev na industrijski valjarni za raztezno reduciranje

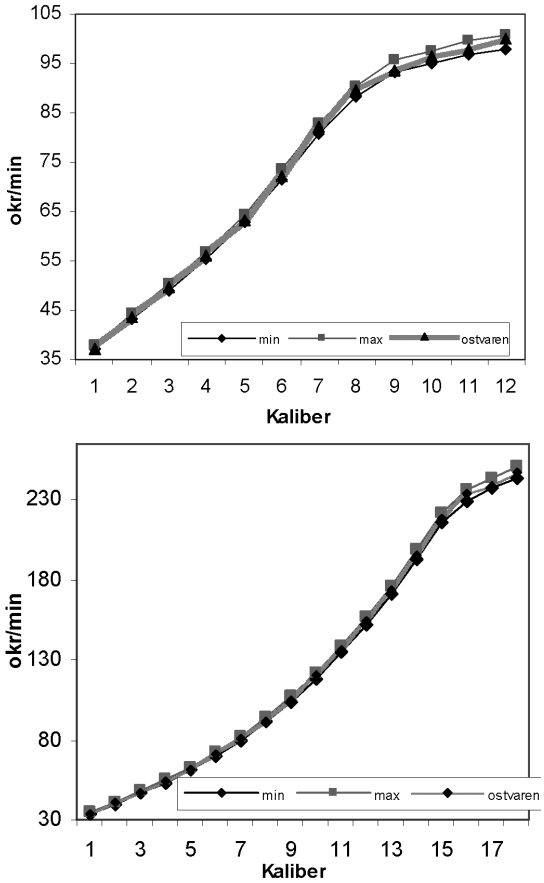


**Figure 8:** Number of revolutions calculated for the tubes: a) $\phi$ 21.3 mm × 2.65 mm and b) $\phi$ 48.3 mm × 3.25 mm

**Slika 8:** Število vrtljev, izračunanih za cevi: a) $\phi$ 21,3 mm × 2,65 mm in b) $\phi$ 48,3 mm × 3,25 mm

On the mill, the welded tubes of $\phi$117.3 mm × 3.8 mm are rolled to tubes of size from $\phi$ 17.1 mm × 2.0 mm to $\phi$ 114.3 mm × 4.5 mm. The pass designing was verified for the tubes $\phi$ 21.3 mm × 2.65 mm and $\phi$ 48.3 mm × 3.25 mm. The rolling of tubes $\phi$ 21.3 mm × 2.65 mm is carried out in 18 passes and of the tubes $\phi$ 48.3 mm × 3.25 mm in 12 passes. For both tube dimensions and for each pass the minimum and maximum number of revolution was calculated, which is shown in **Figure 8**. It is clear from this figure that the calculated values were achieved and the design verified. All the produced tubes have the required mechanical and technological properties and the required dimensional accuracy, thus confirming that the pass design is also reliable for industrial production.

## 8 CONCLUSION

In this article the process of the design of passes is given for the hot-stretch reducing of tubes. The calculations are based on data from references and our own

industrial data. The mutual dependence of the processing parameters is also considered, and the calculation of the tube rate and the reduction for every processing step is explained. Since the reduction of the tube-wall thickness is achieved with stretching, the processing rate and the reduction of the wall thickness are mutually dependent and determine the extent of the internal stresses in the processed material. The corresponding parameters are related through the coefficient of plastic extension, which was also calculated.

The processing parameters are calculated and verified for two tube dimensions in current industrial production. The agreement between the calculated and the obtained dimensions of the tubes confirms the accuracy and the reliability of the designed passes. The rolled tubes have the properties required by the standards and confirm that the relation between the reduction of the wall and the tube diameter as well as the processing rate and the extent of stresses were considered with sufficient accuracy.

$i$ – number of passes of the stretch-reducing mill
$d_0$ – external tube diameter
$d_n$ – external tube diameter in the $i$ – pass
$\Delta d$ – reduction of tube diameter
$s$ – tube-wall thickness
$s_i$ – tube-wall thickness in the $i$ – pass
$C$ – rolling constant
$V_1$ – tube exit rate from the rolls
$A$ – pass surface
$D$ – working diameter of rolls (bottom of passes)
$D_w$ – ideal rolls diameter
$D_{tr}$ – transport diameter of rolls
$a$ – pass width
$b$ – pass height
$n$ – number of revolutions of the rolls
$A$ – area of tube section
$\alpha$ – angle of contact
$\gamma$ – neutral angle in the deformation zone
$\varphi$ – angle change in the deformation zone
$\beta$ – angle of friction
$\mu$ – friction coefficient
$v$ – circumferential velocity of rolls
$v_0$ – tube rate in the deformation zone
$v_\gamma$ – tube rate in the deformation zone at the neutral angle $\gamma$
$v_t$ – tube rate at the exit of deformation zone
$m_1$ – coefficient dependent on rolls quality
$m_2$ – coefficient dependent on rolling rate
$m_3$ – coefficient dependent on steel microstructure
$z$ – coefficient of plastic extension
$z_i$ – coefficient of plastic extension in the $i$- pass
$z_{ku}$ – total coefficient of plastic extension
$z_{sr}$ – average coefficient of plastic extension
$k_f$ – deformation resistance of the rolled material
$\sigma_l$ – axial stress
$\sigma_r$ – radial stress
$\sigma_t$ –tangential stress
$\sigma_{sr}$ – total average stress
$\varepsilon_l$ – lg of axial deformation
$\varepsilon_t$ – lg of tangential deformation
$\varepsilon_r$ – lg of radial deformation
$\upsilon$ – coefficient of the relation of reduction of tube wall and diameter
$T$ – coefficient of correction of the coefficient $z$
$k$ – coefficient of correction of the coefficient z with respect to the diameter reduction

## 9 REFERENCES


[1] S. Rešković, F. Vodopivec; Mater. Tehnol., 42 (**2008**) 6, 257–262
[2] R. Križanić: Technology of stretch reducing, geometrical characteristics of passes and parameters of the manufacturing of tubes, Institute of Metallurgy, Sisak, 1978, 1–24
[3] K. H. Staat: Streckreduzierwalzwerk, Metalurgija, 10 (**1971**), 13–22
[4] H. Molther: Rolling line for the stretch-reducing for tubes, www.freepatententsoline.com
[5] R. Križanić, S. Rešković: Pass determination of rolls for IRS; Proceedings of the Symposium, VII Symposium of roling-mill worker of Yugoslav, OUCM, Beograd, Mavrovo, 1985
[6] A. A. Ševčenko: Continous rolling of tubes, Metalurgizdat, Moskva 1954, p. 188
[7] R. Križanić, M. Šindler, S. Rešković: Development of the IRS computer program, II – Optimisation of the production of small wall welded tubes, Institute of Metallurgy, Sisak, 1979
[8] G. I. Guljajev, P. I. Ivšin: Technology of continuous rolling of tubes without, Metalurgizdat, Moskva 1975, p. 145
[9] S. Rešković: Parameters of working for IRS, Instruction book for the Rolling mill, Ironwork Sisak, Sisak, 1999
[10] R. Križanić: Metalurgija, 26 (**1987**) 4, 109–116
[11] I. Horvat: Calculation of the contact area on the three rolls stretch reducing stand, degree thesis, Faculty of Metallurgy, Sisak, 1983
[12] R. Križanić: Metalurgija, 26 (**1987**) 1/2, 3–11
[13] R. Križanić: Metalurgija, 24 (**1988**) 2, 49–55
[14] W. Demny, H. Molther, H. Gerhards: Process and rolling mill for stretch reducing of tubes, www. freepatententsoline.com
[15] D. Pavlić: Study of the hot rolling of welded tubes on the stretch reducing mill, Degree Thesis, FSB, Zagreb, 1998
[16] R. Križanić: Technology of stretch reducing and geometrical characteristics of passes in the production of welded tubes in the Rolling mill for welded tubes, Institute of Metallurgy, Sisak, 1978

UDK 621.762:669.018.9
Original scientific article/Izvirni znanstveni članek

ISSN 1580-2949
MTAEC9, 44(5)251(2010)

# PREPARATION AND STUDY OF $Mg_2Sn$-BASED COMPOSITES WITH DIFFERENT COMPOSITIONS

## PRIPRAVA IN KARAKTERIZACIJA LASTNOSTI KOMPOZITOV NA OSNOVI $Mg_2Sn$

**Varužan Kevorkijan[1], Srečo Davor Škapin[2]**

[1]zasebni raziskovalec, Betnavska cesta 6, 2000 Maribor, Slovenia
[2]Srečo Davor Škapin, Institut "Jožef Stefan", Jamova 39, 1000 Ljubljana, Slovenia
varuzan.kevorkijan@impol.si

*Prejem rokopisa – received: 2010-02-22; sprejem za objavo – accepted for publication: 2010-03-15*

Single-phase $Mg_2Sn$ powders were successfully reaction-synthesized from the elements and applied for the preparation of $Mg_2Sn$-based composites with different natures, microstructures and combinations of properties. These were fully dense (≥95 % T.D.) Mg- and Al-metal-matrix composites (MMCs) reinforced with either $Mg_2Sn$ particles or mixtures of $Mg_2Sn$ with TiC or $TiB_2$ particulates by the infiltration of porous $Mg_2Sn$ preforms with molten magnesium or aluminium; and (ii) $Mg_2Sn$ intermetallic matrix composites discontinuously reinforced with TiC and $TiB_2$ particles by pressureless sintering.
The microstructures of the composite samples were examined using scanning electron microscopy (SEM-EDS) and X-ray powder diffraction (XRD). The mechanical properties were evaluated by Vickers hardness measurements performed at room temperature, while the fracture toughness of the specimens was determined by applying the indentation method.
Based on the data accumulated, an evaluation of the mechanical properties of these composites on the basis of the volume content of different constituents was performed.
Moreover, the ability of various microstructures obtained with pressureless infiltration and sintering for tailoring the desired combination of mechanical properties. (e.g., toughening in combination with hardness) was also investigated and reported.
Thus, the infiltration led to MMCs with different microstructures and mechanical properties, depending on the infiltrant applied. The samples infiltrated with molten magnesium possessed a characteristic lamellar, sometimes referred to as "Chinese script", eutectic microstructure and thereby an enhanced fracture toughness (up to 7.7 MPa $m^{1/2}$ in non-reinforced and 5.8 MPa·$m^{1/2}$ in reinforced counterparts), in combination with a Vickers hardness superior to those of conventional Mg-Sn alloys. On the other hand, although the mechanical response (Vickers hardness) of the samples infiltrated with aluminium was even better than in the counterparts infiltrated with magnesium, the absence of the "Chinese script" microstructure was observed to have a detrimental influence on the fracture toughness, which was significantly lower in these samples.
The densification of intermetallic matrix composites (IMCs) with a $Mg_2Sn$ matrix discontinuously reinforced with TiC or $TiB_2$ ceramic reinforcement performed by non-reactive, solid-state sintering resulted in samples with a high density (≥95% T.D.) and different combinations of mechanical properties compared to MMCs obtained by infiltration. The Vickers hardnesses of the sintered IMCs were much better than in the MMCs obtained by infiltration, with the exception of the fracture toughness, which was reduced below 1.8 MPa $m^{1/2}$.

Key words: $Mg_2Sn$ powder, synthesis, $Mg_2Sn$-based composites, sintering, infiltration, microstructure development, hardness, fracture toughness

Z reakcijo v trdnem smo iz elementov sintetizirali $Mg_2Sn$. Spojino smo zdrobili in prah uporabili za pripravo vrste kompozitov z različnimi mikrostrukturnimi in mehanskimi lastnostmi. Pripravili smo goste kompozite (≥95 % T. G.): (i) na osnovi kovinske matrice Mg in Al tako, da smo v porozne predoblike spojine $Mg_2Sn$ ter predoblike različnih sestav na osnovi $Mg_2Sn$ in TiC oziroma $TiB_2$ infiltrirali tekoči Mg oziroma Al, in (ii) na osnovi intermetalne spojine $Mg_2Sn$, ki smo jih pripravili s sintranjem $Mg_2Sn$ z dodatkom ojačitvene faze trdin TiC oziroma $TiB_2$.
Mikrostrukturno analizo pripravljenih kompozitov smo opravili z vrstičnim elektronskim mikroskopom in elementno spektroskopsko disperzijsko analizo (EDS) ter z rentgensko praškovno difrakcijo. Mehanske lastnosti, trdoto po Vickersu in zlomno žilavost smo merili pri sobni temperaturi.
Dobljene rezultate smo razložili glede na fazno sestavo pripravljenih kompozitnih vzorcev. Opisali smo odvisnost mehanskih lastnosti infiltriranih in sintranih vzorcev v odvisnosti od mikrostrukturnih karakteristik.
Pri infiltraciji nastajajo kompoziti s kovinsko matrico (KKM) z različno mikrostrukturo in mehanskimi lastnostmi, kar je odvisno od uporabljene kovine, ki jo infiltriramo. Kompoziti na osnovi Mg izkazujejo lamelarno evtektično mikrostrukturo (kitajska pismenka) in izboljšano zlomno žilavost (do 7,7 MPa $m^{1/2}$ neojačani materiali in 5,8 MPa $m^{1/2}$ ojačani kompozitni materiali) in tudi višjo trdnost po Vickersu glede na komercialne Mg-Sn zlitine. Kompoziti na osnovi infiltriranega Al izkazujejo višjo trdnost kot Mg kompoziti, vendar pa nižjo zlomno žilavost, ker ne tvorijo lamelarne mikrostrukture.
Pri sintranju kompozitov na osnovi intermetalne $Mg_2Sn$-matrice, ki so bili ojačani s TiC oziroma $TiB_2$ nastajajo gosto sintrani kompozitni materiali (≥95 % T. G.) z različnimi mehanskimi lastnostmi. Trdota teh materialov je večja, kot jo izkazujejo kompoziti na osnovi kovinske matrice, vendar pa imajo manjšo zlomno žilavost, manj kot 1,8 MPa $m^{1/2}$.

Ključne besede: $Mg_2Sn$-prah, priprava, kompoziti na osnovi $Mg_2Sn$, sintranje, infiltracija, razvoj mikrostrukture, trdota, prelomna žilavost

## 1 INTRODUCTION

Current applications of magnesium stannide ($Mg_2Sn$) are limited to the optimisation of the microstructure and mechanical properties of magnesium [1–7] and in lead-free aluminium alloys [8]. In the Mg-Sn and Mg-Sn-Ca creep-resistant magnesium alloys, $Mg_2Sn$ precipitates are applied as a thermally stable intermetallic phase for suppressing the grain-boundary sliding and dislocation movement, resulting in an improvement of the creep properties.

However, due to its high melting point (770 °C), relatively low density (3.59 g/cm$^3$ – about half that of the density of tin), excellent compressibility (2.83 $10^{-11}$ m$^2$/N, approximately 50 % higher than for $Mg_2Si$) and a thermal expansion coefficient (9.9 $10^{-6}$ K$^{-1}$) similar to some borides and carbides [9,10], magnesium stannide is a promising structural material, particularly in combination with magnesium and aluminium alloys and composites. The Vickers hardness of $Mg_2Sn$ is about 1.2 GPa [7], significantly lower than for $Mg_2Si$ (3.5–7.0 GPa), but still twice as high in comparison with the hardness of Mg-Sn alloys.

In addition, $Mg_2Sn$ is a stoichiometric compound suitable for achieving characteristic eutectic microstructures (i.e., "Chinese-script") and therefore for tailoring the properties of composites (particularly the fracture toughness) with $Mg_2Sn$ appearing as a matrix or a reinforcement phase.

In contrast to numerous investigations carried out in developing Mg-Sn alloys with $Mg_2Sn$ precipitates formed *in situ*, only a limited number of investigations were concerned with the synthesis of $Mg_2Sn$ powder [11] and, to the best of our knowledge, none with its densification, alone or with some other reinforcing phases, i.e., as a matrix for high-temperature composites or as particulate reinforcement in metal matrix composites.

Hence, in the present study, the following investigations were performed in order to demonstrate the potential of $Mg_2Sn$ as an advanced composite matrix or discontinuous reinforcement: (i) the synthesis of $Mg_2Sn$ single-phase powder from the elements; (ii) pressureless sintering and characterisation of $Mg_2Sn$-based intermetallic matrix composites discontinuously reinforced with TiC or $TiB_2$ particles, and (iii) the formation and characterisation of Mg- or Al-metal matrix composites reinforced with either $Mg_2Sn$ particles or mixtures of $Mg_2Sn$ with TiC or $TiB_2$ particulates by the infiltration of porous $Mg_2Sn$ preforms with molten magnesium and aluminium.

## 2 EXPERIMENTAL

In the first part of the experimental work, $Mg_2Sn$ powder was synthesized with a reaction synthesis from the elements. As the source of magnesium and tin, cylindrical samples machined from pure magnesium and tin rods were used. Magnesium and tin samples in three different molar ratios (stoichiometric, with 5 % and 10 % excess of magnesium) were placed in a platinum crucible and heated in a vacuum furnace (for 2 h at 660 °C or for 1 h at 700 °C) in a static atmosphere of argon. This was followed by cooling to room temperature and characterisation of the as-obtained product with optical and scanning electron microscopy (OM and SEM) and X-ray diffraction (XRD). After that, the product was milled in an attrition mill for various milling times (0.5–2 h) in order to achieve the desired morphology of the $Mg_2Sn$ particles. The as-milled $Mg_2Sn$ powders were then applied for various infiltration and sintering experiments.

The infiltration was performed by using porous preforms made from laboratory synthesized $Mg_2Sn$ powder of grade C (**Table 1**) and mixtures of $Mg_2Sn$ powder grade C and commercially available TiC (99.5 %, $d_{50}$ = 4 μm) and $TiB_2$ powders (99.5 %, $d_{50}$ = 6 μm), as listed in **Table 2**. The preforms were isostatically pressed at various pressures (from 80 MPa to 150 MPa) in order to achieve samples with different porosities. The samples obtained were cylinders, 50 mm high and 20 mm in diameter. As infiltrant, Al-*x*Sn and Mg-*x*Sn (*x* = 3%, 5 %) alloys were applied. Al-*x*Sn and Mg-*x*Sn alloys necessary for infiltration were prepared from pure aluminium or magnesium and pure tin powders melted in a graphite crucible with the protection of a fusing agent. The melt was then stirred to ensure homogeneity and, finally, it was cast into a preheated mould. The as-cast ingots were cut and machined into thin cylindrical plates having the same diameter as the $Mg_2Sn$ preforms (20 mm). Finally, a preform sandwiched between two Al-*x*Sn or Mg-*x*Sn plates was placed in a ceramic crucible using the following procedure: the first Al-*x*Sn or Mg-*x*Sn plate was placed on the bottom of crucible and the preform was fixed on it using upper and lower preformatted steel plates. After that, the upper Al-*x*Sn or Mg-*x*Sn plate was placed on it. The volume of the Al-*x*Sn or Mg-*x*Sn plates was calculated to be approximately 50 % higher than the volume of the pores in the preform. The infiltration was conducted by heating the assembly in a vacuum furnace at 730 °C for 1 h, under a static atmosphere of argon.

After completion of the infiltration, the assembly was cooled to room temperature, and then the infiltrated preform was removed from the furnace. The green samples for sintering experiments were formulated by blending the synthesized $Mg_2Sn$ powder (grade C, **Table 1**) with commercial ceramic powders (TiC and $TiB_2$) in appropriate amounts to create IMCs with mass fractions *w* = (10, 30 and 50) % of TiC or $TiB_2$ reinforcement. The powder blends were thoroughly mixed in a planetary mill and subsequently cold compacted. In all cases, the sintering of the compacts was conducted at 750 °C for 1 h in a static atmosphere of argon using a vacuum furnace. The as-synthesized composite samples were cut, machined and polished in accordance with standard procedures.

Microstructural characterization of the fabricated composites was performed with OM and SEM, whereas XRD measurements were applied to the samples to identify the phases and their crystal structure. A quantitative determination of the volume percentage of $Mg_2Sn$ and ceramic particles in the matrix, as well as the retained porosity, was performed with an assessment of optical and scanning electron micrographs of polished composite bars using the point-counting method and image analysis and processing software. The composite

density measurements were carried out using Archimedes' principle, applying absolute ethanol as the immersion fluid. The initial density of the green compacts (preforms and tablets) was calculated from the mass and geometry of the samples.

Vickers hardness (HV) measurements were performed at room temperature on polished composite samples and calculated as the average of six indentations. These measurements were made with a conventional Vickers tester (load: 9.8–24.5 N for 15 s).

Due to their small dimensions and high brittleness, the fracture toughness of the specimens obtained was determined by applying the indentation method [12]. The $K_{IC}$ of the composite samples was determined from submicron-derived indentation cracks and calculated according to the equations proposed by Niihara et al. [13].

## 3 RESULTS AND DISCUSSION

### *3.1 Mechanism of the formation, chemical composition and morphology of laboratory-prepared $Mg_2Sn$ powder*

Depending on the initial composition of the reaction mixture and the heating conditions, the concentration of Mg and Sn impurities in the synthesized $Mg_2Sn$ phase varied significantly.

On applying reaction mixtures with a stoichiometric ratio of elemental magnesium and tin, more than $w$ = 5 % of the tin remained in the reaction product obtained ($Mg_2Sn$ powder grade A, **Table 1**), which was most probably caused by a loss of magnesium. This assumption was additionally confirmed by the experimental finding that the amount of non-reacted tin increased with the increasing temperature of the synthesis.

**Table 1:** Phase composition and morphology of laboratory-prepared $Mg_2Sn$ powders
**Tabela 1:** Fazna sestava in morfologija laboratorijsko izdelanih $Mg_2Sn$ prahov

| Powder | $\varphi(Mg_2Sn)$/% | $\varphi$(Sn)/% | $d_{50}$/μm |
|---|---|---|---|
| Grade A | 95 | 5 | 3.3 |
| Grade B | 97 | 3 | 2.4 |
| Grade C | 99.8 | 0.2 | 2.1 |

On the other hand, by applying a reaction mixture with a small ($x$ = 5 %) excess of magnesium, the amount of non-reacted tin was reduced below 5 % or even below $w$ = 3 % (mass fractions) (grade B, **Table 1**) at a lower temperature of synthesis (660 °C).

Finally, by using a reaction mixture with the mol fraction $x$ = 10 % excess of magnesium, single-phase $Mg_2Sn$ (grade C, **Table 1**) with no Mg or Sn peak detected in the XRD pattern was prepared at 700 °C.

The investigation of the solidified product samples indicated that the reaction mechanism of the $Mg_2Sn$ synthesis is homogeneous nucleation and growth. Based on the phase diagram of the Sn-rich corner in the Mg-Sn binary system [14], it is evident that Mg will start to dissolve into the liquid phase immediately after the temperature exceeds the melting point of Sn (505 K). With increasing temperature, a greater amount of Mg will be dissolved and, after melt saturation, the $Mg_2Sn$ will start to nucleate according to reaction 1:

$$Mg_{(s)} + Sn_{(l)} = Mg_2Sn_{(s)} \quad (1)$$

Above the melting point of magnesium (923 K), the nucleation of $Mg_2Sn$ will continue by nucleation from the saturated liquid phase according to reaction 2:

$$Mg_{(l)} + Sn_{(l)} = Mg_2Sn_{(s)} \quad (2)$$

Thus, to achieve the complete conversion of reactants into $Mg_2Sn$, it is important to preserve a permanent excess of magnesium (approximately $w$ = 10 %) in the system up to the end of the synthesis. The morphology of the laboratory-prepared $Mg_2Sn$ powder, obtained with milling the solidified sample from reactive synthesis, is presented in **Figure 1**. As is evident, the powder obtained is non-agglomerated, with well-shaped individual particles with a size below 5 μm.

The typical phase composition in the synthesized $Mg_2Sn$ powders is reported in **Table 1**. The compositions of various $Mg_2Sn$-TiC and $Mg_2Sn$-$TiB_2$ mixtures used for preforms in the infiltration experiments are listed in **Table 2**.

**Table 2:** The composition of various $Mg_2Sn$-TiC and $Mg_2Sn$-$TiB_2$ mixtures used for preforms preparation in the infiltration experiments
**Tabela 2:** Sestava različnih zmesi $Mg_2Sn$-TiC in $Mg_2Sn$-$TiB_2$, uporabljenih za pripravo predoblik

| Mixture | Initial composition, $\varphi$/% |
|---|---|
| #1 | 100 % $Mg_2Sn$ (grade C) |
| #2 | 75 % $Mg_2Sn$ (Grade C)–25 % TiC |
| #3 | 75 % $Mg_2Sn$ (Grade C)– 25 % $TiB_2$ |
| #4 | 70 % $Mg_2Sn$ (Grade C)–30 % TiC |
| #5 | 70 % $Mg_2Sn$ (Grade C)–30 % $TiB_2$ |

### *3.2 Composites made by pressureless infiltration*

#### 3.2.1 Al-$Mg_2Sn_{(p)}$ and Mg-$Mg_2Sn_{(p)}$

The infiltration of porous $Mg_2Sn$ preforms (composition #1, **Table 2**) with molten Al resulted in fully dense composite samples with a continuous aluminium-based matrix, reinforced with $Mg_2Sn$ particles and $Mg_2Sn$ precipitates appearing near the primary $Mg_2Sn$ particles, **Figure 2a**.

On the other hand, samples fully infiltrated with molten magnesium have a characteristic lamellar "Chinese script" eutectic microstructure, **Figure 3a**, and completely different mechanical properties, **Table 3**.

In both cases, due to the complete and non-reactive wetting of the $Mg_2Sn$ preform skeleton with molten Mg or Al, under atmospheric pressure the infiltration proceeded spontaneously. The absence of chemical reactions between the preform skeleton and the molten infiltrants

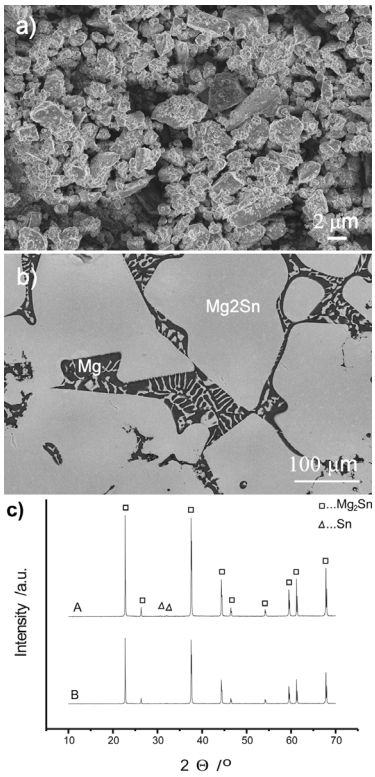


**Figure 1: a**) SEM micrograph of $Mg_2Sn$ powder (grade B) after milling, **b**) SEM micrograph of as-synthesized $Mg_2Sn$ and **c**) X-ray powder diffraction pattern of the prepared compound $Mg_2Sn$: A – grade B powder (**Table 1**), and B – grade C powder (**Table 1**)

**Slika 1: a**) SEM-posnetek $Mg_2Sn$ prahu (tip B) po mletju, **b**) SEM-posnetek vzorca $Mg_2Sn$ pred mletjem in **c**) XRD-difraktogram sintetizirane $Mg_2Sn$-spojine: A – tip B (**Tabela 1**) in B-tip C (**Tabela 1**)

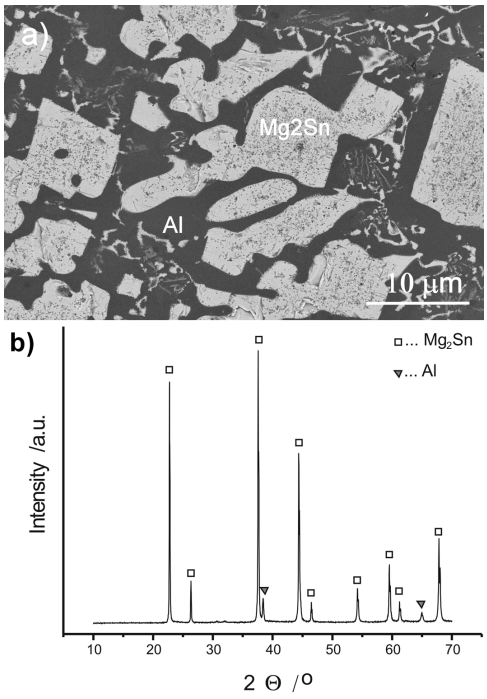


**Figure 2: a**) SEM micrograph and **b**) X-ray powder-diffraction pattern of the pressurelessly infiltrated $Mg_2Sn$-Al composite sample

**Slika 2: a**) SEM-posnetek in **b**) XRD-difraktogram $Mg_2Sn$-Al-kompozita, pripravljenega z infiltracijo

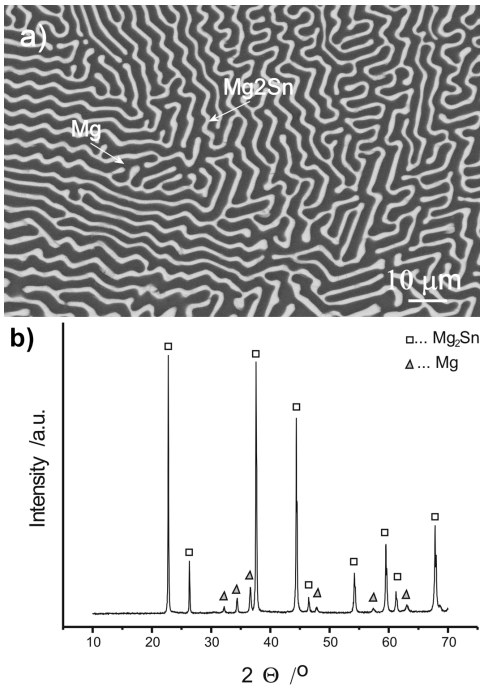


**Figure 3: a**) SEM micrograph and **b**) X-ray powder diffraction pattern of the $Mg_2Sn$-Mg composite sample infiltrated at 730 °C showing a lamellar structure consisting of $Mg_2Sn$ "Chinese-script" in a matrix of magnesium

**Slika 3: a**) SEM-posnetek in **b**) XRD-difraktogram $Mg_2Sn$-Mg-kompozita, infiltriranega pri 730 °C z značilno lamelarno mikrostrukturo ojačitve v Mg matriki

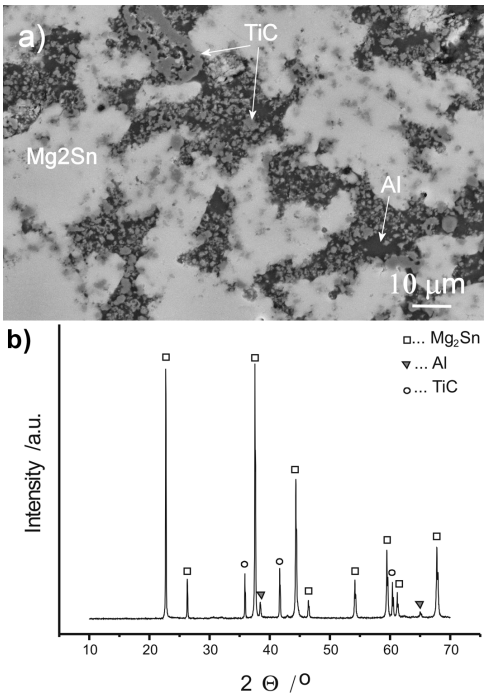


**Figure 4: a**) SEM micrograph and **b**) XRD spectrum of pressureless infiltrated Al-Sn-$Mg_2Sn_{(p)}$-$TiC_{(p)}$ composite sample with an initial composition of the preform skeleton of $\varphi$ = 69 % $Mg_2Sn$, $\varphi$ = 29 % TiC and $\varphi$ = 2 % Al (volume fraction $\varphi$/%)

**Slika4: a**) SEM posnetk in **b**) XRD difraktogram vzorca Al-Sn-$Mg_2Sn_{(p)}$-$TiC_{(p)}$ – kompozita, izdelanega z infiltriracijo predoblike na osnovi 69 % $Mg_2Sn$, 29 % TiC in 2 % Al (volumenski delež $\varphi$/%)

**Table 3:** Average room-temperature Vickers hardness and fracture toughness of Al-$Mg_2Sn$ composites prepared by pressureless infiltration
**Tabela 3:** Povprečne vrednosti trdote po Vickersu in prelomne žilavosti, izmerjene pri sobni temperaturi na vzorcih Al-$Mg_2Sn$-kompozitov, izdelanih s postopkom infiltracije

| Composite composition $\varphi$/% | Retained porosity $\varphi$/% | Density $\rho$/(g/cm$^3$) | Vickers hardness (GPa) | $K_{IC}$/ (MPa m$^{1/2}$) |
|---|---|---|---|---|
| 18 % Al-82 % $Mg_2Sn$ | 2.2 ± 0.2 | 3.5 ± 0.4 | 0.87 ± 0.09 | 3.4 ± 0.4 |
| 29 % Al-71 % $Mg_2Sn$ | 3.5 ± 0.4 | 3.4 ± 0.3 | 0.82 ± 0.08 | 4.7 ± 0.5 |
| 38 % Al-62 % $Mg_2Sn$ | 4.7 ± 0.5 | 3.3 ± 0.3 | 0.75 ± 0.08 | 5.3 ± 0.5 |
| 19 % Al-81 % $Mg_2Sn$ | 2.0 ± 0.2 | 3.6 ± 0.4 | 0.88 ± 0.09 | 3.9 ± 0.4 |
| 28 % Al-72 % $Mg_2Sn$ | 3.2 ± 0.3 | 3.5 ± 0.4 | 0.83 ± 0.08 | 4.8 ± 0.5 |
| 38 % Al-62 % $Mg_2Sn$ | 3.9 ± 0.4 | 3.4 ± 0.3 | 0.79 ± 0.08 | 5.6 ± 0.6 |

**Table 4:** Average room-temperature Vickers hardness and fracture toughness of Mg-Sn-$Mg_2Sn$ composites prepared by pressureless infiltration
**Tabela 4:** Povprečne vrednosti trdote po Vickersu in prelomne žilavosti, izmerjene pri sobni temperaturi na vzorcih Mg-Sn-$Mg_2Sn$-kompozita, izdelanega s postopkom infiltracije

| Composite composition $\varphi$/% | Retained porosity $\varphi$/% | Density $\rho$/(g/cm$^3$) | Vickers hardness (GPa) | $K_{IC}$/ (MPa m$^{1/2}$) |
|---|---|---|---|---|
| 20 % Mg-80 % $Mg_2Sn$ | 2.2 ± 0.2 | 3.3 ± 0.3 | 0.66 ± 0.07 | 4.7 ± 0.5 |
| 28 % Mg-71 % $Mg_2Sn$ | 3.5 ± 0.4 | 3.1 ± 0.3 | 0.72 ± 0.07 | 6.5 ± 0.7 |
| 41 % Mg-59 % $Mg_2Sn$ | 4.7 ± 0.5 | 2.9 ± 0.3 | 0.77 ± 0.08 | 7.3 ± 0.7 |
| 19 % Mg-81 % $Mg_2Sn$ | 2.0 ± 0.2 | 3.4 ± 0.4 | 0.61 ± 0.06 | 5.4 ± 0.5 |
| 31 % Mg-69 % $Mg_2Sn$ | 3.2 ± 0.3 | 3.1 ± 0.4 | 0.69 ± 0.07 | 6.6 ± 0.7 |
| 38 % Mg-62 % $Mg_2Sn$ | 3.9 ± 0.4 | 3.0 ± 0.3 | 0.71 ± 0.07 | 7.7 ± 0.8 |

was proved with the corresponding X-ray diffraction patterns, **Figures 2b** and **3b**.

As evident from **Tables 3** and **4**, the Vickers hardnesses of the Al-$Mg_2Sn$ and Mg-$Mg_2Sn$ MMCs are improved with increasing the amount of $Mg_2Sn$ particulate reinforcement. However, regarding the fracture toughness, quite the opposite behaviour was observed. The fracture toughness of Al-$Mg_2Sn$ and Mg-$Mg_2Sn$ MMCs decreases with an increasing amount of $Mg_2Sn$ particulates.

Comparing the mechanical properties of the Al-$Mg_2Sn$ and Mg-$Mg_2Sn$ MMCs, it is found that the Vickers hardness is evidently better in the samples infiltrated with aluminium. However, the fracture toughness is an exception, becoming greater (almost doubled) in the samples infiltrated with magnesium.

The extraordinary fracture toughness of Mg-$Mg_2Sn$ MMCs is caused by their characteristic lamellar structure consisting of $Mg_2Sn$ "Chinese script" in a matrix of a magnesium solid solution.

### 3.2.2 Al-$Mg_2Sn_{(p)}$-$TiC_{(p)}$ and Al-$Mg_2Sn_{(p)}$-$TiB_{2(p)}$

Preforms made from mixtures of laboratory-synthesized $Mg_2Sn$ powder and commercially available TiC and $TiB_2$ powders (compositions #1, #2, #3 and #4), were also successfully pressurelessly infiltrated with molten aluminium, resulting in samples with almost theoretical density and interesting combinations of mechanical properties.

The microstructure of infiltrated samples consisted of a co-continuous network of $Mg_2Sn$ phase interpenetrated by an aluminium matrix with finely dispersed TiC or $TiB_2$ particles, **Figures 4** and **5**. The absence of secondary phases, **Figure 5b**, indicates that in this case the spontaneous infiltration also proceeded as a non-reactive process.

The reinforcement of an Al matrix with TiC or $TiB_2$ particles resulted in a marked improvement in the Vickers hardness. As evident from **Table 5**, the Vickers hardness of Al-$Mg_2Sn$-TiC and Al-$Mg_2Sn$-$TiB_2$ composites was approximately 50 % higher than in non-reinforced Al-$Mg_2Sn$ samples, **Table 3**.

An examination of the fracture toughness, **Table 5**, revealed that the toughness of the MMCs was inversely proportional to the total amount of reinforcing phase. Moreover, it became lower when replacing some of the $Mg_2Sn$ particles with more brittle TiC or $TiB_2$ particulates. This is well documented in **Tables 3 and 5** for samples with approximately the same total amount of particulate reinforcement.

### 3.2.3 Mg -$Mg_2Sn_{(p)}$-$TiC_{(p)}$ and Mg-$Mg_2Sn_{(p)}$-$TiB_{2(p)}$

The experiments showed that the infiltration of $Mg_2Sn$-TiC and $Mg_2Sn$-$TiB_2$ preforms with molten magnesium proceeded spontaneously, without a chemical reaction between the preform skeleton and the molten magnesium. By adjusting the porosity of the preforms within the range the volume fractions of 30 % to 35 %, composites with different compositions listed in Table 6 were routinely fabricated. At 900 °C, the infiltration was complete within 1h, resulting in composite samples with less than $\varphi$ = 5 % of retained porosity.

The resulting composite samples have a typical eutectic microstructure showing a lamellar structure consisting of $Mg_2Sn$ "Chinese script" in a matrix of

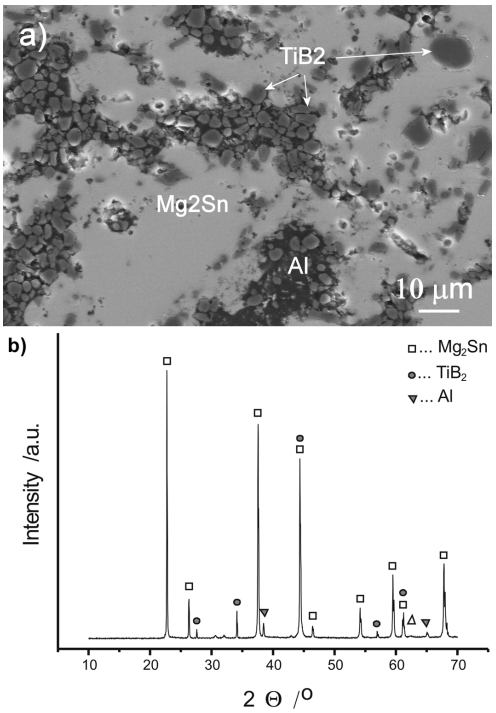


**Figure5: a**) SEM micrograph and **b**) XRD spectrum of pressurelessly infiltrated Al-Sn-$Mg_2Sn_{(p)}$-$TiB_{2(p)}$ composite sample with an initial composition of the preform skeleton $\varphi$ = 75 % $Mg_2Sn$, $\varphi$ = 25 % $TiB_2$.

**Slika 5: a**) SEM-posnetek in **b**) XRD-defraktogram vzorca Al-Sn-$Mg_2Sn_{(p)}$-$TiB_{2(p)}$ –kompozita, izdelanega iz predoblike na osnovi $\varphi$ = 75 % $Mg_2Sn$ in $\varphi$ = 25 % $TiB_2$

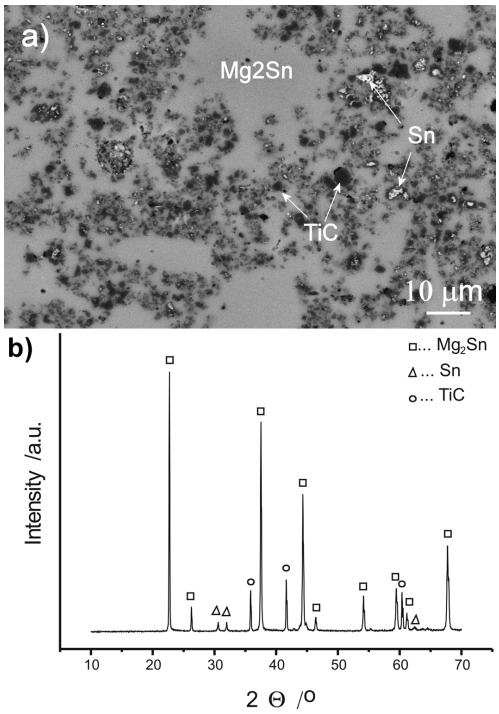


**Figure7: a**) SEM micrograph and **b**) XRD spectrum of pressurelessly sintered $Mg_2Sn$-Sn-$TiC_{(p)}$ composite sample with the initial composition $\varphi$ = 67 % $Mg_2Sn$, $\varphi$ = 3 % Sn and $\varphi$ = 30 % TiC

**Slika7: a**) SEM-posnetek in **b**) XRD-difraktogram $Mg_2Sn$-Sn-$TiC_{(p)}$ -kompozita, izdelanega s sintranjem vzorcev, sestavljenih iz $\varphi$ = 67 % $Mg_2Sn$, $\varphi$ = 3 % Sn in $\varphi$ = 30 % TiC

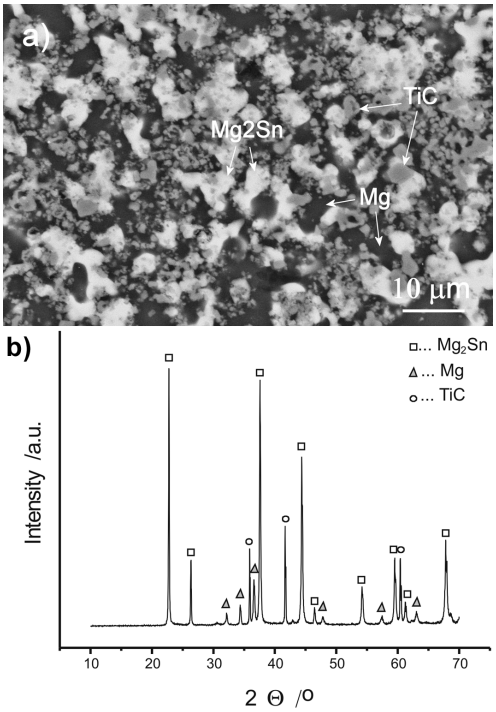


**Figure6: a**) SEM micrograph and **b**) XRD spectrum of Mg-Sn-$Mg_2Sn_{(p)}$-$TiC_{(p)}$ with an initial composition of the preform skeleton $\varphi$ = 70 % $Mg_2Sn$ and $\varphi$ = 30 % TiC

**Slika6: a**) SEM-posnetek in **b**) XRD-defraktogram vzorca Mg-Sn-$Mg_2Sn_{(p)}$-$TiC_{(p)}$-kompozita, izdelanega z infiltracijo predoblike na osnovi $\varphi$ = 70 % $Mg_2Sn$ in $\varphi$ = 30 % TiC

magnesium solid solution, additionally reinforced with fine TiC or $TiB_2$ particles, **Figures 7a and 8a**.

From the X-ray diffraction patterns of the composite samples, it is evident (**Figure 7b and 8b**) that besides $Mg_2Sn$ reinforcement and irrespective of the matrix composition, no secondary phases were detected, which indicates that the pressureless infiltration of $Mg_2Sn$ preforms with molten Mg-Sn-based alloys was not chemically assisted. A detailed SEM examination of interface regions of all the samples also confirmed the absence of chemical reactions between the composite constituents listed above.

Regarding the mechanical properties of the Mg-$Mg_2Sn$-TiC and Mg-$Mg_2Sn$-$TiB_2$ composite samples, which are summarized in **Table 6**, an increase in the particulate content ($Mg_2Sn$ and TiC or $TiB_2$) was observed to improve the Vickers hardness, while at the same time reducing the fracture toughness. In addition, the Vickers hardness of the Mg-$Mg_2Sn$-TiC and Mg-$Mg_2Sn$-$TiB_2$ composite samples was found to be better than in the non-reinforced counterparts, while the fracture toughness was about 25 % lower.

Compared to the Al-$Mg_2Sn$-TiC or Al-$Mg_2Sn$-$TiB_2$ counterparts, the reduction of Vickers hardness is only slight. On the other hand, the fracture toughness of the Mg-$Mg_2Sn$-TiC or Mg-$Mg_2Sn$-$TiB_2$ composites is almost twice as high as in their Al-$Mg_2Sn$-TiC or Al-$Mg_2Sn$-$TiB_2$ counterparts, which is due to the lamellar structure

consisting of the $Mg_2Sn$ "Chinese script" in a matrix of magnesium.

### *3.3 Composites made by pressureless sintering*

3.3.1 $Mg_2Sn$-Sn-$TiC_{(p)}$ and $Mg_2Sn$-Sn-$TiB_{2(p)}$ composites made by pressureless sintering

Pressureless sintering of green samples made either from as-milled $Mg_2Sn$ powders of grade A and B, **Table 1**, or mixed with various amounts of TiC or $TiB_2$ particles, resulted in dense composite specimens with a retained porosity of less than the volume fraction $\varphi$ = 5 %. In contrast, pressureless sintering of green samples made either from as-milled $Mg_2Sn$ powder of grade C, **Table 1**, or mixed with various amounts of TiC or $TiB_2$ particles, was found to be incomplete, with more than $\varphi$ = 10 % of retained porosity.

**Table 5:** Average room-temperature Vickers hardness and fracture toughness of Al-Sn-$Mg_2Sn_{(p)}$(grade C)-$TiC_{(p)}$ and Al-Sn-$Mg_2Sn_{(p)}$(grade A)-$TiB_{2(p)}$ composites prepared by pressureless infiltration

**Tabela 5:** Povprečne vrednosti trdote po Vickersu in prelomne žilavosti, izmerjene pri sobni temperaturi na vzorcih Al-Sn-$Mg_2Sn_{(p)}$(tip C)-$TiC_{(p)}$ and Al-Sn-$Mg_2Sn_{(p)}$(tip A)-$TiB_{2(p)}$- kompozitov, izdelanih s postopkom infiltracije

| Composite composition $\varphi$/% | Retained porosity $\varphi$/% | Density $\rho$/(g/cm$^3$) | Vickers hardness (GPa) | $K_{IC}$/ (MPa m$^{1/2}$) |
|---|---|---|---|---|
| 28%Al-48%$Mg_2Sn$-23 %TiC | 1.9 ± 0.2 | 3.6 ± 0.2 | 1.29 ± 0.13 | 2.8 ± 0.3 |
| 36%Al-46%$Mg_2Sn$-18 %TiC | 2.2 ± 0.2 | 3.5 ± 0.2 | 1.14 ± 0.11 | 3.1 ± 0.3 |
| 28%Al-49%$Mg_2Sn$-23%$TiB_2$ | 3.5 ± 0.4 | 3.6 ± 0.2 | 1.38 ± 0.14 | 2.7 ± 0.3 |
| 35%Al-46%$Mg_2Sn$-19%$TiB_2$ | 4.7 ± 0.5 | 3.5 ± 0.2 | 1.26 ± 0.13 | 3.0 ± 0.3 |

**Table 6:** Average room-temperature Vickers hardness and fracture toughness of Mg- $Mg_2Sn_{(p)}$-$TiC_{(p)}$ and Mg-$Mg_2Sn_{(p)}$-$TiB_{2(p)}$ composites prepared by pressureless infiltration

**Tabela 6:** Povprečne vrednosti trdote po Vickersu in prelomne žilavosti, izmerjene pri sobni temperaturi na vzorcih Al-Sn-$Mg_2Sn_{(p)}$(tip C)-$TiC_{(p)}$ in Al-Sn-$Mg_2Sn_{(p)}$(tip A)-$TiB_{2(p)}$-kompozitov, izdelanih s postopkom infiltracije

| Composite composition $\varphi$/% | Retained porosity $\varphi$/% | Density $\rho$/(g/cm$^3$) | Vickers hardness (GPa) | $K_{IC}$/ (MPa m$^{1/2}$) |
|---|---|---|---|---|
| 29% Mg-47%$Mg_2Sn$-1%Al-23 %TiC | 1.9±0.2 | 3.4±0.2 | 1.16±0.12 | 4.9±0.5 |
| 36%Mg-38%$Mg_2Sn$-7%Al–19%TiC | 2.2±0.2 | 3.5±0.2 | 1.0±0.19 | 5.8±0.6 |
| 29%Mg-48%$Mg_2Sn$–1%Al-22%$TiB_2$ | 3.5±0.4 | 3.3±0.2 | 1.24±0.12 | 4.4±0.4 |
| 35%Mg-39%$Mg_2Sn$–7%Al-19%$TiB_2$ | 4.7±0.5 | 3.3±0.2 | 1.13±0.11 | 5.3±0.5 |

**Table 7:** Average room-temperature Vickers hardness and fracture toughness of sintered $Mg_2Sn$ -Sn-TiC samples.

**Tabela 7:** Povprečne vrednosti trdote po Vickersu in prelomne žilavosti, izmerjene pri sobni temperaturi na vzorcih, sintranih $Mg_2Sn$ -Sn-TiC-kompozitov

| Composite initial composition $\varphi$/% | Retained porosity $\varphi$/% | Density $\rho$/(g/cm$^3$) | Vickers hardness (GPa) | $K_{IC}$/ (MPa m$^{1/2}$) |
|---|---|---|---|---|
| 97% $Mg_2Sn$ (grade A)-3% Sn | 4.8 ± 0.5 | 3.7 ± 0.2 | 1.0 ± 0.1 | 1.7 ± 0.2 |
| 87% $Mg_2Sn$ (grade A)-3% Sn-10% TiC | 3.5 ± 0.4 | 3.8 ± 0.2 | 1.4 ± 0.1 | 1.4 ± 0.1 |
| 68% $Mg_2Sn$ (grade A)-2% Sn-30% TiC | 4.3 ± 0.4 | 4.1 ± 0.4 | 1.5 ± 0.2 | 1.0 ± 0.1 |
| 49% $Mg_2Sn$ (grade A)-1% Sn-50% TiC | 4.9 ± 0.5 | 4.3 ± 0.5 | 1.8 ± 0.2 | 0.7 ± 0.1 |
| 95% $Mg_2Sn$ (grade B)-5% Sn | 3.1 ± 0.3 | 3.8 ± 0.5 | 0.9 ± 0.1 | 1.8 ± 0.2 |
| 86% $Mg_2Sn$ (grade B)-4% Sn-10% TiC | 2.7 ± 0.3 | 3.8 ± 0.3 | 1.0 ± 0.1 | 1.4 ± 0.1 |
| 66% $Mg_2Sn$ (grade B)-3% Sn-30% TiC | 3.9 ± 0.4 | 3.9 ± 0.4 | 1.3 ± 0.1 | 1.1 ± 0.1 |
| 48% $Mg_2Sn$ (grade B)-2% Sn-50% TiC | 4.1 ± 0.5 | 4.1 ± 0.5 | 1.7 ± 0.2 | 0.6 ± 0.1 |

**Table 8:** Average room-temperature Vickers hardness and fracture toughness of sintered $Mg_2Sn$-Sn-$TiB_2$ composite samples

**Tabela 8:** Povprečne vrednosti trdote po Vickersu in prelomne žilavosti, izmerjene pri sobni temperatri na vzorcih, sintranih $Mg_2Sn$-Sn-$TiB_2$-kompozitov

| Composite initial composition) $\varphi$/% | Retained porosity $\varphi$/% | Density $\rho$/(g/cm$^3$) | Vickers hardness (GPa) | $K_{IC}$/ (MPa m$^{1/2}$) |
|---|---|---|---|---|
| 97 % $Mg_2Sn$ (grade A)-3 % Sn | 4.8 ± 0.5 | 3.7 ± 0.2 | 1.0 ± 0.1 | 1.7 ± 0.2 |
| 87 % $Mg_2Sn$ (grade A)-3 % Sn-10 % $TiB_2$ | 3.5 ± 0.4 | 3.8 ± 0.2 | 1.5 ± 0.1 | 1.3 ± 0.1 |
| 68 % $Mg_2Sn$ (grade A)-2 % Sn-30 % $TiB_2$ | 4.3 ± 0.4 | 4.1 ± 0.4 | 1.7 ± 0.2 | 0.8 ± 0.1 |
| 49 % $Mg_2Sn$ (grade A)-1 % Sn-50 % $TiB_2$ | 4.9 ± 0.5 | 4.3 ± 0.5 | 1.9 ± 0.2 | 0.6 ± 0.1 |
| 95 % $Mg_2Sn$ (grade B)-5 % Sn | 3.1 ± 0.3 | 3.8 ± 0.5 | 0.9 ± 0.1 | 1.8 ± 0.2 |
| 86 % $Mg_2Sn$ (grade B)-4 % Sn-10 % $TiB_2$ | 2.7 ± 0.3 | 3.8 ± 0.3 | 1.0 ± 0.1 | 1.4 ± 0.1 |
| 66 % $Mg_2Sn$ (grade B)-3 % Sn-30 % $TiB_2$ | 3.9 ± 0.4 | 3.9 ± 0.4 | 1.6 ± 0.1 | 1.0 ± 0.1 |
| 48 % $Mg_2Sn$ (grade B)-2 % Sn-50 % $TiB_2$ | 4.1 ± 0.5 | 4.1 ± 0.5 | 2.0 ± 0.2 | 0.5 ± 0.1 |

The microstructure of the sintered samples reinforced with ceramic particulates is presented in **Figures 7 and 8**. The composites obtained consist of a continuous $Mg_2Sn$ matrix and TiC or $TiB_2$ ceramic particulate reinforcement dispersed around the sintered $Mg_2Sn$ grains and small Sn inclusions. In contrast, the microstructure of the dense, non-reinforced samples was uniform, with fully sintered $Mg_2Sn$ grains and Sn inclusions.

The SEM-EDS evaluation of the samples and the XRD measurements imply that the $Mg_2Sn$-TiC and $Mg_2Sn$-$TiB_2$ systems are non-reactive, without secondary phases formed during the sintering, and that the sintering proceeded via a non-reactive mechanism, assisted by the liquid Sn phase. The mechanical properties of the sintered samples are listed in **Tables 7 and 8**.

The Vickers hardness of the pressurelessly sintered samples was found to be enhanced with an increasing amount of particulate reinforcement in the $Mg_2Sn$ matrix, **Table 2**. In addition, the Vickers hardness measurements also confirmed that the sintering of samples with the same initial volume fraction of TiC or $TiB_2$ reinforcement resulted in composites with similar hardnesses. This is most probably caused by the similar microstructures of the $Mg_2Sn$-TiC and $Mg_2Sn$-$TiB_2$-composite samples, the same sintering mechanism and almost the same hardness of the TiC and $TiB_2$ reinforcing particulates.

## 4 CONCLUSIONS

The reactive synthesis of $Mg_2Sn$ from the elements resulted in a high-yield, single-phase product with less than the mass fraction 0.2 % of impurities (Mg or Sn), depending on the composition of the initial reactive mixture.

1. Additional crushing and subsequent milling of the reaction product (i.e., in a planetary mill) was found to be an easy operation, enabling the cost-effective preparation of $Mg_2Sn$ powders with an average particle size of less than 5 μm, suitable for the production of $Mg_2Sn$-based advanced composites.
2. Depending on the selected synthesis technique of (i) **pressureless infiltration** of porous $Mg_2Sn$, $Mg_2Sn$-TiC and $Mg_2Sn$-$TiB_2$ preforms with molten aluminium and magnesium, or (ii) **pressureless sintering** of green $Mg_2Sn$-TiC and $Mg_2Sn$-$TiB_2$ compacts, $Mg_2Sn$-based composites of different nature, microstructure and combination of properties were successfully prepared, demonstrating the significant potential of the $Mg_2Sn$ phase as a composite matrix and of the particulate reinforcement.
3. The investigation of the effect of different microstructures developed in $Mg_2Sn$-based composites on their mechanical properties (hardness and toughness) revealed that $Mg_2Sn$, as the stoichiometric compound, could be useful for tailoring an optimum combination of these properties.
4. The pressureless infiltration of porous $Mg_2Sn$, $Mg_2Sn$-TiC and $Mg_2Sn$-$TiB_2$ preforms with molten magnesium and aluminium resulted in dense (≥95 % T.D.) metal matrix composites with a metallic matrix discontinuously reinforced with $Mg_2Sn$ and TiC or $TiB_2$ particulates. The infiltration proceeded spontaneously, without detectable chemical reactions between the preform skeleton and the molten infiltrants.
5. The composite samples infiltrated with molten magnesium possessed the characteristic lamellar "Chinese script" eutectic microstructure, while in samples infiltrated with molten aluminium the appearance of fine $Mg_2Sn$-Sn precipitates in an Al matrix, mostly in the vicinity of the initially introduced $Mg_2Sn$ particles, was observed.
6. In preforms with the addition of TiC or $TiB_2$ ceramic reinforcement, the microstructure development during the infiltration occurred in the same way as in their non-reinforced counterparts. Because of the low temperature of the preform infiltration (750 °C), the particulate reinforcements remained chemically inert in contact with molten magnesium or molten aluminium, resulting in a final microstructure of infiltrated composite samples the same as in the non-reinforced counterparts. The only difference was observed inside the Al or Mg phases, which were completely reinforced with TiC or $TiB_2$ particles.
7. The microstructure of the composite samples obtained by pressureless infiltration could be tailored to consist of a continuous aluminium or magnesium matrix, discontinuously reinforced with $Mg_2Sn$ of different morphologies (particulates in samples infiltrated with aluminium and the characteristic "Chinese script" eutectic phase in samples infiltrated with magnesium) and, when added, TiC or $TiB_2$ reinforcements. Such a microstructure design was projected in order to achieve an optimum combination of enhanced fracture toughness (particularly improved by the "Chinese script" phase appearing in samples infiltrated with magnesium), with tensile properties and a hardness superior to that of conventional Mg-Sn alloys.
8. The Vickers hardness was found to be better in samples infiltrated with aluminium than in counterparts infiltrated with magnesium. On the other hand, quite the opposite behaviour was found with regard to the fracture toughness. Due to their characteristic lamellar structure consisting of $Mg_2Sn$ as the "Chinese script" in the matrix, composite samples infiltrated with magnesium possessed an enhanced fracture toughness almost twice that of the counterparts infiltrated with aluminium, in which the $Mg_2Sn$ phase appeared as particulates.
9. Within each single group of infiltrated samples (i.e., samples with the same ***qualitative*** composition), the Vickers hardness was enhanced, while the fracture

toughness decreased with an increasing total amount of particulate reinforcement.

10. Pressureless sintering of green samples from $Mg_2Sn$ powders with 3–5% of free Sn, or from mixtures of these powders with various amounts of TiC or $TiB_2$ particles, resulted in dense composite specimens with a porosity of less than the volume fraction $\varphi$ = 5 %. In contrast, pressureless sintering of green samples from $Mg_2Sn$ powder without free Sn or a mixture of the same powder with various amounts of TiC or $TiB_2$ particles was found to be incomplete, with more than $\varphi$ = 10 % of porosity.
11. The composites obtained consisted of a continuous $Mg_2Sn$ matrix and TiC or $TiB_2$ ceramic particulate reinforcement dispersed around the sintered $Mg_2Sn$ grains and small Sn inclusions. In contrast, the microstructures of the dense, non-reinforced samples were uniform, with fully sintered $Mg_2Sn$ grains and Sn inclusions.
12. During sintering, the formation of secondary phases was not observed. Densification of composite samples proceeded with non-reactive sintering, assisted by molten tin
13. The Vickers hardness of the sintered samples (intermetallic matrix composites with a $Mg_2Sn$ matrix discontinuously reinforced with TiC or $TiB_2$ ceramic reinforcement) was significantly improved in comparison with the metal matrix composites obtained by infiltration. The exception was the fracture toughness, which in the sintered samples was reduced to approximately one-third or even one-quarter of the values measured in the metal matrix composites obtained by infiltration.
14. With densities higher than the density of aluminium and magnesium alloys, $Mg_2Sn$-based composites have a limited potential for the weight reduction of structural parts. However, some of the $Mg_2Sn$ composites (especially Mg-$Mg_2Sn$ metal matrix composites) could offer a unique combination of properties, including the ability of the composite microstructure (lamellar, consisting of the $Mg_2Sn$ "Scinese script" in a magnesium solid solution) to develop a toughening mechanism in combination with improved tensile properties and hardness.

## Acknowledgement

This work was supported by funding from the Public Agency for Research and Development of the Republic of Slovenia, as well as the Impol Aluminium Company and Bistral, d. o. o. from Slovenska Bistrica, Slovenia, under contract No. 1000-07-219308.

## 5 REFERENCES

[1] N. Hort, Y. Huang, T. A. Leil, P. Maier, K. U. Kainer, Adv. Eng. Mat., 8 (**2006**) 5, 359
[2] N. Hort, Y. Huang, K. U. Kainer, F. Moll, K. U. Kainer, Adv. Eng. Mat., 8 (**2006**) 4, 235
[34] J. Gröbner, A. Janz, A. Kozlov, Dj. Mirković, R. S. Fetzer, JOM, 60 (**2009**) 12, 32
[4] M. Zhang, W. Z. Zhang, G. Z. Zhu, Scrpita Materialia 59 (**2008**), 866
[5] Z. Min, Z. W. Zheng, Z. G. Zhen, Y. Kun, Trans. Nonferrous Met. China 17 (**2007**), 1428
[6] Z. X. Ping, C. Y. Gui, X. Y. HUa, Trans Nonferrous Met. Soc. China 18 (**2008**), s299
[7] B. H. Kim, J. J. Jeon, K. C. Park, B. G. Park, Y. H. Park, I. M. park, Archives of Materials Science and Engineering, 30 (**2008**) 2, 93
[8] S. Koch, H. Antrekowitsch, BHM, 153 (**2008**) 7, 278
[9] O. Madelung, U. Rössler, M. Schulz, Non-tetrahedrally bonded elements and binary compounds I, Springer-Verlag, 1998, 1–3
[10] C. Zhang, P. Han, X. Yan, C. Wang, L. Xia, B. Xu, J. Phys. D: Appl. Phys., 42 (**2009**), 1. (doi: 125403)
[11] W. Y. Feng, D. W. Bo, Z. T. Young, Trans. Nonferrous Met. Soc. China, 19 (**2009**), 1196
[12] K. Kondoh, H. Oginuma, T. Aizawa, Materials Transactions, 42 (**2001**), 1293
[13] K. Niihara, R. Morena, D. P. Hasselman, J. Mater. Sci. Lett. 1 (**1982**), 13
[14] A. A. Nayeb-Hasemi, J. B. Clark, J. Bull. Alloy Phase Diagrams 63 (**1984**), 467

UDK 617.3:617.57:669.295:621.9
Original scientific article/Izvirni znanstveni članek

ISSN 1580-2949
MTAEC9, 44(5)261(2010)

# OSSEOINTEGRATION AND REJECTION OF A TITANIUM SCREW

## OSEOINTEGRACIJA IN ZAVRNITEV TITANOVEGA VIJAKA

**Grega Klančnik[1], Miro Zdovc[2], Uroš Kovšca[2], Borut Praček[3], Janez Kovač[3], Janez Rozman[4]**

[1]University of Ljubljana, Faculty of Natural Science and Technology, Aškerčeva cesta 12, SI-1000, Ljubljana, Slovenia
[2]University of Nova Gorica, Material Characterization Graduate Study Programme, Vipavska 13, Rožna Dolina, 5000 Nova Gorica, Slovenia
[3]Jožef Stefan Institute, Jamova cesta 39, SI-1000 Ljubljana, Slovenia
[4]ITIS, d. o. o., Center for Implantable Technology and Sensors; Lepi pot 11, SI-1000, Ljubljana, Slovenia
grega.klancnik@ntf.uni-lj.si

*Prejem rokopisa – received: 2009-12-01; sprejem za objavo – accepted for publication: 2010-04-22*

In the present study, a rejected titanium implant, an orthopaedic screw removed from a patient, was investigated. The screw was implanted into the metacarpal bone for one year and was removed due to irritation. The first signs of irritation were indicated three months after the implantation. After the removal, the signs of irritation disappeared. AES and EDS analyses showed that the surface of the screw was significantly different from the bulk material. The high contamination of the surface layer was found to be caused by the screw-manufacturing process, which is considered to be the main reason for the rejection of the implant.

Keywords: orthopaedics, titanium implant, titanium screw, contamination, AES, EDS

V predstavljeni študiji smo preiskali zavrnjen titanov vijak, ki je bil odstranjen pacientu. Vijak je bil privit v dlančnico in po enem letu odstranjen zaradi razdraženosti okoliškega tkiva, ki se je pojavila v prvih treh mesecih po implantaciji. Po odstranitvi razdraženosti ni bilo več. AES analiza in EDS analiza sta pokazali, da se površina močno razlikuje od notranjosti vijaka. Odkrita je bila kontaminacija površine, ki je tehnološke narave in se zato predvideva, da je bil to glavni razlog zavrnitve implantata.

Ključne besede: ortopedija, titanov implantat, titanov vijak, kontaminacija, AES, EDS

## 1 INTRODUCTION

Titanium alloys are commonly used as biomaterials and, like stainless steels, are used in orthopaedics. Titanium is a superior orthopaedic material because it has a high compatibility in contact with bone tissue and is more corrosion resistant than stainless steels. In addition, because of its low tension modulus (55–100 GPa), titanium implants tend to be handling-friendly during the placement. However, one of the most common problems with titanium alloys is related to the contamination of the implant oxide surface with metal ions, which can contribute to the rejection of the implant (**Figure 1**).


**Figure 1:** Titanium screw – rejected implant
**Slika 1:** Titanov vijak – zavrnjeni implantat

### *1.1 Osseointegration*

The term "osseointegration" describes the process of having a stable, loaded implant in direct contact with the bone. Biomaterials with the so-called osseointegrability, e.g., commercially pure (CP) titanium with a low iron content, CP tantalum and calcium hydroxyapatite (HA),[1] are widely used. Stainless steels are also widely used for orthopaedic applications. Classical 316L can, for example, provide a natural surface oxide coating like titanium and titanium alloys. If we compare titanium (CP) with 316L, exposed to physiological fluids, no reactions are usually present. However, stainless-steel implants, after a longer implantation time, release metal ions, $Cr^{6+}$, $Ni^{2+}$, $Mo^{6+}$ and $Fe^{3+}$, into the surrounding tissue. A test of cytotoxicity performed on rate bone-marrow stromal cells showed the following order of toxicity: Cr > Mo = Fe > Co >Ni. All these ions can cause local inflammation by ion accumulation inside the body.[2] Because the surface of the implant is so important when it is in contact with the bone, tissue and particular cells, biochemical modification is used for a better and faster integration.[1]

### *1.2 Rejection of the implant*

Two of the most common reasons for rejection of the implant are the mechanical damage that occurs during the procedures for implantation and the friction between the two pieces (the plates and the screw).[2] Titanium

alloys have a high coefficient of friction, which can cause irritation when an implant rubs with the soft tissue or when new particles are formed during the placement. With the loss of fixation at the interface of the bone and the titanium implant, titanium splinters may be formed and influence the integration strength.[2] Because it is newly formed, the surface with titanium dioxide is very reactive with respect to contamination and this is considered to be an important variable for further storage until use. Dental titanium implants, however, failed to osseointegrate when the surface was contaminated with iron, zinc, tin and lead.[1,4]

### *1.3 Formation of calcium phosphate*

Calcium phosphate is the name given to a family of minerals consisting mainly of $Ca^{2+}$ with $PO_4^{3-}$ or $P_2O_7^{4-}$ and hydroxyapatite ($Ca_{10}(PO_4)_6(OH)_2$), and bone mineral is one of them. The biology of the interaction with titanium and titanium-based alloys has been studied extensively. The bone formation around the implant derives from the adjacent bone bed, which grows towards the implant. The implant surface is a highly attractive substrate for the bone cells (osteoblasts). Bone tissue is a mineralized connective tissue; it is composed of cells, called osteoblasts, that deposit a matrix of type-I collagen and also release calcium, magnesium and phosphate ions and combine with the collagenous matrix into the crystalline mineral hydroxyapatite. After a certain time of exposure of the implant to the internal environment of the body, the result is a relatively thick surface oxide layer (the natural oxidation of titanium surfaces inside the bone or body fluid) augmented with the ions, mainly calcium and phosphorous.[2,5]

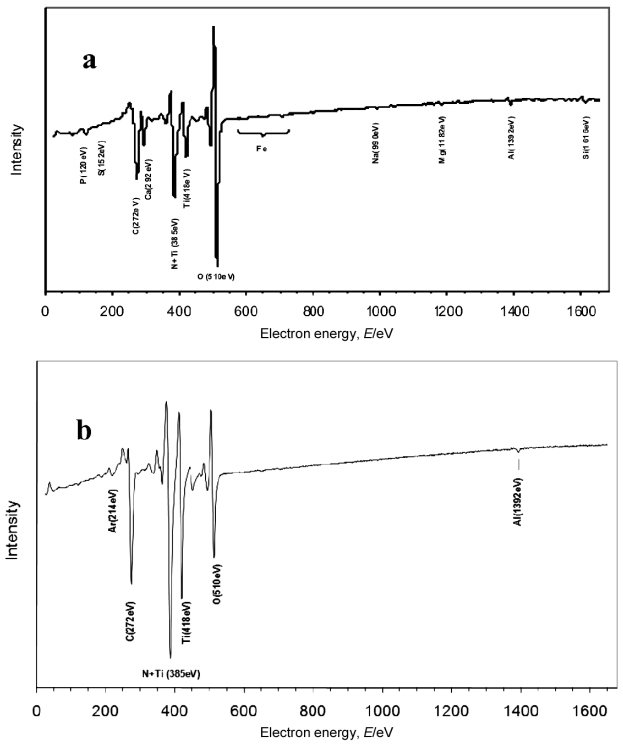


**Figure 2:** AES spectrum of the screw surface: (a) surface before and (b) after ion sputtering

**Slika 2:** AES-spekter površine vijaka: (a) površina pred ionskim jedkanjem in (b) po njem

## 2 EXPERIMENTAL

The investigation was aimed at the detection of possible reasons for the rejection of a titanium screw inserted into the metacarpal bone. After removal, the screw was investigated with Auger Emission Spectroscopy (AES) PHI SAM, model 545A. The first energy spectrum was recorded from the head surface of the screw and the last spectrum after ion etching with $Ar^+$. On a metallographically prepared sample, one AES spectrum was also recorded to detect the chemical composition under the surface of the screw. The sputtering rate was determined with a Ni/Cr reference and was found to be 2 nm/min. For the chemical analyses of possible phases, an investigation of the microstructure was made with a JEOL 5610 electron microscope and an EDS spectrometer. The investigated surface was also examined with an Olympus CX61 optical microscope and a DP70 video camera.

## 3 RESULTS

The AES analysis of the retrieved screw surface after one year of implantation is shown in **Figure 2a, b**.

Calcium and phosphorus were both found to be the electrolyte constituents of the body fluid, and both are related to the formation of calcium phosphate. The presence of oxygen, nitrogen, titanium, silicon, aluminium and iron was also established (**Figure 2 a**). However, the last recorded AES spectrum, at the end of the ion etching inside the oxide layer, did not reveal the presence of iron (**Figure 2 b**). A trace of argon was found, because of the ion etching with $Ar^+$. The presence of carbon on the screw's surface is related to the atmospheric contamination. The AES depth profile in **Figure 3 a** shows a high concentration of carbon, which is a result of backscattering.

The presence of an oxidized surface suggests a strong affinity for oxygen (Figure 3a). The AES depth profile of the titanium screw's surface revealed a surface contaminated with iron deep inside the oxide layer (**Figure 3 b**). However, the AES spectrum of the bulk material, in **Figure 4**, does not show the presence of any iron.

Oxygen is always present in trace amounts. **Figure 4** shows that inside the screw, in the titanium, an alpha structure is also present. The bulk of the screw was investigated with SEM and EDS (**Figure 5**).

EDS analysis (**Figure 5 a**) and AES spectrum of the bulk material (**Figure 4**) revealed no aluminium, silicon or iron in the bulk material. The chemical composition of

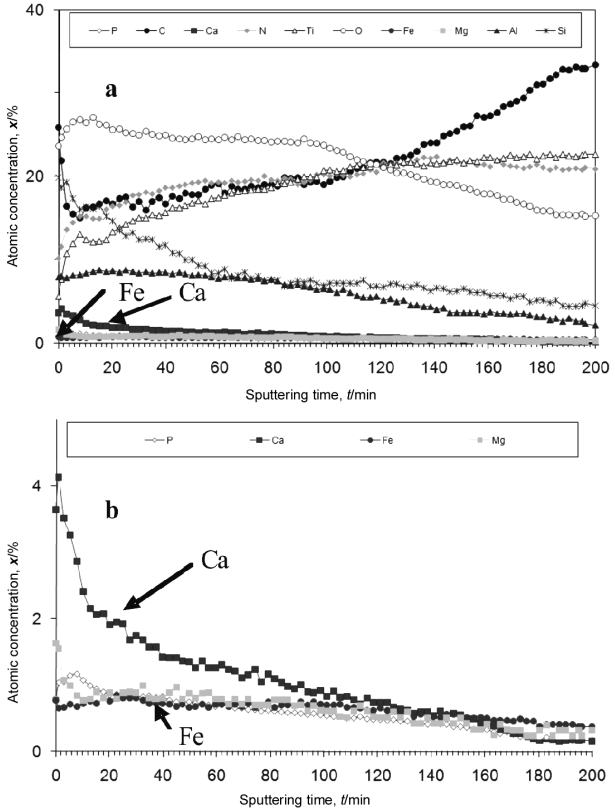


**Figure 3:** AES analysis: (a) depth profile of titanium screw (b) contamination with iron

**Slika 3:** AES-analiza: (a) profilna analiza titanovega vijaka (b) kontaminacija z železom

the titanium screw's surface strongly differs from the bulk composition.

The EDS analysis of the precipitates also revealed the presence of carbon (**Figure 5 b**). The detection of the x-ray signal with the EDS system is difficult for carbon on account of its low atomic number. The results from the EDS analyses in **Figures 5 and 6** hint at the presence of titanium carbides. The micrograph in **Figure 5** revealed a 14-µm-thick layer of titanium with a reduced presence, or absence, of precipitates. As already discussed, the absence of other elements was established.

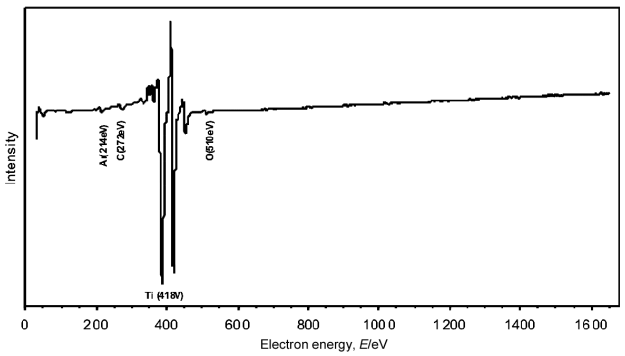


**Figure 4:** AES spectrum of the bulk material

**Slika 4:** AES-spekter osnovnega materiala

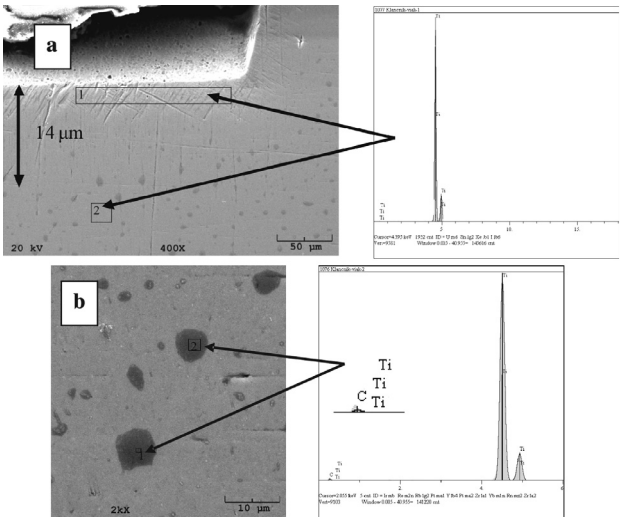


**Figure 5:** SEM micrograph and EDS analysis: (a) bulk material and (b) precipitates

**Slika 5:** SEM-posnetek in EDS analiza: (a) osnovnega materiala in (b) precipitatov

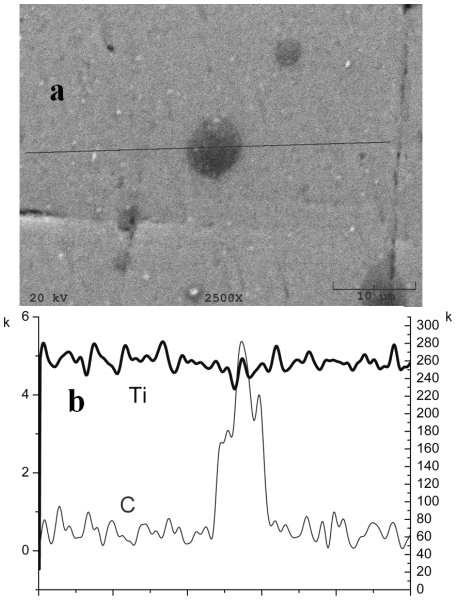


**Figure 6:** EDS line analysis: (a) SEM micrograph and (b) EDS line analysis

**Slika 6:** EDS-linijska analiza: (a) SEM-posnetek in (b) EDS-linijska analiza

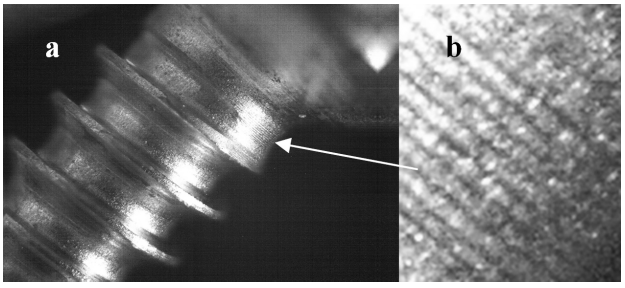


**Figure 7:** Macrograph of titanium screw: (a) surface and (b) turning grooves of the screw

**Slika 7:** Slika titanovega vijaka: (a) površina in (b) sledi obdelovalnega orodja

The evidence of the machining of the screw is represented in **Figure 7**. The shape of the grooves indicates that the screw was not polished before the implantation.

## 4 DISCUSSION

Due to the golden-like colour of the surface of the screw and the nitrogen found with the AES analysis, it can be concluded that the surface of the screw was nitrided (**Figure 1, 3 a**). This titanium nitride provides a relatively stable surface (better wear resistance and hardness). The presence of aluminium and silicon could be assigned to the technology of the production (blasting the surface with alumina and silica particles, contamination with silicon oils, etc.). Furthermore, the high concentration of silicon on the surface of the screw could possibly result from an unintentional deposition during the manufacture. This fact was confirmed by the corresponding concentration gradient over the sputtering time. Siliconization increases the resistance of titanium to oxidation because it dissolves in the $TiO_2$ surface layer and reduces the diffusion rate of the oxygen atoms through this layer.[6] Nevertheless, silicon increases the activity of osteoblasts and favours the formation of the appatite layer.

The presence of aluminium and silicon in the $TiO_2$ coating lowers the friction coefficient of the surface and becomes more compatible in terms of orthopaedic practice.[7] The presence of aluminium in the oxide layer, however, confirms the existence of stable $Al_2O_3$ oxide. Aluminium is capable of forming the most stable oxide; it can also form at room temperature and could form the piece of necrotic bone that has detached from the sound bone (the toxic response of the body). From the AES spectrum of the oxide layer it seems that a relatively high concentration of aluminium is present. Aluminium particles on the surface could weaken the stable position of the implant and cause irritation. It can be concluded from the AES analysis (**Figure 4**) that the presence of aluminium on the surface was not correlated with the bulk material.

The penetration depth of the calcium and phosphorous was determined to be over 400 nm and shows the quality of the osseointegration. From the AES spectrum in **Figure 3 b**, the presence of iron was not detected deeper than 0.4 μm, and iron was not detected in the basic (inner) material (**Figure 4**).

## 5 CONCLUSIONS

From the results of the AES and EDS analyses, several conclusions can be drawn. The retrieved titanium implant is unalloyed (alpha) titanium strengthened with titanium carbides. The presence of calcium and phosphorous was also established, 0.4 μm deep into the oxide surface layer, which confirms the quality of the osseointegration of the bone with the screw, and the bone as the source of calcium and phosphate ions involved in the metabolic functions. The nucleation of the growth of calcium phosphate started from the bone and from the implant surface. With interconnected pores the osteoblast cell adhesion, differentiation, proliferation as well as biomineralization were possible, relatively deep inside the oxide surface. Aluminium and silicon were found in higher concentrations and can influence the friction factor. A lower friction factor can strongly reduce the possibility of inflammation when an implant is rubbing against soft tissue. The existence of an ideal friction coefficient is impossible because it would differ from patient to patient. The aluminium contamination is relatively high when we consider that the bulk material is commercial titanium. Aluminium and iron oxides should be considered as being in the group of capsule-forming metal surfaces and the reason for retrieving the implant. Iron was found deep inside the oxide layer. The screw surface was examined with a stereo microscope and machining grooves were observed. The AES depth profile revealed that the screw surface was contaminated with iron, which could be the result of using an iron-containing steel tool. The accumulation of iron as well as the high contamination with aluminium at the interface of the implant and soft tissue can cause inflammation and irritation, which can form splinters at the implant–bone interface.

## 6 REFERENCES

[1] D. M. Brunette, P. Tengvall, M. Textor, P. Thomsen; Titanium in medicine; Springer, (**2001**)

[2] J. W. Nicholson; The Chemistry of medical and dental materials; The Royal society of Chemistry, (**2002**)

[3] M. G. Choi, H. S. Koh, D. Kluess, D. O'Conner, A. Mathur, G. A. Truskey, Janet Rubin, D. F. Zhou, K. L. P. Sung; PNAS; 102 (**2005**) 12, 4578–4583

[4] G. A. A.Castilho, M. D.Martins, W. A. A. Macedo; Surface characterisation of titanium based dental implants; Brazilian journal of physic; 36 (**2006**), 1004–1008

[5] E. R. Hitzky, K. Ariga, Y. Lvov; Bio-inorganic Hybrid Nanomaterials; Willey-Vch Verlag, (**2008**)

[6] D. Vojtěch, T. Kubatik; Siliconizing as a method for improving the resistance of titanium to oxidation; Mater. Tehnol., 37 (**2003**), 381–384

[7] E. A. Levashov, D. M. Shtansky, N. A. Gloushankova, I. V. Reshetov; Biocompatible multicomponent nanostructured coatings for medical implants; Avalible from world wide web: http://www.faqs.org/patents/app/20090050017

UDK 620.193:669.35'5'6:730(497.4)
Original scientific article/Izvirni znanstveni članek

ISSN 1580-2949
MTAEC9, 44(5)265(2010)

# CORROSION INVESTIGATION OF THE PREŠEREN MONUMENT IN LJUBLJANA

## KOROZIJSKA PREISKAVA PREŠERNOVEGA SPOMENIKA V LJUBLJANI

**Mirjam Bajt Leban, Viljem Kuhar, Tadeja Kosec, Andraž Legat**

Slovenian National Building and Civil Engineering Institute, Dimičeva 12, 1000 Ljubljana, Slovenia
mirjam.leban@zag.si

*Prejem rokopisa – received: 2010-03-30; sprejem za objavo – accepted for publication: 2010-04-13*

The investigated monument, erected in honour of the Slovenian poet France Prešeren, was unveiled in 1905 in Ljubljana, and restored in 1970. Its appearance differs considerably from the original as a result of corrosion. The strong interaction between atmospheric pollutants and the bronze alloy in Ljubljana city centre has resulted in the formation of a secondary patina. With the aim to determine the corrosion state of the Prešeren monument and to ensure the data for the next restoration procedure, a chemical and physical examination was performed. The composition of the patina was analysed using energy-dispersive spectroscopy coupled with scanning electron microscopy and a non-destructive method for determining the alloy composition was used. The different types of patina were studied.

Key words: Prešeren monument, bronze, patina, corrosion, urban atmosphere

Spomenik v spomin pesniku Francetu Prešernu v Ljubljani je bil odkrit l. 1905, renoviran pa l. 1970. Danes je njegov zunanji videz zaradi bolezni brona precej drugačen od tistega ob postavitvi. Največji razlog za to je onesnaženje okolja v centru Ljubljane. Da bi ugotovili korozijsko stanje Prešernovega spomenika in pridobili potrebne podatke za predvidene restavratorske posege, smo izvedli kemijske in fizikalne analize brona spomenika. Sestavo patin smo analizirali z energijsko disperzijsko spektroskopijo rentgenskih žarkov, kemijsko sestavo brona pa z nedestruktivno metodo.

Ključne besede: Prešernov spomenik, bron, patina, korozija, mestna atmosfera

## 1 INTRODUCTION

Artistic sculptures exposed outdoors are subjected to many environmental pollutants and other influences [1]. Bronze is a copper–tin alloy, sometimes referred to as phosphor bronze, and may contain other alloying elements, such as zinc, lead, etc. [2]. Copper is a commonly used material in statuary art, and it is heavily affected by ageing; however, the rate of ageing depends strongly on the exposure conditions. Bronze forms a protective oxide layer, also referred to as natural patina, when exposed to humid aerated environments. Furthermore, harmful factors include humidity, oxygen, UV light, biological pollution, etc., that can change the appearance of sculptures significantly.

The duration of patina [3–6] formation depends on the atmosphere. It can last from 20 to 100 years in rural sites, up to 10 years in urban centres, and up to 1 year in littoral zones [7]. Nowadays, with the aim to achieve the desired visual effect on bronze surfaces, artificial patination [7–11] is used. Bronze-brown or green casts patinas are used on statues exposed to the open air. The desired colours can be obtained by using various recipes and concentrations of one or more chemical compounds [12].

In order to ensure the quality of the maintenance and the long-term protection of outdoor sculptures against corrosion, various parameters should be taken into account. The most important parameters are: bronze quality, type of surface, chemical cleaning and subsequent treatment, and the type of corrosive atmosphere. In addition, the chemical composition of different parts of the bronze sculpture should be determined, as well as the type and intensity of the corrosion processes should be evaluated.

### *1.1 Prešeren's monument in Ljubljana*

The monument erected in honour of the Slovenian poet France Prešeren was unveiled on the 10th of September 1905. The author of the monument was the Slovenian sculptor Ivan Zajec and the architecture for the statue was designed by the architect Maks Fabiani. The monument consists of a statue of the poet (Prešeren) and a statue of his poetic Muse (Muza), in her hand holding a sprig of laurel (**Figure 1**). Two reliefs – "Fisherman (Ribič)" on the north side (**Figure 2**) and "Črtomir's Farewell to Bogomila (Slovo Črtomira od Bogomile)" – on the south side of the pedestal (**Figure 3**) are also constituent parts of the monument. The main statues and both reliefs were cast in bronze in the renowned Vienna foundry.

The monument was partly restored after 1970. The old patina was mechanically removed, although not completely. Once this procedure was finished, the monument was most likely artificially patinated with green patina. Subsequently, influenced by the corrosive environment and rinsing by water, at different locations on the monument different types of patina were formed

**Figure 1: S**tatue of the poet France Prešeren, with the statue of the poetry Muse above, holding a sprig of laurel in her hand
**Slika 1:** Kip pesnika Franceta Prešerna s kipom pesnikove Muze, ki drži v roki lovorjevo vejico

and various colours of green and pale green patinas developed as secondary corrosion products. The purpose of our work was to determine the corrosion state of the Prešeren monument and to provide the necessary data to be used in future restoration interventions.

## 2 EXPERIMENTAL

In order to identify the corrosion processes on the monument, samples of the corrosion products were mechanically scrapped off selected sites of the monument, as well as off both side reliefs. A non-destructive method of chemical analysis for the bronze was applied on these areas, using a portable instrument, i.e., a *Niton – Xli/XLp 800 Series Analyser and XDXRF – energy dispersive x-ray fluorescence*. A calibration of the *Niton – Xli/XLp 800 Series Analyser* apparatus was made before and after the analysis, using control etalons of the qualities C260C (Cartridge brass), C464 (Naval brass); C443 (Admiralty brass) and C110 (electrolytic copper) – UNS identification – *The Unified Numbering System*. In the laboratory, the corrosion products were examined with a scanning electron microscope SEM (JEOL JSM – 5500 LV Japan (*Japan*)) and analyzed with electron-dispersive spectroscopy (EDX, Oxford Inca, *Oxford Instrument Analytical, UK*) at an accelerating voltage of 20 kV.

**Figure 2:** Relief "Fisherman"
**Slika 2:** Relief "Ribič"

**Figure 3:** Relief "Črtomir's Farewell to Bogomila"
**Slika 3:** Relief "Slovo Črtomira od Bogomile"

## 3 RESULTS

### *3.1 Results of the chemical analysis of the bronze*

The results of the chemical analysis of the bronze alloy at different parts of the monument are given in mass fractions (*w*/%) in **Table 1**.

In addition to a certain content of elements, such as Cu, Sn, Pb, Zn, Ni and Fe, which are prescribed for bronzes, minor quantities of Ag, W, Mn, Cr, V, Ti, Al, Mo, Nb and Co were detected, also. The presence of Fe, Al and Mn confirmed the impurity of bronze. The presence of phosphorus and sulphur is common and expected in such alloys, but cannot be determined by the application of the applied method because the detection of the elements is limited.

### *3.2 Results of EDS (Energy-Dispersive X-ray Spectroscopy) analysis of patinas formed on the monument*

Samples of patinas were taken from different sites of bronze before any renovation on the stone part of the monument. Powder patina samples from internal and external layers were analyzed deposed on a carbon surface. The elemental compositions of the different corrosion layers are reported in **Table 2**. The EDS results of the most representative sites of the monument analyses are given in mass fractions (*w*/%).

**Table 1:** Results of the chemical analysis of the bronze (mass fractions, *w*/%)
**Tabela 1:** Rezultati kemijske analize brona (masni deleži, *w*/%)

| Site *w*/% | Cu | Sn | Pb | Zn | Ni | Fe | Rest |
|---|---|---|---|---|---|---|---|
| Fisherman | 87.76 | 6.37 | 1.74 | 3.28 | 0.18 | 0.10* | 0.57 |
| Farewell | 87.25 | 7.17 | 1.74 | 3.07 | 0.09 | 0.11 | 0.57 |
| Prešeren | 88.51 | 4.78 | 1.34 | 4.61 | 0.12 | 0.19 | 0.45 |
| Muse | 87.03 | 6.74 | 1.64 | 3.72 | 0.14 | 0.21 | 0.97 |
| C922** | 86– 90 | 5.5–6.5 | 1–2 | 3–5 | 0–1.0 | <0.25 | – |
| *** | <0.10 | 0.18 | 0.04 | 0.20 | 0.10 | 0.04 | – |

Remarks:
* – below the detection limit of the analyser;
** – regulation for C922 bronze quality (UNS identification);
*** – detection limits of Niton – Xli/XLp 800 Series Analyser.

**Table 2:** Results of the EDS analysis of the different patinas of the monument and reliefs
**Tabela 2:** Rezultati EDS-analize različnih patin na spomeniku in reliefih

| Site of patina take off | Patina colour, other properties *w*/% | C | O | Si | S | Cl | Cu | Sn | Pb | Rest |
|---|---|---|---|---|---|---|---|---|---|---|
| Farewell | white – green | 26.80 | 31.76 | 1.40 | 3.30 | 0.25 | 34.30 | 0.27 | 0.43 | 1.49 |
| Farewell | black – thick layer | 4.79 | 42.58 | 0.52 | 6.33 | – | 42.76 | 1.16 | 0.85 | 1.08 |
| Fisherman | bronze red – brown | 46.25 | 31.82 | 6.29 | 0.17 | 0.25 | 11.82 | 1.94 | 0.63 | 0.83 |
| Fisherman | green – white | 42.47 | 34.39 | 7.07 | 0.24 | 0.28 | 12.30 | 2.19 | 0.17 | 0.89 |
| Fisherman | light green – thin layer | 6.72 | 30.26 | – | 2.03 | – | 43.68 | 12.79 | 2.15 | 2.37 |
| Fisherman | bronze black – thin layer | 4.61 | 30.75 | 0.23 | 1.36 | – | 49.92 | 7.71 | 3.16 | 2.26 |
| Prešeren | black – thin layer | 5.26 | 43.14 | 0.39 | 7.76 | 0.46 | 40.06 | 0.32 | 1.27 | 1.34 |
| Muse | black – thin layer | 6.61 | 32.18 | 1.91 | 4.97 | 0.70 | 49.05 | 0.01 | 0.90 | 3.67 |
| Prešeren | black brown – thin layer | 9.16 | 50.15 | 0.39 | 6.02 | – | 32.10 | 0.38 | 0.81 | 0.99 |
| Prešeren | light green | 4.10 | 48.37 | 0.29 | 6.18 | – | 38.70 | 1.89 | 0.44 | 0.03 |
| Prešeren | black brown – thin layer | 4.77 | 38.37 | 0.28 | 2.88 | – | 41.73 | 8.89 | 1.02 | 2.06 |
| Muse | green-white – thin layer | 11.09 | 34.29 | 1.11 | 4.93 | 0.23 | 45.62 | 0.66 | 0.80 | 1.27 |

The corrosion activators (ions that initiate corrosion, $Cl^-$ and $S^{2-}$ in this case) that caused particular patina on different sites of the sculptures and monuments as well as the type of bronze patinas that were formed can be concluded from the composition of the most typical elements of the corrosion products given in **Table 2**.

The content of oxygen was higher in the case of the Prešeren and Muse statues. These patinas were taken from sites that are exposed at different angles of inclination. Moreover, the content of carbon is lower in the case of corrosion products formed on exposed surfaces at different angles of inclination. The content of sulphur is substantially higher in the case of a multi-angle exposure. The presence of zinc in the corrosion products is low and it does not vary on the exposure sites.

## 4 DISCUSSION

### *4.1 Visual observations*

The visual examination of the monument and the composition of the bronze and the patina indicate that secondary patinas were formed on the sites where there was a non-uniform leaching action of the rain. On the other hand, at sites where the leaching action of the rain is weaker (dark, almost black surfaces), the internal layer of the patina consisted of cuprite ($Cu_2O$). The external layer consisted mostly of copper sulphates (bronhanite and antlerite), copper chloride–hydroxide (atacamite) and other compounds originating from environmental contamination [13]. On some hardly accessible sites (the Prešeren and Muse statues), where the leaching action of the acid rain (pH < 5) was not as strong, the layer of secondary corrosion products was very thick (up to 0.5 mm).

Only a few corrosion activators accumulated on the dark (green to black colours) surfaces with the thinner patina layer (the bronze shine through the layer is clearly visible). These surfaces are smooth and the bronze is not deeply etched. The leaching action was observed in detail and similar observations were made [14]. On such surfaces the presence of copper chlorides was low or even non-existent, while copper oxides and sulphates were dominant.

On the surfaces with the green-grey and white coloured patina substrate, the secondary patina layer consisted mainly of copper oxides, sulphates, chlorides, carbonates and plaster. As heavily soluble compounds, carbonates were not leached by rain. On the other hand, the secondary layer of corrosion products on the surfaces, affected by the leaching action of the rain, was pale green and had a powdery non adhesive texture.

Flow-off water zones of light green colour were formed on the sites of the intensive corrosion products. A minor area on the south side of the monument, known as *Ribič* relief, has a red-brown bronze surface. The internal patina layer consists mostly of cuprite, whereas the secondary layer is very thin. The patina in the vertical zones is primarily of soluble corrosion products consisting of copper carbonates.

Since many different patinas were formed over the entire surface of the monument and different conditions regulated the water flow-off, it can be assumed that severe corrosion (e.g., bronze disease) was activated because of the relatively aggressive atmosphere. The surface of the reliefs is smoother than the surface of the monument, which is the main reason for the smaller corrosion damage.

The depth of the pitting corrosion on particular sites could not be estimated without a prior patina removal. The damage is not severe, yet it could have a crucial influence on the appearance of the monument details – locally corrosion damage causes an etched appearance of the surface.

### *4.2 EDXRF analysis*

The results of the bronze chemical analysis suggest that both sculptures were made from the bronze C922 according to the requirements of the standard UNS [2]. As presented in **Table 1**, the contents of Sn and Pb in some analyses deviate from their contents prescribed in the standards. However, the chemical composition analyzed on the bronze surface (where the EDXRF analysis was made) can differ slightly from the bulk composition. Regardless of this fact, it can be assumed that the bronze in both sculptures, as well as that in the side reliefs, is homogeneous. Its purity is comparable to currently valid regulations. Therefore, it can be concluded that the casting process of all the component parts of the monument included in this investigation was under quality control.

### *4.3 EDS analysis*

The results of the EDS analyses of the different patinas scraped off different sites of the monument indicate that the main contributions to the corrosion processes and to the formation of patinas are effected by environmental pollution (the pollution in the centre of Ljubljana is an urban atmosphere), acid rain, salt aerosol due to winter salting of the roads, dust, soot and bird excrements. The patina on the bronze statue consists of an internal, usually thinner, layer and a thicker, external layer. A schematic presentation is given in **Figure 4**. The internal patina layer consists of copper and tin oxides. The analyses have also proved the presence of copper carbonate and alloying elements. The thin layers of dark brown-black, red-brown and green patina corrosion products do not contain chloride compounds.

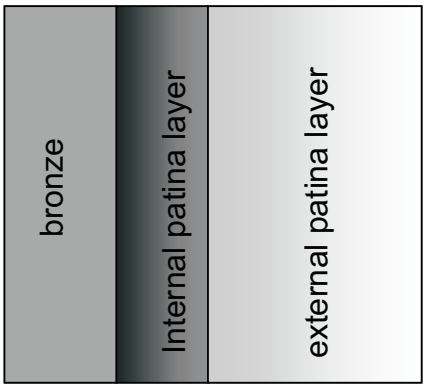


**Figure 4:** Schematic presentation of patina layers on bronze
**Slika 4:** Shematska predstavitev plasti patin na bronu

In the secondary-external layer of brown-black, black-green and green-white patina, the following predominant compounds were found: copper oxides, copper hydroxisulphates, as well as sulphides, chlorides and carbonates of copper and its alloying elements.

The sites where the water rinsing was not highly intensive have a relatively stable, predominantly black, patina. The vertical and horizontal surfaces have been affected by intensive rinsing. The leaching activity of the urban rain is therefore stronger and the colour of the patina is pale green-white.

The presence of Cl, Mg, K and Ca in the corrosion products is a consequence of the bronze's contamination with de-icing salts. Although the content of these elements is not high, they are in sufficient quantities to trigger corrosion and "bronze disease". The presence of chlorides and moisture is the cause for copper dissolution. The formation of sulphur compounds of copper and its alloying elements as well as carbonates in corrosion products is probably the consequence of acid rain (carbon and sulphur acid), air pollution (above all $SO_2$), and moisture. Copper hydroxi-sulphates are soluble in water – they form green-white lines on the sides of bronze sculptures. The content of zinc in the corrosion products is minimal and it can be assumed that the bronze of the sculptures and reliefs is not sensitive to dezincification. However, Bernardi and coauthors found that Cu and Pb in bronze type G85 progressively form insoluble corrosion compounds, while Zn continuously dissolves without forming detectable insoluble products [15]. They also claim that the absence of dissolved tin is remarkable.

Pollution with sand powder and soot might be the reason for the detected presence of Al, Si and C in the corrosion products.

## 5 CONCLUSION

Based on a visual examination, a chemical analysis of the bronze, and an EDS analysis of the patinas formed on Prešeren's monument in Ljubljana, the following conclusions were drawn:

- The sculptures of Prešeren's monument in Ljubljana were made from bronze C922. The purity of the bronze indicates that the casting process of this monument was strongly controlled.
- Regardless of the corrosion processes and the age of the bronze monument (approximately 100 years), the corrosion damage to the bronze alloy is insignificant, and the patina formation only disturbs the monument's visual/aesthetic appearance.
- The variety of patinas formed on the different sites of the monument under different conditions of wetting/drying/rinsing shows that the corrosion (bronze disease) is a consequence of the aggressive urban atmosphere.
- In order to maintain the bronze statue and to keep the appearance as long as possible, the protection of the bronze prepatinated surface is strongly advised.

## 6 REFERENCES

[1] P. A. Schweitzer, Fundamentals of metallic corrosion: Atmospheric and media corrosion of metals, corrosion engineering handbook, CRC press, 2nd Ed. 2007

[2] P. A. Schweitzer, Metallic materials – physical, mechanical, and corrosion properties, 1st Ed., Marcel Dekker, New York, 2003

[3] C. Chiavari, A. Colledan, A. Frigani, G. Brunoro, Corrosion evaluation of traditional and new bronzes for artistic castings, Mat. Chem. Phys., 10 (**2005**), 252–259

[4] F. Gallese, G. Laguzzi, L. Luvidi, V. Ferrari, S. Takacs and G. Venturi Pagani Cesa, Comparative investigation into the corrosion of different bronze alloys suitable for outdoor sculptures, Corros. Sci., 50 (**2008**) 954–961

[5] D. A. Scott, An examination of the patina and corrosion morphology of some roman bronzes, Journal of the American Institute for Conservation, 33 (**1994**), 1–23

[6] D. L. Hamilton, Conservation of cuprous metals (Copper, Bronze, Brass), Conservation Research Laboratory, Texas A&M University, 2000, Available from Word Wide Web: http://nautarch.tamu.edu/crl/conservationmanual/ConservationManual.pdf

[7] Introduction to patinas on brass, bronze and cooper, available from Word Wide Web: http://www.sciencecompany.com/patinas/patina-sintro.htm

[8] Green patina finishes, Available from Word Wide Web: http/www.cooper.org/resources/properties/protection/green.html

[9] Brown statuary finishes, Available from Word Wide Web: http/www.cooper.org/resources/properties/protection/brown.html

[10] M. Parmenter, Bronze patina basics, 1999, Available from Word Wide Web: http://www.whiteriverfoundry.com/bronze_patina_basics.htm

[11] Introduction to patinas on brass, bronze and cooper, patina formulas for brass, bronze and copper, Science Company, Available from Word Wide Web: http://www.sciencecompany.com/patinas/patinaformulas.htm

[12] R. Huges, M. Rowe, The colouring, bronzing and patination of metals, Thames and Hudson, London, 1991

[13] C. Chiavari, K. Rahmouni, H. Takenouti, S. Joiret, P. Vermaut and L. Robbiola, Composition and electrochemical properties of natural patinas of outdoor bronze monuments, Electrochim. Acta, 52 (**2007**), 7760–7769

[14] E. Bernardi, C. Chiavari, B. Lenza, C. Martini, L. Morselli, F. Ospitali, L. Robbiola, The atmospheric corrosion of quaternary bronzes: The leaching action of acid rain, Corros. Sci., 51 (**2009**), 159–170

[15] E. Bernardi, C. Chiavari, C. Martini, L. Morselli, The atmospheric corrosion of quaternary bronzes: An evaluation of the dissolution rate of the alloying elements Applied Physics A: Materials Science & Processing, 92 (**2008**), 83–89

### Acknowledgments

The research work presented in this paper was performed under the auspices and initiative of the Municipality of Ljubljana (Mestna občina Ljubljana).

UDK 622.332/333(497.115)
Original scientific article/Izvirni znanstveni članek

ISSN 1580-2949
MTAEC9, 44(5)271(2010)

# THE MICROFLORA AND PHYSICO-CHEMICAL PROPERTIES OF LIGNITE FROM THE MIRASH MINE, NEAR KASTRIOT

## MIKROFLORA IN FIZIKALNO-KEMIJSKE LASTNOSTI LIGNITA IZ RUDNIKA MIRASH PRI KASTRIOTU

**Fatime Plakolli[1], Luljeta P. Beqiri[2], Agron Millaku[3]**

[1]Faculty of Education, Rr. Agim Ramadani 10000 Pristine, Kosovo
[2]University of Pristine, Faculty of Mine and Metallurgy, Mitrovica, Kosovo
[3]Ministry of Environment and Spatial Planning, Rilindja K3, Kosovo
fatimekoka2008@hotmail.com

*Prejem rokopisa – received: 2010-03-08; sprejem za objavo – accepted for publication: 2010-04-29*

Coal, as an important source of energy, is very often the subject of study for scientists from the areas of chemistry, physics, technology, and biology, etc. In Kosovo, large deposits of coal, in the form of lignite, can be found. Lignite is mostly used to produce electrical energy; however, the interest of the country of Kosovo is to study many of the aspects of lignite.

In this paper an analysis of the microflora of lignite from the mine in the locality of Mirash, near Kastriot, is presented. With modern microbiological methods, the density, assortment, and some of the morphological and physiological characteristics of bacteria (heterotrophic, proteolytic, amilolytics, lypolytic and celulolytic) were determined and aerobic bacteria and fungi (yeasts and moulds) were investigated also. The samples of lignite were analyzed for physic–chemical attributes, for example, a determination of ash, and of C, O, H, N, S, carbonates, silicates, etc. The biomass of the isolated microflora from lignite was submitted for a chemical analysis and an astounding number of bacterial microflora and fungal was found. A composition chemical link between the coal and the microbial biomass was observed: the values of C, O, N, and H were found to be approximately similar in the coal and the bacterial mass.

Key words: coal, lignite, bacterial and fungal microflora, energy, carbonates, silicates, biomass

Premog kot pomemben vir energije je pogosto predmet študija znanstvenikov s področja kemije, fizike, tehnologije, biologije in drugih ved. Na Kosovu so velike količine premoga v obliki lignita. Največ lignita se uporablja za proizvodnjo električne energije, zato je razumljiv interes kosovske družbe in znanosti za njegovo vsestransko preučevanje. V tem prispevku je predstavljena analiza mikroflore lignita iz rudnika Mirash pri Kastriotu. Z modernimi mikrobiološkimi metodami so bile določene gostota, razvrstitev, morfološke in fiziološke značilnosti bakterij (heterotrofnih, proteolitičnih, alilolitičnih, lipolitičnih in celulitičnih). Istočasno so bile preiskane tudi aerobne bakterije in glive (kvasovke in plesni). Vzorci lignita so bili analizirani in določene so bile fizikalno-kemične lastnosti, kot so: vsebnost pepela, vsebnosti C, O, H, N, S, karbonatov, silikatov in podobnega. Biomasa izolirane mikroflore iz lignita je bila kemijsko analizirana. Najdeno je osupljivo veliko število bakterijske mikroflore in gliv v lignitu in opažena je bila povezava med kemijsko sestavo premoga in biomaso mikrobov. Vsebnosti C, O, N in H so bile približno enake v premogu in v masi bakterij.

Ključne besede: premog, lignit, mikroflora bakterij in gliv, energija, karbonati, silikati, biomasa

## 1 INTRODUCTION

Coal is considered to be a very important source of energy, and it has been used since the earliest times (before the new era). The economic development of society during the past 1000 years was based on coal as a source of energy (1). Oil and its derivatives are also an important source of energy, and by the beginning of the second half of the 20th Century it had achieved primacy as a source of energy. Nowadays, an interest in coal has once again emerged, because 80 % of fossil fuel reserves are coal as compared to 18 % for oil.

Actually, 45 % of the globally generated energy is generated with coal, as compared to 30 % from oil and 14 % from natural gas (2). Coal is a fossil fuel; it is an organic sedimentary rock; and it is formed by the accumulation of organic matter (plant debris).

This process usually takes place in waterlogged environments (water basins, lakes, marshes, swamps) (3). Coalification covers a number of geological periods, which can be used to determine the geological history of the Earth's crust (4). For this reason, the process of coal formation took place as a result of a number of different factors (pressure, humidity, lack of air, microbiological reactions, physical and chemical reactions, etc.). The best way to describe this complex process, which took place over millions of years, is the accumulation of dead organic (plant) matter that subsequently forms coal. The composition of coal is very complex; however, it consists mainly of carbon (between 60 % and 95 %). Thus, it has a very wide range of uses and a characteristic structure. Coal contains the following biogenic elements: carbon, hydrogen, oxygen and sulfur. From the biochemical point of view coal contains the same elements as did the tropical plants from which it was formed: oils, resins, etc. It ranges in color between black and brownish-black. Its strength is between 0.5 kg/cm$^2$ and 2.5 kg/cm$^2$ and its specific weight is 1–1.7.

Coals are divided into humic (formed by the degradation of land plants) and sapropelic (algae and fungi) (5) and it is found in the form of sedimentary rocks. After the fossilization the organic matter was submitted to degradation and in specific circumstances a new matter was formed, which served as the skeleton for the formation of coal. The following can be found in plant cells: cellulose, hemicellulose, lignin, proteins, oils, waxes, resins, cutin, etc. Through the interaction of micro-biological, physical and chemical, as well as geological factors, the organic matter turns into a mass called torv (peat), lignite and other kinds of coal. The coalification process has two phases: humification and carbonization. During the process of humification, organic materials, under the influence of the above-mentioned factors, turn into torv (peat) – humus. The peat is then degraded by microorganisms. Bacteria are known to degrade organic matter and cellulose, on which occasion enzymes and biocatalyzers are produced and affect the oxidoreduction process, as well. Micro-organisms affect the inorganic matter by increasing the mineral solubility (7).

According to several authors (8, 9, 10), upon the degradation of peat, microorganisms reduce their activity as a consequence of the formation of antiseptic substances, such as phenols (8).

During the second phase, torv or sapropel will turn into anthracite, lignite, coal, etc (9).

In aerobic conditions, 80 % of the organic matter is lost, whereas in anaerobic conditions only 5 % of the organic matter is lost (10). During the degradation of the organic matter proteolytic microorganisms degrade proteins. Then the degradation of the oils by lipolytic microorganisms and that of cellulose by cellulolytic microorganisms follows and afterwards, the degradation of hemicellulose, lignin, cutin and eventually resins, occurs.

The influence of physical and chemical factors in the formation of coal is characterized by increased pressure and the catalytic influence of minerals and gases together with water, temperature and pH. From the petrographic point of view lignite is xylitic. Geological data show that the Kosovo Coal Basin dates back to the Pliocene (approximately 2.5 million years ago). This tectonic basin was formed during the Oligocene (other layers were sedimented on top of it during the late Tertiary Period). Its reserves are estimated to 2.2 billion tons and could be as high as 10 billion tons. According to (11), the ecoregions in the Kosovo basin during the Pliocene consisted of wetlands, hills and mountains. Based on the ecological conditions, in which certain groups of plants lived, the following wetland vegetation zones existed (12):

1) Submerged aquatic plants (Myriophyllum)
   a) floating plants
   b) emergent plants (Graminea and Cyperaceae)
2) Mountain vegetation zone (Taxodiaceae)
3) Shrub zone (Polipodiaceae)
4) Dry forest zone (Sequoia forests) (14)

II. Hilly region

Forest zone: Salix, Alnus, Populus (15)
Deciduous forest zone: Querqus, Fagus, Carpinus, Tilia, Castanea, Acer, etc.

III. Mountainous region: Pinus, Picea, Abies, Laryx (16).

From these groups of plants the coal was formed. According to several references, coal and different microorganisms co-existed since the time the deposit was formed, around 2.5 million years ago. They have survived in a latent or dormant state, which slowed down their metabolism in order to survive the unfavorable conditions. The other form is called spores or endo-spores, and many scientific papers have dealt with coal and microorganisms.

It was established that certain species of bacteria can clean coal and improve its quality, e.g., leptospirillum, ferroxidans and thiobacillus ferroxidans. These species have been bred to use phenol as their only source of food (17) and pseudomonas and arthrobacter have degraded coal molecules by "eating" sulfur and other contaminants.

Bacteria increase the intensity of methane degradation (attested in the labs of the US Energy Department). The digestive system of the above-mentioned bacteria eliminates harmful pollutants and helps the production of clean coal (18). Certain strains (Pseudomonas) can degrade or ferment, coal derivatives (fenatren) producing $CO_2$ and $H_2O$: Fenatren – 1 – hydroxyl 2 – naphtoic acid – salicylic acid – catechol – $CO_2$+$H_2O$ (19). The bacteria digest the carbon in the rocks and produce natural gas for a period of about 10–1000 years (21) and lock methane at the bottom of the sea in anaerobic conditions. The aim of this study was to determine the presence of the bacterial and fungal microflora in the lignite from the Mirashi-Kastrioti Coal Mine. The presence of heterotrophic, proteolytic, amilolytic, lipolytic, cellulolytic, aerobic bacteria and fungi was studied in order to get an idea about the existing microflora at the time when the lignite was formed.

Furthermore, the aim of this study was to determine the composition of the ash, biogens and bacterial biomass in the lignite from the Mirashi Coal Mine. The authors were motivated by the claim (6) that hopanoids, the compounds in the membranes of prokaryotic cells (as well as bacteria), can be found in great abundance here (as well as by the data on the amount of carbon in the coal of the Kosova basin). It must be stressed that hopanoids are the main constituents of coal (90 %). Scientific data show that the membranes of prokaryotic cells (bacteria, cyanobacteria) have the most hopanoids.

Since the organic material (in coal) consists largely of bacteria in the form of kerogen, which is the organic precursor of petroleum, it becomes obvious that hopa-

noids or bacteriohopanetetrol are isolated from kerogen. In order to verify the relation between the accumulation of kerogens and bacterial activity, the authors (20, 23) have demonstrated the importance of bacteria in the formation of fossil fuels and the degradation of organic matter.

## 2 MATERIAL AND METHODS

Lignite samples from the Mirashi Coal Mine in the vicinity of Kastriot were used as study material and samples of dry and wet coal were examined. For the physico-chemical analysis of the coal (lignite), gravimetric, chromatographic and spectrophotometric methods were used. The following parameters were determined: moisture, ash, combustible volatile matter, lower calorific value, fixed carbon, total sulfur, organic sulfur, inorganic sulfur, $SiO_2$, $Al_2O_3$, $Fe_2O_3$, CaO, magnesium oxide and sulfur oxide.

A lump of coal was first examined. Later it was subjected to grinding and mixed with sterilized tap water in order to determine the presence of microflora on its surface and interior. Modern methods were applied to determine the presence of microflora (Standard Methods for the Examination of Water and Wastewater, APHA – last edition). The presence of biogens was determined using a sophisticated apparatus (VARIO MACRO CHNS). Initially, wet coal was dried at a temperature of 105 °C for 2 h. A sample of coal with a weight of 75 mg to 125 mg was used. The minimum weight for a reliable analysis was 40 mg. First, the content of biogens present in the lignite, the ratio between C and N, C and H as well as C and S were determined. Then the presence and the amount of biogens in the bacterial biomass isolated from the lignite were determined using the same apparatus.

## 3 RESULT WITH DISCUSSION

### *3.1 Microbiological analysis of lignite*

The microbiological, physical and chemical results were obtained in the three-month period of March, April and May. The results represent the arithmetical average of three measurements. Wet coal was used due to the fact that it had a higher density of microorganisms.

**Table 1:** Heterotrophic bacteria and physiological groups isolated from lignite
**Tabela 1:** Heterotrofne bakterije in fiziološke skupine, izolirane iz lignita

| Bacterial group | Unit | Number | *x*/% |
|---|---|---|---|
| Heterotrophic bacteria (saprophytic) | mL | 28,855,000 | 100 |
| Proteolytic | mL | 3,375,000 | 11.49 |
| Amilolytic | mL | 4,900,000 | 16.98 |
| Lipolytic | mL | 2,380,000 | 8.24 |
| Cellulolytic | mL | 3,200,000 | 11.08 |
| Sporogenic (microaerophilic) | mL | 15,000,000 | 51.98 |
| Total | | 28,855,000 | 99.97 |

(The amount of substance fraction, *x*/%)

**Table 2:** Fungal microflora isolated from the lignite of the Mirashi Coal Mine.
**Tabela 2:** Mikroflora gliv, izoliranih iz lignita iz premogovnika Mirashi

| Fungi type | Unit | Number | *x*/% |
|---|---|---|---|
| Mold | mL | 16,000,000 | 66.66 % |
| Yeast | mL | 8,000,000 | 33.33 % |
| Total | | 24,000,000 | 99.99 |

**Table 3:** Some physical parameters of the lignite from the Mirashi Coal Mine (March, April and May 2008)
**Tabela 3:** Nekaj fizikalnih parametrov lignita iz premogovnika Mirashi (marec, april in maj 2008)

| Month | *w*(M)/% | *w*(A)/% | *w*(Vm)/% | *Hu*/(MJ/kg) |
|---|---|---|---|---|
| March | 41.30 | 12.84 | 41.27 | 8.563 |
| | 44.64 | 16.49 | 38.87 | 7.809 |
| | 42.35 | 18.9 | 35.94 | 6.889 |
| April | 41.30 | 19.20 | 37.35 | 7.332 |
| | 42.20 | 15.1 | 39.37 | 7.966 |
| | 41.25 | 15.15 | 38.95 | 7.834 |
| May | 42.40 | 12.80 | 39.31 | 7.947 |
| | 42.32 | 17.79 | 35.67 | 6.804 |
| | 42.30 | 19.60 | 36.88 | 7.184 |
| | 40.28 | 13.74 | 36.82 | 7.165 |
| Average value | 42.03 | 16.16 | 38.04 | 7.549 |

Legend: M – moisture content, A – ash content, Vm – volatile matter, *Hu*/(MJ/kg) – lower calorific value.

The data show that the sporogenic bacteria (51.98 %) dominate the microflora, followed by the proteolytic bacteria (11.49 %) and amilolytic (16.98 %). The results of the analysis prove that the physiological groups listed in **Table 1** were present in the plant matter from which the lignite was formed. Based on the results in **Table 1** (according to which a single group may contain up to 28,855,000 bacteria), we can conclude that 1 t of lignite contains about $28.8 \cdot 10^{12}$ microorganisms, as was stated by other authors as well (6).

According to **Table 2**, just 1 g of lignite with moisture content contains 16 million mold cells (66.6 %). The remaining 33.33 % are yeast cells.

### *3.2 Physical and chemical analysis*

The above-mentioned lump of coal was used to determine the content of moisture and ash, combustible volatile matter as well as the lower calorific value of the coal (**Table 3**).

The lower calorific value of lignite present in **Table 4** was 8027 MJ.

CaO and $SiO_2$ are the main components in the ash of the coal from the Mirashi Coal Mine. The large concentration of CaO shows that it originates from limestone sedimentary rock. The large presence of $SiO_2$ shows that the lignite originates from silica algae (silica rich soil) (**Table 5**).

**Table 4:** Content of components important for the caloric value of lignite (Mirashi Coal Mine March, April and May 2008)
**Tabela 4:** Vsebnost komponent pomembnih za kalorično vrednost lignita (premogovnik Mirashi, marec, april in maj 2008)

| No | Analyzed parameters | Content, *w*/% |
|---|---|---|
| 1 | Coke | 34.06 |
| 2 | Fixed carbon | 18 |
| 3 | Vaporizing matter | 20.2 |
| 4 | Volatile matter | 39.64 |
| 5 | Total sulfur | 0.78 |
| 6 | Other | 7.52 |

**Table 5:** Chemical composition of ash of lignite from the Mirashi Coal Mine (March, April and May 2008)
**Tabela 5:** Kemijska sestava pepela v lignitu iz premogovnika Mirashi (marec, april in maj 2008)

| Components Content, *w*/% | |
|---|---|
| $SiO_2$ | 27.48 |
| $Al_2O_3$ | 11.82 |
| $Fe_2O_3$ | 7.46 |
| CaO | 37.33 |
| MgO | 3.2 |
| $SO_2$ | 9.6 |
| Other | 3.11 |

**Table 6:** Content of biogens (C, N, S, H) in lignite from the Mirashi Coal Mine
**Tabela 6:** Vsebnost biogenov (C, N, S, H) v lignitu iz premogovnika Mirashi

| | Sample weight | Unit | Sample | *m*(C)/*m*(N) ratio | Content, *w*/% |
|---|---|---|---|---|---|
| First measurement | 40.4 | mg | lignite | 43.06 | *w*(N) = 1.096 *w*(C) = 47.19 *w*(S) = 1.268 *w*(H) = 4.383 |
| Second measurement | 40.0 | mg | lignite | 45.55 | *w*(N) = 1.032 *w*(C) = 47 *w*(S) =1.347 *w*(H) = 4.392 |
| Third measurement | 40.8 | mg | lignite | 49.23 | *w*(N) = 1.055 *w*(C) = 51.92 *w*(S) = 1.381 *w*(H) = 4.405 |
| Average value | | | | 45.94 | *w*(N) = 1.061 *w*(C) = 48.73 *w*(S) = 1.332 *w*(H) = 4.36 |

**Table 7:** Presence of biogens (C, N, S, H) in the microbial biomass isolated from lignite of the Mirashi Coal Mine
**Tabela 7:** Prisotnost biogenov (C, N, S, H) v biomasi mikrobov, izoliranih iz lignita iz premogovnika Mirashi

| Measurement | Sample weight m/mg | Sample | C/N ratio *w*(C)/*w*(N) | Content, *w*/% |
|---|---|---|---|---|
| First measurement | 84–95 | Microbial biomass *w*(C)/*w*(N) = 2.07 | N:<br>C:<br>S:<br>H: | 21. 34<br>44.36<br>0.77<br>7.18 |
| Second measurement | 84–95 | *w*(C)/*w*(N) = 2.07 | N:<br>C:<br>S:<br>H: | 21.53<br>44.75<br>0.72<br>7.31 |
| Third measurement | 84–95 | *w*(C)/*w*(N) = 2.08 | N:<br>C:<br>S:<br>H: | 21.42<br>44.68<br>0.70<br>7.24 |
| | *w*(AV)/*w*(N) = 21.43; *w*(C) = 44.59; *w*(S) = 0.73; *w*(H) = 7.24 | | | |

### *3.3 The presence of biogens (C, N, S, H) in the analyzed coal and in the microbial biomass isolated from the same*

Data in **Table 6** show that carbon is the main component in biogenic coal (48.73). The average value of *m*(C)/*m*(N) ratio is 45.94.

The data in **Table 7** confirm, once again, the domination of carbon in the microbial biomass isolated from the lignite of the Mirashi Coal Mine. The results show that there is a resemblance in the constitution of the biogens in the coal and those in the bacterial biomass. It has been confirmed that during the Pliocene the vegetation in the Kosovo basin consisted of 132 different types of plants with numerous sub-types, grasses, aquatic plants, trees, etc. A number of authors (11, 12, 13, 14, 15) have reconstructed the vegetation of that period by comparing the fossil pollen grains and spores from the Pliocene with those from the present day. The same plants can nowadays be found in the area of the Kosovo coal basin.

## 4 CONCLUSION

Based on the investigations performed, the following conclusions can be drawn:

- The lignite from the coal mine in Mirash (Kastriot) has a high density of microorganisms, i.e., 28,855,000 microorganisms per gram or $28 \cdot 10^{12}$ microorganisms per ton.
- Among the isolated microorganisms we have determined the presence of bacteria, molds and yeasts (gram positive, negative and variable). The most common shapes were rods, spheres and spirals.
- Forty pure cultures were isolated (with typical representatives).
- Due to it physical and chemical characteristics the lignite from the Kosovo basin is of a better quality than that of other basins in the region.
- The presence of biogens (C, N, H, S) in the coal and the microbial biomass provides evidence of their functional interaction during the process of coal formation.
- The number of microorganisms in 1 g of lignite is evidence that most of the microorganisms are deposits of hopanoids, respectively carbon.
- The fossil pollen grains and spores found in different horizontal and vertical layers of the Kosovo coal basin give us a picture of the vegetation of the area from which the lignite was formed.

## 5 REFERENCES


[1] M. Berisha: Studij distribucije nekih elemenata u substance Kosovskog uglja. Doctor's Thesis. Prirodno matematiqki fakultet. PMF, Prishtina, 1982, p. 7–9

[2] Ll. A, Munro: Chemistry in engineering, Prentice Hall. (Inc), 1964

[3] P. Nikolić, D. Dimitrijević: Monografija savremena administracija. Beograd, (3, 9, 13, 175) 1980

[4] A Towle: Modern biology, Rinehard Winston, 1990, 221, 353–354

[5] Z. i J. Aljančič: Ugalj kao izvoz energije, Naučna knjiga, Beograd, 1951

[6] L. Prescott, J. Harley, D. Klein: Microbiology. Fourth ed. McGraw-Hill, 1999, 41–42

[7] C. L. Brierly: Microbiologycal minig. Science American, 247 (**1982**) 2, 44–53

[8] P. Atlas: Microorganisms and petroleum pollutants. BioScience, 28 (**1978**) 6, 378–391

[9] D. Allen: Coal. Abana (Appalachian Blacksmiths), 2003

[10] H. H. Lowny, F. Wily: Chemistry of coal utilization, 1963, 208

[11] V. Nikolić: Proučavanje spora i polena iz pliocenskog lignita Kosovskog basena sa osvrtom na današnji izgled vegetacije Kosova. Prirodnjački museum u Beogradu, 1966

[12] M. Atanacković: Pliocen Kosovskog basena. Geološko paleontološka studija. Zavod za geološka istraživanja C. Gore. Knj. III. Titograd, 1959

[13] E. Nagy: Polynoloische Untersuchung der am Fusse des Matra-Gebirges galagenten ober panonischen, 1952

[14] M. Janković: Fitoekologija sa osnovama Fitocenologije i pregledom tipova vegetacija na Zemlji. Naučna knjiga, Beograd, 1963

[15] I. Horvat: Sistematski odnosi termofilnih hrastova i borovih šuma jugoistočne Evrope. Biolcai glasnik, 12 (**1959**), 1–2

[16] N. Pantić: Paleobotanika, Naučna knjiga, Beograd, 1960

[17] M. Plakolli: Examination of phenolic degrading ability of bacterial cultures isolated from phenolic waste water of the place drying of the plant "Kosova" Acta Biol. Med. Exp., 10 (**1985**), 5–12

[18] M. Lin, E. Premuzič: Coal – purifying bacteria, Brookhaven National Laboratory, New York, 2001

[19] M. Rogoff, I. Wender: Bacterial oxidation of phenanthrene, Bureau de Mines, U.S Department of Interior Region V Bruceton, Pennsylvania, 1956

[20] Ourisson et al: The microbial origin of fossil fuels. Sci. Am. 251 (**1984**) 2, 44–51

[21] A. Martini: Green Car Congress Ecology. University of Massachusetts, 2008

[22] D. Valentine: Bacteria keep undersea methane out of the atmosphere. Santa Barbara, California USA, 2007

[23] P. Luger et al: The crystal structure of Hop-17 (21)-en-3B-y1 acetate of Pluchea pteropoda Hemsl. Vietnam. Cryst. Res. Technol. 35 (**2002**) 3, 355–362

UDK 620.18:546.48:669.4:633.31
Original scientific article/Izvirni znanstveni članek

ISSN 1580-2949
MTAEC9, 44(5)277(2010)

# CADMIUM AND LEAD ACCUMULATION IN ALFALFA (MEDICAGO SATIVA L.) AND THEIR INFLUENCE ON THE NUMBER OF STOMATA

## AKUMULACIJA KADMIJA IN SVINCA V RASTLINI LUCERNA (MEDICAGO SATIVA L.) IN NJUN VPLIV NA ŠTEVILO LISTNIH POR

**Arsim Bytyqi[1], Enver Sherifi[2]**

[1]Štore Steel Company, d. o. o. Železarska cesta 3, Štore, Slovenia
[2]Department of Biology, Faculty of Natural Sciences, University of Prishtina, Mother Teresa Street, 10000 Priština, Kosovo
arsim.bytyqi@imt.si

*Prejem rokopisa – received: 2009-12-09; sprejem za objavo – accepted for publication: 2010-06-08*

Accurate measurements of the heavy-metal contents in polluted areas are required to assess the potential ecological risks in these areas. Chemical and biological indicators are of interest when they provide information about the concentration and accumulation of heavy metals in the environment. This study was conducted in order to investigate heavy-metal accumulation and the effect on alfalfa (Medicago sativa L.) at different distances from the road. The total content of heavy metals was determined using atomic absorption spectrophotometry. The present results showed a variation that indicated that Pb and Cd had the highest concentration in all the sampling areas near the road. According to the results of the present study, the concentration of heavy metals has an influence on the number of stomata in both the adaxial and abaxial surfaces of the leaves, particularly in locations where the concentrations of Pb and Cd were higher. The results showed that the plant demonstrated a physiological response to the heavy-metal pollution, which suggests that roadside plants are indicators of heavy-metal accumulation and the effect on the environment.

Key words: concentration of Pb and Cd, Medicago sativa L., adaxial stomata, abaxial stomata

Za oceno ekološke obremenjenosti na območjih, ki so onesnažena s težkimi kovinami, moramo izvajati natančne in drage meritve, če hočemo najti kemične in biološke pokazatelje, ki kažejo na kopičenje težkih kovin v okolju – organizmih. Naredili smo raziskavo kopičenja težkih kovin in njihovih posledic na rastlino lucerna (Medicago sativa L.) na različnih oddaljenostih od ceste. Skupna vsebnost težkih kovin je bila določena z atomsko absorpcijsko spektrofotometrijo. Najvišje koncentracije težkih kovin Pb in Cd so bile dosežene v bližini ceste. Prav tako smo ugotovili korelacijo med koncentracijo težkih kovin v rastlini in številom por na obeh straneh listov. Višja koncentracija težkih kovin v rastlini je povezana z večjim številom listnih por. Rezultati so pokazali, da se rastline fiziološko odzovejo na prisotnost težkih kovin, zato je stanje teh rastlin v okolju lahko pokazatelj onesnaženja okolja s težkimi kovinami.

Ključne besede: koncentracija Pb in Cd, Medicago sativa L.,, zgornja pora, spodnja pora

## 1 INTRODUCTION

The contribution of cars and other road transport to the global emission of atmospheric pollutants is increasing. In parallel with the rapid growth in industrialization, environmental pollution is increasing, with heavy metals like lead and cadmium constituting a significant part. These elements are released into the environment as a result of a wide range of industrial activities. The contamination of heavy metals in the environment is of major concern because of their toxicity and the threat to human life and the environment.[16] Heavy metals are considered to be the main sources of pollution in the environment, since they have a significant effect on its ecological quality. Some heavy metals at low doses are essential micronutrients for plants, but in higher doses they may cause metabolic disorders and growth inhibition for most of the plant species.[12]

In monitoring urban pollution there is a need to consider the materials that cause the occurrence of pollutants. Among toxic metals, lead and cadmium appear to be the most dangerous to the environment.[11] Lead and cadmium cause toxicity and environmental impact, although this toxicity is entirely dependent on the concentration and environmental parameters.

Investigations concerning the concentration of lead and cadmium in alfalfa (Medicago Sativa L.) at different distances from the road and their influence on some morph-anatomic parameters are presented in this study.

## 2 MATERIAL AND METHODS

Three sites were selected for the collection of 60 plants of Medicago sativa along the Lipjan–Prizren road (**Figure 1**).

1. Location I Lipjan
2. Location II Shtime
3. Location III Suharek

The plant samples were cut off at 2 cm or 3 cm above the soil and stored in plastic bags. In every location the plants were collected at two different distances from the

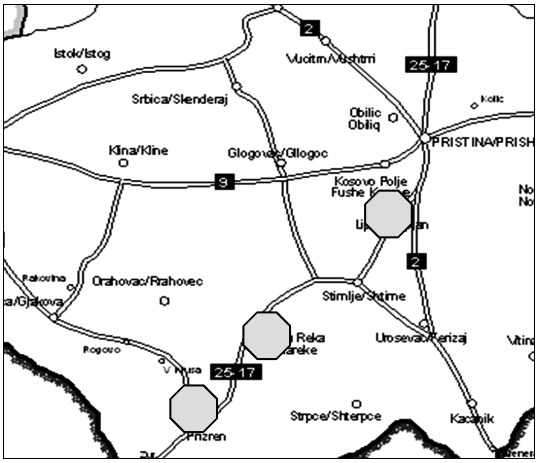


**Figure 1:** Location sketch map of the investigated area.
**Slika 1:** Lokacijska skica zemljevida področja raziskav

road where lead and cadmium were determined in the tissue extracts of all the specimens.

All the samples were dried in a thermostat at a temperature of 105 °C for three hours. The digestion of the plant samples was carried out using an acid solution with a 20 : 2 : 1 ratio of nitric acid ($HNO_3$), perchloric acid ($HClO_4$), and sulfuric acid ($H_2SO_4$). A portion of 3 g of each sample was weighed and transferred into a 250 mL beaker. The samples were heated to boiling until the white color appeared. Then the samples were acid washed, filtered into the (100 ml) flask, which was added up to the mark with distilled water. The filtered samples were then analyzed for heavy-metal concentration in plant tissues using Atomic Absorption Spectrophotometer.

The stomata number was measured in microscopic fields of leaf impressions taken from the middle parts of leaves. Leaf epidermis imprints of the adaxial and abaxial leaf surfaces were then removed using transparent sticky tape and placed on a microscopic slide. The stomata number was expressed as the number per microscopic field at a magnification of (10X40). Ten fields were assessed in every specimen and the variable was analyzed using Excel computer software.

## 3 RESULTS AND DISCUSSION

In **Table 1** the concentrations of heavy metals in three different localities are presented. Based on the results related to location 1 (Lipjan), the greatest quantity of cadmium and lead was established in the specimens taken near the road where the average content of cadmium and lead was 1.38 μg/g and 0.814 μg/g, respectively. Research data revealed that recently this highway has been an intensive source of pollution with heavy metals. Heavy-metal accumulation in plant tissues (leaves, stem) was due to the foliar absorption from the surroundings (vehicle sources). According to the results, lead exhibited high levels of contamination closer to the highway. The smallest content of lead (0.21 μg/g) was noted in specimens taken at a distance of 10 m from the highway. The quantity of cadmium in this location was higher in specimens taken near the highway (1.38 μg/g), while the smallest concentration of the cadmium was characteristic for specimens taken at a distance of 10 m from the highway (0.61 μg/g). The general decrease in the concentration of metals with distance from the highway indicates their relation to traffic. This is attributed mainly to the aerial deposition of metal particulates from motor vehicles.[14] The results of the investigation show that the concentration of cadmium in the plant samples varied between 1.38 μg/g and 0.61 μg/g. The accumulation of the selected metals varied greatly among the plant species and the uptake of an element by a plant is primarily dependent on the plant species, its inherent controls and the soil quality.[10]

The alfalfa plant has a high potential to uptake toxic metals like cadmium and lead.[9] Alfalfa has the ability to accumulate concentrations of heavy metals well above the tolerance levels of other plants, which may be due to the presence of specialized chemical functional groups responsible for metal tolerance and accumulation.[1] Various studies have shown the heavy contamination of roadside vegetation with lead. Heavy metals could be absorbed in investigated samples by clay minerals, Fe oxides and/or organic matter. They could also be incorporated into the structures of carbonates.[13]

Based on the results of locality II (Shtime), it is evident that the content of metals grows as the distance between the place of the specimen collection and the road with heavy traffic decreases. The highest content of cadmium and lead in this locality was in specimens taken near the highway (0.29 μg/g, 1.47 μg/g). The concentration of both metals in this location for specimens taken at a distance of 10 m from the highway varied in the range (0.24 μg/g to 1.05 μg/g). These high concentrations may be due to the aerial deposition of heavy metals over a long period of time. A significant correlation was noted between the number of passing petrol vehicles and the lead concentration in the particulate deposits collected from different designated sites (lead in deposits 14.4 μg/g, lead in leaves 1.78 μg/g).[4]

According to the results in location III (Suharek), as distinguished from the first two locations, the highest content of cadmium was in the specimens taken at a distance of 10 m from the highway (2.29 μg/g). The lowest content of cadmium is observed in specimens taken near the highway (1.52 μg/g) **Table 1**. Based on the results obtained, we can conclude that the quantity of lead at this location, as in the two other locations, was greater near the highway (0.79 μg/g), whereas the lowest quantity was observed in specimens taken at a 10m distance from the road (0.16 μg/g) (**Table 2**). Positive and negative correlations are found in the metal concentration at different distances from the highway. Comparatively speaking, almost all the samples collected

**Table 1:** Cadmium accumulation (µg/g) in alfalfa (Medicago sativa L.) at different distances from the road
**Tabela 1:** Akumulacija Cd (v µg/g) v rastlini lucerna (Medicago sativa L.) pri različnih oddaljenostih od ceste

| Localities and individuals examined | 1 | 2 | 3 | 4 | 5 | 6 | 7 | 8 | 9 | 10 | X | S | SX | V | Lsd 0.05 | Lsd 0.01 |
|---|---|---|---|---|---|---|---|---|---|---|---|---|---|---|---|---|
| P1. 1 m | 0.6 | 0.59 | 0.28 | 0.33 | 0.76 | 4.52 | 0.58 | 2.48 | 0.47 | 3.15 | 1.38 | 1.47 | 0.46 | 1.06 | 0.16 | 0.23 |
| P2. 1 m | 0.56 | 0.36 | 0.29 | 3.68 | 0.26 | 3.05 | 0.26 | 3.3 | 2.69 | 0.23 | 1.47 | 1.49 | 0.47 | 1.01 | 0.36 | 0.5 |
| P3. 1 m | 3.41 | 0.79 | 0.26 | 0.78 | 0.22 | 1.14 | 2.81 | 0.42 | 2.94 | 2.42 | 1.52 | 1.23 | 0.39 | 0.81 | 0.21 | 0.3 |
| P1. 10 m | 3.33 | 0.22 | 0.39 | 0.25 | 0.19 | 0.26 | 0.51 | 0.25 | 0.35 | 0.35 | 0.61 | 0.9 | 0.3 | 1.5 | 0.16 | 0.23 |
| P2. 10 m | 1.05 | 0.26 | 2.83 | 0.22 | 0.22 | 2.69 | 0.45 | 0.19 | 0.51 | 0.38 | 2.74 | 1.1 | 0.3 | 1.1 | 0.36 | 0.5 |
| P3. 10 m | 0.42 | 0.19 | 2.87 | 4.9 | 2.82 | 2.74 | 5.21 | 0.19 | 0.29 | 3.27 | 2.29 | 1.9 | 0.6 | 0.8 | 0.21 | 0.3 |

**Table 2:** Lead accumulation (µg/g) in alfalfa (Medicago sativa L.) at different distances from the road
**Tabela 2:** Akumulacija Pb (v µg/g) v rastlini lucerna (Medicago sativa L.) pri različnih oddaljenostih od ceste

| Localities and individuals examined | 1 | 2 | 3 | 4 | 5 | 6 | 7 | 8 | 9 | 10 | X | S | SX | V | Lsd 0.05 | Lsd 0.01 |
|---|---|---|---|---|---|---|---|---|---|---|---|---|---|---|---|---|
| P1. 1 m | 1.05 | 0.26 | 0.75 | 0.25 | 0.51 | 1.78 | 0.73 | 0.23 | 0.92 | 1.61 | 0.81 | 0.54 | 0.17 | 0.67 | 0.58 | 0.08 |
| P2. 1 m | 0.28 | 0.29 | 0.26 | 0.09 | 0.72 | 0.39 | 0.23 | 0.03 | 0.09 | 0.49 | 0.29 | 0.2 | 0.06 | 0.7 | 0.003 | 0.004 |
| P3. 1 m | 0.66 | 0.82 | 0.39 | 0.84 | 0.61 | 0.95 | 1.02 | 0.58 | 1.61 | 0.43 | 0.79 | 0.35 | 0.11 | 0.44 | 0.02 | 0.03 |
| P1. 10 m | 0.32 | 0.32 | 0.13 | 0.19 | 0.23 | 0.26 | 0.03 | 0.12 | 0.09 | 0.45 | 0.21 | 0.1 | 0.04 | 0.58 | 0.58 | 0.08 |
| P2. 10 m | 0.45 | 0.19 | 0.29 | 0.41 | 0.16 | 0.12 | 0.13 | 0.16 | 0.25 | 0.22 | 0.24 | 0.1 | 0.03 | 0.47 | 0.003 | 0.004 |
| P3. 10 m | 0.22 | 0.09 | 0.16 | 0.43 | 0.09 | 0.03 | 0.06 | 0.13 | 0.19 | 0.23 | 0.16 | 0.6 | 0.03 | 0.68 | 0.02 | 0.03 |

X- Arithmetic mean, S-Standard deviation, SX- Standard error, V-Coefficient of variability, Lsd- Least Significant Difference

**Table 3:** Number of stomata in the abaxial and adaxial surfaces per 1 mm$^2$ in alfalfa (Medicago sativa L.) for locality I near the road
**Tabela 3:** Število por na obeh straneh listov (zgornja in spodnja) na 1 mm$^2$ pri rastlini lucerna (Medicago sativa L.) v bližini ceste

| | Lower leaf | | | | Medium leaf | | | | Upper leaf | | | |
|---|---|---|---|---|---|---|---|---|---|---|---|---|
| | Upper surface | | Lower surface | | Upper surface | | Lower surface | | Upper surface | | Lower surface | |
| No. | X | V | X | V | X | V | X | V | X | V | X | V |
| 1 | 142.8 | 0.26 | 111.9 | 0.25 | 170.8 | 0.23 | 88.3 | 0.36 | 218 | 0.31 | 139.9 | 0.24 |
| 2 | 102.5 | 0.24 | 86.9 | 0.32 | 44.1 | 0.39 | 86.9 | 0.25 | 145.8 | 3 | 122.2 | 0.25 |
| 3 | 85.4 | 0.24 | 78 | 0.3 | 86.9 | 0.36 | 153 | 0.2 | 54.5 | 0.35 | 107.5 | 0.32 |
| 4 | 98.3 | 0.37 | 79.5 | 0.24 | 112.2 | 0.3 | 91.3 | 0.37 | 88.7 | 0.39 | 82.4 | 0.33 |
| 5 | 83.9 | 0.2 | 91.3 | 0.26 | 88.3 | 0.23 | 95.7 | 0.37 | 76.5 | 0.27 | 129.6 | 0.29 |
| 6 | 79.6 | 0.45 | 98.6 | 0.44 | 58.92 | 0.39 | 98.6 | 0.28 | 84.9 | 0.27 | 72.1 | 0.27 |
| 7 | 67.7 | 0.2 | 82.4 | 0.22 | 63.3 | 0.29 | 57.4 | 0.18 | 70.7 | 0.36 | 66.2 | 0.18 |
| 8 | 234.2 | 0.29 | 98.6 | 0.33 | 64.8 | 0.3 | 51.5 | 0.2 | 252.2 | 0.26 | 67.7 | 0.38 |
| 9 | 109 | 0.27 | 94.2 | 0.43 | 91.3 | 0.27 | 82.4 | 0.25 | 69.2 | 0.52 | 107.5 | 0.54 |
| 10 | 200.1 | 0.31 | 69.2 | 0.4 | 116.3 | 0.26 | 98.6 | 0.29 | 141.4 | 0.23 | 57.4 | 0.35 |
| X | 120.3 | | 89 | | 114.5 | | 90.3 | | 122.2 | | 95.2 | |
| Lsd 0.05 | 183.2 | | 129 | | 17.9 | | 80.3 | | 204.9 | | 43.9 | |
| Lsd 0.01 | 257.1 | | 181.1 | | 25.1 | | 112.8 | | 287.6 | | 61.1 | |

from site A, which was directly at the border of the road, showed a higher lead concentration than the site-B samples. The average lead concentration in C. sativa in the study area was 3.6 mg kg$^{-1}$, whereas the average concentration of this metal at the control site was 0.94 mg kg$^{-1}$.[2]

### *3.1 Lead and cadmium affect the number of stomata in alfalfa (Medicago sativa L.)*

A number of stomata were examined on the abaxial and adaxial leaf surfaces. All the specimens were gathered at the three localities marked on the map. Based on the results (related to the effect of these heavy metals on the number of stomata) it is observed that at location I in three researched leaves (lower, medium, upper) the largest number of stomata per 1 mm2 on the surfaces of the leaves was found in plants examined near the road (156.5 mm$^2$, 165.7 mm$^2$, 197.8 mm$^2$). The difference between the specimens in terms of stomata number on both the abaxial and adaxial surfaces of the leaves was also significant (**Table 3**). In all the specimens examined at different distances from the road the largest number of stomata per 1 mm$^2$ was on the upper leaf (**Table 4**). In the same location the smallest number of stomata was found in specimens taken at a distance of 10 m from the road (116.4 mm$^2$, 143.4 mm$^2$, 159.6 mm$^2$). It was reported that the lead concentration in leaves of Soybean

**Table 4:** Number of stomata in abaxial and adaxial surfaces per 1 mm$^2$ in alfalfa (Medicago sativa L.) for locality I 10 m distance from the road
**Tabela 4:** Število por na obeh straneh listov (zgornja in spodnja) na 1 mm$^2$ pri rastlini lucerna (Medicago sativa L.) na oddaljenosti 10 m od ceste

| | Lower leaf | | | | Medium leaf | | | | Upper leaf | | | |
|---|---|---|---|---|---|---|---|---|---|---|---|---|
| | Upper surface | | Lower surface | | Upper surface | | Lower surface | | Upper surface | | Lower surface | |
| No. | X | V | X | V | X | V | X | V | X | V | X | V |
| 1 | 76.5 | 0.15 | 82.4 | 0.42 | 147.3 | 0.2 | 102 | 0.18 | 153.1 | 0.36 | 79.5 | 0.42 |
| 2 | 88.3 | 0.39 | 107.5 | 0.35 | 89.8 | 0.35 | 103 | 0.34 | 170.8 | 0.09 | 103.1 | 0.27 |
| 3 | 126.6 | 0.22 | 98.6 | 0.29 | 111.9 | 0.19 | 109 | 0.18 | 179.7 | 0.12 | 131 | 0.23 |
| 4 | 79.5 | 0.23 | 67.7 | 0.26 | 178.2 | 0.27 | 121 | 0.39 | 154.6 | 0.36 | 107.5 | 0.34 |
| 5 | 122.2 | 0.23 | 110.4 | 0.26 | 181.1 | 0.14 | 131 | 0.31 | 148.7 | 0.23 | 111.9 | 0.29 |
| 6 | 98.6 | 0.26 | 107.5 | 0.24 | 162 | 0.28 | 119 | 0.25 | 188.5 | 0.17 | 151.7 | 0.4 |
| 7 | 172.3 | 0.27 | 148.7 | 0.38 | 144.3 | 0.36 | 118 | 0.17 | 107.5 | 0.32 | 88.3 | 0.19 |
| 08 | 86.9 | 0.28 | 107.5 | 0.28 | 147.3 | 0.23 | 121 | 0.24 | 100 | 0.37 | 75.1 | 0.35 |
| 9 | 136.9 | 0.38 | 73.6 | 0.24 | 139.9 | 0.29 | 137 | 0.24 | 160.5 | 0.21 | 119.3 | 0.28 |
| 10 | 176.7 | 0.27 | 178.2 | 0.14 | 132.5 | 0.36 | 97.4 | 0.27 | 232.7 | 0.37 | 173.8 | 0.41 |
| X | 116.4 | | 108.2 | | 143.4 | | 115.8 | | 159.6 | | 114.1 | |
| Lsd 0.05 | 183.2 | | 67.7 | | 213.4 | | 22.3 | | 175.4 | | 15.5 | |
| Lsd 0.01 | 257.1 | | 95.1 | | 299.5 | | 31.3 | | 146.2 | | 21.8 | |

X-Arithmetic mean, V-Coefficient of variability, Lsd- Least Significant Difference.

**Table 5:** Number of stomata in abaxial and adaxial surfaces per 1 mm$^2$ in alfalfa (Medicago sativa L.) for locality II near the road
**Tabela 5**: Število por na obeh straneh listov (zgornja in spodnja) na 1 mm$^2$ pri rastlini lucerna (Medicago sativa L.) v bližini ceste

| | Lower leaf | | | | Medium leaf | | | | Upper leaf | | | |
|---|---|---|---|---|---|---|---|---|---|---|---|---|
| | Upper surface | | Lower surface | | Upper surface | | Lower surface | | Upper surface | | Lower surface | |
| No. | X | V | X | V | X | V | X | V | X | V | X | V |
| 1 | 190 | 0.26 | 100.1 | 0.31 | 83.9 | 0.5 | 60.3 | 0.17 | 136 | 0.5 | 117.8 | 0.42 |
| 2 | 219.4 | 0.16 | 145.8 | 0.29 | 173.8 | 0.33 | 191.4 | 0.23 | 307.8 | 0.1 | 145.8 | 0.24 |
| 3 | 109 | 0.36 | 89.8 | 0.29 | 95.7 | 0.31 | 60.3 | 0.4 | 331.4 | 0.1 | 169.3 | 0.34 |
| 4 | 60.3 | 0.38 | 63.3 | 0.51 | 122.2 | 0.18 | 95.7 | 0.44 | 268 | 0.25 | 132.5 | 0.25 |
| 5 | 166.4 | 0.37 | 119.3 | 0.47 | 114.8 | 0.28 | 54.5 | 0.22 | 164.9 | 0.32 | 120.7 | 0.47 |
| 6 | 76.5 | 0.26 | 45.6 | 0.31 | 132.5 | 0.2 | 97.2 | 0.21 | 85.4 | 0.43 | 85.4 | 0.46 |
| 7 | 82.4 | 0.25 | 89.8 | 0.28 | 79.5 | 0.29 | 89.8 | 0.28 | 136.9 | 0.27 | 66.2 | 0.24 |
| 8 | 101.6 | 0.3 | 73.6 | 0.29 | 175.2 | 0.18 | 85.4 | 0.35 | 284.2 | 0.23 | 114.8 | 0.45 |
| 9 | 182.6 | 0.39 | 104.5 | 0.3 | 184.1 | 0.12 | 103.1 | 0.39 | 142.8 | 0.27 | 106 | 0.34 |
| 10 | 63.3 | 0.34 | 54.5 | 0.28 | 89.8 | 0.33 | 67.7 | 0.47 | 94.2 | 0.32 | 88.3 | 0.38 |
| X | 125.1 | | 88.6 | | 125.1 | | 90.5 | | 195.1 | | 114.6 | |
| Lsd 0.05 | 46.5 | | 45.8 | | 27.5 | | 4.6 | | 93.8 | | 35.3 | |
| Lsd 0.01 | 65.2 | | 64.2 | | 38.6 | | 6.45 | | 131.6 | | 49.5 | |

X-Arithmetic mean, V-Coefficient of variability, Lsd- Least Significant Difference.

**Table 6:** Number of stomata in abaxial and adaxial surfaces per 1 mm$^2$ in alfalfa (Medicago sativa L.) for locality II 10 m distance from the road
**Tabela 6:** Število por na obeh straneh listov (zgornja in spodnja) na 1 mm$^2$ pri rastlini lucerna (Medicago sativa L.) na oddaljenosti 10 m od ceste

| | Lower leaf | | | | Medium leaf | | | | Upper leaf | | | |
|---|---|---|---|---|---|---|---|---|---|---|---|---|
| | Upper surface | | Lower surface | | Upper surface | | Lower surface | | Upper surface | | Lower surface | |
| No. | X | V | X | V | X | V | X | V | X | V | X | V |
| 1 | 160.8 | 0.23 | 109 | 0.17 | 104.5 | 0.31 | 73.6 | 0.33 | 190 | 0.27 | 111.9 | 0.37 |
| 2 | 73.6 | 0.24 | 89.7 | 0.33 | 169.3 | 0.51 | 45.6 | 0.42 | 172.3 | 0.21 | 60.3 | 0.28 |
| 3 | 69.2 | 0.49 | 51.5 | 0.31 | 150.2 | 0.4 | 53 | 0.35 | 116.3 | 0.33 | 79.5 | 0.35 |
| 4 | 117.8 | 0.38 | 65.4 | 0.24 | 97.2 | 0.4 | 77.9 | 0.49 | 97.2 | 0.25 | 67.9 | 0.22 |
| 5 | 86.9 | 0.48 | 60.3 | 0.4 | 110.4 | 0.41 | 67.7 | 0.34 | 182.6 | 0.35 | 94.2 | 0.43 |
| 6 | 113.4 | 0.21 | 57.4 | 0.22 | 128.1 | 0.39 | 54.5 | 0.27 | 86.9 | 0.25 | 53 | 0.27 |
| 7 | 72.1 | 0.31 | 45.6 | 0.4 | 79.5 | 0.29 | 50 | 0.41 | 119.3 | 0.6 | 51.5 | 0.39 |
| 8 | 67.7 | 0.21 | 170.8 | 0.23 | 66.2 | 0.4 | 57.4 | 0.42 | 64.8 | 0.29 | 160.5 | 0.31 |
| 9 | 147.3 | 0.45 | 55.9 | 0.45 | 88.3 | 0.36 | 86.3 | 0.46 | 76.5 | 0.36 | 53 | 0.28 |
| 10 | 75.1 | 0.46 | 82.4 | 0.41 | 151.7 | 0.3 | 82.4 | 0.33 | 116.3 | 0.38 | 60.3 | 0.33 |
| X | 120.3 | | 78.8 | | 89.6 | | 64.8 | | 120.1 | | 79.2 | |
| Lsd 0.05 | 46.5 | | 45.8 | | 27.5 | | 4.6 | | 93.8 | | 35.3 | |
| Lsd 0.01 | 65.2 | | 64.2 | | 38.6 | | 6.45 | | 131.6 | | 49.5 | |

X-Arithmetic mean, V-Coefficient of variability, Lsd- Least Significant Difference.

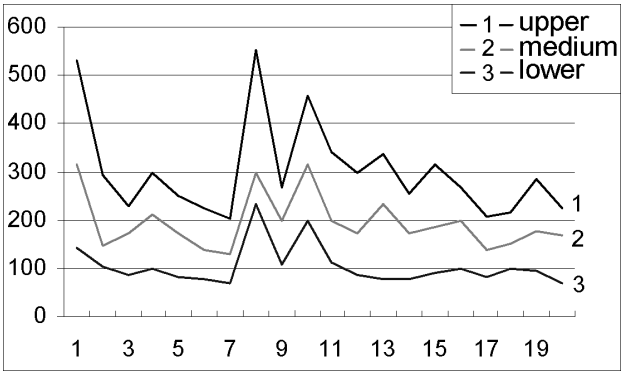


**Figure 2:** Number of stomata in abaxial and adaxial surfaces of leaves at location III near the road

**Slika 2:** Število por na obeh straneh listov (zgornja in spodnja) v bližini ceste na 1 mm$^2$

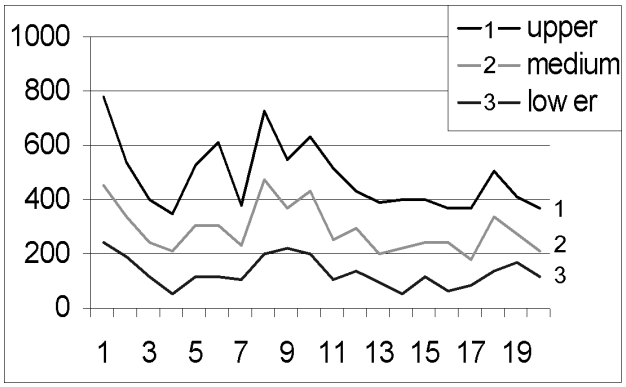


**Figure 3:** Number of stomata in adaxial and abaxial surfaces of leaves at location III 10 m from the road

**Slika 3:** Število por na obeh straneh listov (zgornja in spodnja) na oddaljenosti 10 m od ceste na 1 mm$^2$

(Glycine Max) increased the number of stomata per unit area.[5] Metals can be transported via an apoplastic system and immobilized in the cell walls. Toxic metals become a real threat to plants, mainly when they reach the cytosol of the cell. The data clearly indicate that even very low levels of heavy metals in the soil may have an influence on plant growth.[3]

The number of stomata in the leaf epidermis of Cucumis sativa was increased after cultivation at various Pb rates (10, 20, 40) mg dm$^{-3}$ (1297.6 mm$^2$ 1714.8 mm$^2$, 1979.5 mm$^2$). After the treatment with lead the cucumber leaves exhibited a great number of stomata per unit area.[6] Positive and negative correlations were noticed among the metal concentrations and the number of stomata on the upper and lower surfaces of the leaves. Based on the results at location II (**Table 5, 6**) it was observed that both the adaxial and abaxial surfaces of the leaf had a significantly lower stomata number in individuals examined at a distance of 10 m from the road. An increase in the number of stomata per unit area with a simultaneous reduction in the size of the guard cells appeared due to a self-defense system, which is developed in plants under stress conditions and provided the support to the plant for their survival in the contaminated environment.[15]

The stomata number on the leaf for both the adaxial and abaxial leaf surfaces is shown in **Figure 2 and 3**. With the adaxial leaf surface of all individuals examined at locality III the largest number of stomata per 1 mm$^2$ was found in the upper leaf surface of the specimens gathered from near the road, while the smallest number was in the lower leaf surfaces. A significantly higher stomata number was found on the upper leaf surfaces (95.2 mm$^2$) compared with two other leaves (medium and lower). The experimental data confirmed the tendency of the increase in the stomata number with industrial pollution at the site II (213.5 mm$^2$) compared with the control site (205.4 mm$^2$), and again showed statistically insignificant differences between the control plants and those from the site with high traffic.[8] From this it can be concluded that heavy metals at millimolar concentrations inhibit stomata movements. At higher concentrations, they interfere with metabolic processes and inhibit growth, sometimes leading to plant death.[7]

## 4 CONCLUSIONS

At three different locations, 60 plant samples of Medicago sativa were collected at different distances from the road and the concentration of Pb, Cd and the number of stomata in the adaxial and abaxial leaf surfaces were determined.

The analysis of the statistical and comparative variance of all examined parameters, the LSD and the coefficient of correlation between the distances from the road were deduced. The greatest content of heavy metals (Pb, Cd) in all localities examined was found in the specimens taken near the road. The lowest quantity of concentration of these metals was found in specimens at a distance of 10 m from the road, with the exception of location III, where the content of Cd was higher at a distance from the road. The concentration of metals decreased with increasing distances from the highway and lead seems to be the most adapted tracer of highway contamination.

The largest number of stomata per 1 mm$^2$ at locality I was found in the lower leaf (197.8 mm$^2$). Also at localities II and III, the number of stomata for the medium and lower leaf was lower than for the upper leaf. This study has shown that the street plants are relatively contaminated with heavy metals. Finally, the results obtained in this research work are a significant reference value for future studies of these areas and other regions as well.

## 5 REFERENCES

[1] A. Sekara, M. Poniedzialek, J. Ciura, E. Jedrsezezyk. Zinc and coper accumulation and distribution in the tissues of the nine crops: implication in phytoremediation. Polish Journal of Environmental Studies 14, (**2005**) 6, 829–835

[2] Huma Pirzada, Audil Rashid. Multivariate analysis of selected roadside plants (Dalbergia sissoo, and Canabis sativa) for lead pollution monitoring. Pak. J. Bot. 41 (**2009**) 4, 1729–1736

[3] Peter Ryser, Wendy R. Sauder. Effects of heavy metal contaminated soil on growth phenology and boimass turnover of Hieracium piloselloides. Environmental Pollution. 140 (**2006**), 1, 52–61

[4] Aydinalp, C., Marinova, S. Lead in particulate deposits and in leaves of roadside plants. Polish Journal of Environmental Studies, 13 (**2004**) 2, 233–235

[5] Elbieta Weryszko-Chmielewska, Miroslava Chwil. Lead-induced histological and ultrastructural changes in the leaves of soybean (Glycine Max). Soil Science and Plant Nutrition., 51 (**2004**) 2, 203–212

[6] Miroslawa Chwil. The influence of lead on structure of Cucumis sativus L. leaves. Folia Horticulturae, 17 (**2005**) 2, 11–22

[7] H. M. Yang, X. Y. Zhang, G. X. Wang. Effects of heavy metals on stomatal movements in broad bean leaves. Russian journal of plant physiology. 51 (**2004**) 4, 464–468

[8] Ivanka Dimitrova, Lilyana Yurukova. Bioindication of anthropogenic pollution with Plantago lanceolata (Plantaginaceae): metal accumulation, morphological and stomatal leaf characteristics. Phytologia Balcanica 11 (**2005**) 1, 86–89

[9] Anamika Singh, Susan Eapen, M. H. Fulekar. Potential of Medicago sativa for uptake of cadmium from contaminated environment. Rom. Biotechnol. Lett., 14 (**2009**) 1, 4164–4169

[10] Riffat Nasem Malik, Syed Zahor, Ishfaq Nazir. Heavy Metal contamination and accumulation in soil and wild plant species from industrial area of Islamabad, Pakistan. Pak. J. Bot., 42 (**2010**) 1, 291–301

[11] Shinggu, D. Y., Ogugbuaja, V. O., Barminas, J. T., Toma, I. Analysis of street dust for heavy metal pollutants in Mubi, Adamawa State, Nigeria. International Journal of Physical Sciences 2 (**2007**) 11, 290–293

[12] J. R. Peralta, L. Gardea-Torresdey, K. J. Tiemann, Gómez S., Arteaga E., Rascon, J. G. Parsons. Study of the effects of heavy metals on seed germination and plant growth on alfalfaplant (Medicago sativa) grown in solid media. Environmental Science and Engineering. 15 (**2000**) 4, 135–140

[13] Aleš Plesničar, Nina Zupančič. Heavy Metal contamination of roadside soil along Ljubljana-Obrežje highway. Materials and geoenvironment. 52 (**2005**) 2, 403–418

[14] C. L. Ndiokwere. A study of heavy metal pollution from motor vehicle emissions and its effect on roadside soil, vegetation and crops in Nigeria. Environmental pollution. 7 (**2003**) 1, 35–42

[15] Rafia Azmat, Saba Haider, Hajra Nasreen. A Viable Alternative mechanism in adapting the Plants to heavy metal Environment. Pak. J. Bot., 41 (**2009**) 6, 2729–2738

[16] Lena Q. Ma., Gade N. Rao. Chemical fractionation of cadmium, copper, nickel and zinc in contaminated soils. Journal of Environmental Quality. 26 (**1997**) 1, 259–264

UDK 620.179.11:621.794:621.8
Professional article/Strokovni članek

ISSN 1580-2949
MTAEC9, 44(5)283(2010)

# THE SELECTION AND DEVELOPMENT OF TRIBOLOGICAL COATINGS

## IZBIRA IN RAZVOJ TRIBOLOŠKIH PREVLEK

**Yuriy Kharlamov[1], Vladimir Dal[1], Ilija Mamuzić[2], Larysa Lopata[3], G. S. Pisarenko[3]**

[1]East Ukraine National University, Faculty of Applied Mechanics and Material Science, Kvartal Molodesnij, Lugansk 91034, Ukraine
[2]Metallurgy Faculty of the University of Zagreb, Aleja narodnih heroja 3, 44103 Sisak, Croatia
[3]Institute for Problems of Strength of the National Academy of Sciences of Ukraine, Kiev, Ukraine
yuriy.kharlamov@gmail.com

*Prejem rokopisa – received: 2010-02-01; sprejem za objavo – accepted for publication: 2010-03-10*

The main objectives of this study are the strategy and methodology for selecting the optimal surface treatment for a given tribological application. The classification of the main methods of the coating processes and the surface modification is given and the scheme of the development of the operation technology of the surface treatment and coating deposition is proposed. The main initial data are: the structure of tribological system (TrS); the individual properties of the TrS parts; the lubricant properties; the method of lubrication of the TrS parts; the properties of the surrounding environment; the external influences on the TrS; the technological limitations on the TrS parts treatment; and the managerial and economic limitations. The selection of the surface technology method includes the following steps: the preliminary analysis of the TrS part interaction; the development of models of friction and the wear process of the TrS parts; the choice of rational values of the parameters of the surface layers of the TrS parts; the choice of the rational composition and the structure parameters of the surface layers of the TrS parts; the choice of a rational technological route and the methods of the surface treatment of the TrS parts; the experimental examination of surface-strengthened materials and the TrS and the correction of the surface-treatment technology.

Key words: coatings, friction pair solid surfaces contact, surface engineering, tribological system

Glavni cilj tega članka sta strategija in metodologija optimalne izbire metode za utrditev površine za neko tribološko uporabo. Dana je razvrstitev glavnih metod in procesov obdelave površine in nanosa prevlek ter predložena je shema razvoja tehnologije obdelave površine in nanosa prevlek. Najbolj pomembni začetni podatki: struktura tribološkega sistema (TrS); lastnosti posamičnih delov TrS; lastnosti maziv za TrS; lastnosti okolja; zunanji vplivi na TrS; tehnološke omejitve obdelave TrS-delov; poslovne in ekonomske omejitve. Metoda izbire površinske tehnologije ima naslednje korake: izbira racionalnih parametrov za površinske plasti TrS-delov; izbira racionalnih parametrov sestave in strukture površinskih plasti TrS-delov, izbira racionalne tehnologije za površinsko obdelavo TrS-delov; eksperimentalna preiskava površinsko utrjenih plasti TrS-delov in popravki tehnologije za površinsko utrditev.

Ključne besede: prevleke, torni par kontakta trdih površin, utrditev površine, tribološki sistem

## 1 INTRODUCTION

The use of surface engineering methods in tribological applications is growing and will continue to grow, as evidenced by a literature survey [1–9]. A surface treatment in the form of coatings and films and the modification of surface layers can offer certain economic and technical advantages over the use of materials without the surface-strengthening treatment. Their main advantage is that the strengthened surface layers allow the base material of tribological system (TrS) parts to be optimized for strength purposes, while the surface layer is optimized for reducing the wear and increasing the corrosion resistance, promoting film lubrication, enhancing lubricant effectiveness, the modification of surface function, etc. Furthermore, replacing the surface layer by coating deposition during repair may be more cost effective than the manufacture of a new TrS part. But the principal disadvantage in using coatings concerns the possibility of the separation from the base material of TrS part during use. While the discussions that follow emphasize the considerations important in the selection of tribological surface treatment, it should be noted that other alternatives might exist for any particular problem. This could involve, for example, use of a more effective lubricant, or a redesign of the tribological system's elements, the use of more effective methods of lubrication, the development of new or the use of improved materials, etc.

## 2 CLASSIFICATION OF SURFACE-ENGINEERING METHODS

Many technological methods and processes of surface engineering are available for the modification of surface characteristics. Tribological surface-treatment methods are used for different purposes: 1. Replacing surfaces with coatings and the deposition of films; 2. Surface modification (surface alloying and/or microstructure is altered); and 3. Combination of methods for coating deposition and surface modification. A wide variety of surface-modification methods are available for tribological purposes. The main categories are: 1. Modification of surface layers in the process of shape processing; 2. Heat (volume) treatment; 3. Surface heat treatment; 4. Treatment by surface plastic deformation; 5. Surface thermomechanical treatment; 6. Surface

alloying; 7. Chemical and thermochemical treatment, including microarc oxidization; 8. Ion implantation; 9. Formation of a surface-layer composite structure by the introduction of hardening phase particles; 10. Others and hybrid methods.

Resurfacing essentially replaces the surface layer of a base material (or previously deposited coating) with another having more desirable friction and wear properties. Usually, the new surface is harder than the surface replaced, but not always. A wide variety of coating compositions is available. Each of these compositions can be applied by a variety of processes. The main categories of the coating-deposition processes are: Electroplating; Electrophorus; Electroless plating; Welding; Thermal spraying; Physical Vapour Deposition; Chemical Vapor Deposition (CVD); Immersion on melt; Electro-spark alloying; Electro-magnetic alloying; Bonding of powder layers; Solid phase plating (bonding of plates); Painting; and Continuous deposition of films in process of friction (rotaprint, from environment, etc.).

Some of these application processes are very simple and inexpensive, such as painting. Others are very complex, either requiring vacuum processing or requiring a series of treatments and pre-treatment. Some of them can be applied in the field, while others can only be applied at particular facilities. There is no shortage of tribological coatings and surface layers to try for almost any need. The primary problem that exists is knowing which surface treatment to select for any given application. A related problem is that surface treatment developers often do not know where their coatings should be used or what coating or kind of surface modification to develop to meet a particular need. There is a need for a strategy or methodology for selecting a surface-layer composition and structure, and the methods for obtaining a given tribological application. In this paper such a strategy is proposed and elements of that strategy are discussed.

## 3 SOLID SURFACE CHARACTERISTICS

The difficulties of the selection of surface-treatment methods are connected with a very large number of parametric variables of solid surface quality, which could be described by the following ensemble of characteristics

$$K \supseteq G_{ex} \cup G_{in} \cup S_c \cup S_s \cup Ph_c \cup Ph_s \cup Ch_c \cup Ch_s \cup Df_c \cup Df_s \cup St_c \cup St_s \cup Pmp_c \cup Pmp_s \cup Ptp_c \cup Ptp_s \cup ...$$

where $G_{ex}$ is an ensemble of characteristics that are characterized by the geometry parameters of the external surface of the strengthened layer and in its turn could be characterized by the ensemble $G_{ex} \supseteq G_{exw} \cup G_{exm}$, where $G_{exw}$ and $G_{exm}$ are ensembles of the parameters of waviness and roughness of the surface, respectively; $G_{in}$ is the ensemble of parameters that are characterized by the geometry parameters of the internal surface of the strengthened layer (or coating) and in its turn could be characterized by the ensemble $G_{ix} \supseteq G_{ixw} \cup G_{ixm}$; $S_c$ and $S_s$ are the ensembles of the parameters that are characterized by the geometry configuration inaccuracy of the surface of the strengthened layer (or coating) and its interface with main material, respectively; $Ph_c$ and $Ph_s$ are the ensembles of parameters that can be characterized; $Ch_c$ and $Ch_s$ are the chemical compositions; $St_c$ and $St_s$ are the ensembles of parameters that are characterized by the structure; $Df_c$ and $Df_s$ are the ensembles of parameters that are characterized by the deformation; $Pmp_c$ and $Pmp_s$ are the ensembles of the parameters that are characterized by the physico-mechanical properties; $Ptp_c$ and $Ptp_s$ are the ensembles of the parameters that are characterized by the thermophysical properties; the indices *c* and *s* are for the strengthened layer (or coating) and the structure of near-surface layer of the main material and/or the transition zone, respectively.

In searching for the optimal solution of a particular tribological problem it is necessary to consider the ensemble of parameters that is characterized by the assembly and friction surface working conditions

$$TrS \supseteq E \cup C_e \cup L_e \cup F \cup M_e \cup W_e$$

where $E$ is the ensemble of the characteristics of the TrS workpieces; $L_e$ is the ensemble of the characteristics of the linking between workpieces; $F$ is the ensemble of the kind of friction and its main characteristics; $M_e$ is the ensemble of the mutual shifting of the TrS workpieces; $W_e$ is the ensemble of the wear characteristics of the TrS.

For dataware of the choice of the surface-treatment method it is necessary to elaborate the ensemble of the parametric variables of the solid surface quality that influences on the wear-resistance at different kinds of wear and control may affect the wear resistance

$$QPSS_i \supseteq G_{exi} \cup G_{ini} \cup S_{ci} \cup S_{si} \cup Ph_{ci} \cup Ph_{si} \cup Ch_{ci} \cup Ch_{si} \cup Df_{ci} \cup Df_{si} \cup St_{ci} \cup St_{si} \cup Pmp_{ci} \cup Pmp_{si} \cup Ptp_{ci} \cup Ptp_{si} \cup ...$$

where the index mark "i" is given for a certain kind of wear. Furthermore, it is necessary to elaborate the ensemble of parametric variables of the solid surface quality that is possible to control for each method of surface treatment and to determine the limits of this control.

$$QPSS_j \supseteq G_{exj} \cup G_{inj} \cup S_{cj} \cup S_{sj} \cup Ph_{cj} \cup Ph_{sj} \cup Ch_{cj} \cup Ch_{sj} \cup Df_{cj} \cup Df_{sj} \cup St_{cj} \cup St_{sj} \cup Pmp_{cj} \cup Pmp_{sj} \cup Ptp_{cj} \cup Ptp_{sj} \cup ...$$

where the index mark "j" is given for a certain kind of surface treatment.

## 4 METHODOLOGY FOR THE SELECTION OF THE SURFACE-ENGINEERING METHODS

Coating deposition and surface modification have rapidly evolved in recent decades from simple and traditional methods to extremely sophisticated techno-

logies. These developments are part of an effort to eliminate the limitations imposed by oil-based lubrication and are changing the general perception of the limits of wearing contacts [6]. Knowledge of the mechanisms behind these improvements in lubrication and wear resistance is, in most cases, very limited. The methods employed in most studies on surface coatings and modification are empirical and there is relatively little information available on which surface technology is the most suitable for a particular application. Prior to selecting the coating material and the technological method it is necessary to determine the prime objective that could be used to reduce the friction or suppress the wear – or both. During the selection of the most effective surface material and process to suppress wear in a particular situation, the prevailing wear mechanism must first be recognized and assessed.

In the last years, much research is being carried out in the field of tribological coatings and surface treatment, and although they are being increasingly used in practice, little is still known about their properties and their tribological behaviour, especially for new, advanced surface technology. Different types of coatings of the same composition have different mechanical and tribological properties, depending mainly on the type of deposition process and the substrate material. Furthermore, due to the specific test methods and conditions for given applications or research facilities of an organization, it is seldom possible to compare the results obtained by different researches. The selection of a coating-material and coating-process combination for a specific substrate can be complex. There are a great number of possible combinations, not all of which lead to satisfactory solutions [1,6–9]. To overcome these problems, the strategy and the methodology for the selection of the optimal tribological coatings and the surface treatment for a given application are proposed.

The selection of the types of surface-strengthening treatment include the following stages, shown in **Figure 1**:

1. study of the initial data, including: composition and internal relations of the TrS (parts; relations between them; lubricant; surrounding environment); individual properties of the TrS parts, including the geometry parameters of the parts and the friction surfaces (macro- and micro-geometry) and the properties of the main material; the lubricant properties (volume and surface properties, chemical and physical, etc.); the aggregate properties of the lubricant and the TrS parts (the adsorption properties, moistness, etc.); the lubrication manner influencing, at first, on techniques and the lubrication type; the properties of the surrounding environment (the chemical composition, the corroding influence, the humidity, the temperature, the pressure, etc.); external influences on the TrS (kinetic – sliding (rolling) the velocity *V*, the hydrodynamic velocity; the dynamic – mechanical force, the pressure *P*, the electric field parameters; the thermal – temperature $\vartheta_0$, the thermal flow, the thermal gradient); the technological limitations on the TrS parts treatment (the shape and the sizes of the parts and surfaces, the materials, the variability of the properties, the technological heredity, etc.); the managerial and economic limitations (the required productivity, the presence of equipment, the materials, the energy sources and others, the sanitary, hygienic and ecological demands, the permissible expenses, etc.).
2. the determination of the TrS parts' interaction during the static and dynamic conditions (adhesion, adsorption, chemosorption, oxidation, corrosion, diffusion, elastic strain, plastic deformation, micro-cutting, scratching, structure and phase transformation, etc.).
3. the development of the scheme of the TrS action, including the preliminary determination of the TrS characteristics for describing the input values *X* transformation in the output values *Y*

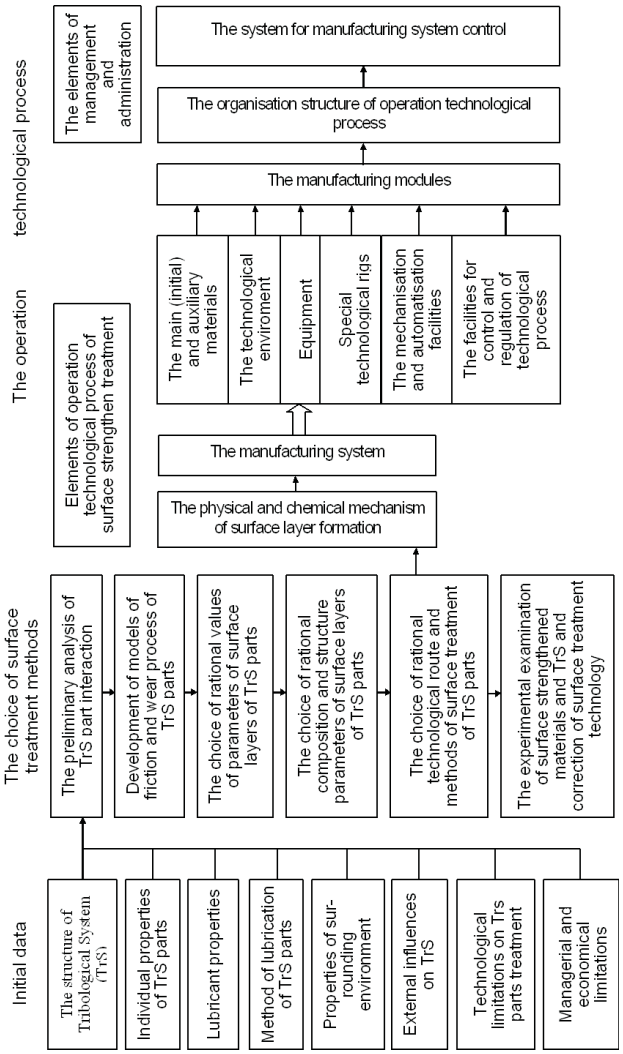


**Figure 1:** Scheme of the development of the operation technology of the surface-strengthening treatment

**Slika 1:** Shema razvoja operacij tehnologije za utrditev površine

$$\{X\} = \{P,V,\vartheta_0\} \Rightarrow \{Y\} = \{F_t,Z,P_t\}$$

where $F_t$ is the friction resistance, $Z$ is the wear and seizure, $P_t$ is the accompanying processes.

4. the development of the models of friction and the wear process of the TrS parts (physical, mathematical, imitative, analogue);
5. the determination of the rational values of the parameters of the surface layers' properties by using the models of friction and wear (by obtaining the permissible values of *Y*);
6. the selection of the rational composition and the structure of the surface layer of the TrS parts (we must take into account the existing analogues and also the structure–properties correlations);
7. the determination of the direction of the surface-strengthening treatment of the friction surface of the TrS parts: or the surface layers' modification, or the coating deposition or their combination;
8. the determination of the list of possible physico-chemical methods of surface-strengthening treatment;
9. the preliminary selection of the optimal methods of surface-strengthening treatment by using elected criterions of optimisation and the maintenance of the required technique-economic limitations;
10. the experimental test of the surface-strengthening treatment in the laboratory or the empirical-industrial conditions;
11. the preliminary projection of the operating methods of the surface treatment – equipment, the special technological rigs, the technological variables, the technological environment, the facilities of the mechanisation, the robotisation and the automation, the methods of management and control, the techno-economic comparison of the operating variants;
12. the clarification of the relationships between the operation technology of the surface-strengthening treatment and the manufacturing procedure of the TrS parts' production; the correction of the structure for both processes for the purpose of their optimisation;
13. the final selection of the surface-strengthening treatment methods, the development of measures for the reliability of the maintenance of the demanded characteristics of the technological process; the development of a project for the processing system of the surface treatment.

The selection of the optimal methods of the surface-strengthening treatment usually realized by employing technical criteria to secure the required TrS tribotechnical characteristics according to scheme, shown in **Figure 2**. In the case of the presence of some equivalent surface-treatment variants on the tribotechnical characteristics for the final selection economic criteria are used. The system of the selection of the optimal surface-strengthening treatment includes the scheme of the TrS action and the database of the multitude of surface-strengthening treatment classes and the methods' characteristics. Preliminarily, by using the technological limitations, other initial data and the database, one could select a recommended group of parameters of the surface layers' quality, which promoted the increasing wear resistance. The next would be the selection of respective methods of surface-strengthening treatment, which allowed a control of the desirable parameters of the surface-layer quality. Then, with use of the earlier developed model of friction and wear for the TrS we can make a more detailed valuation of the selected decision, including the calculation and the experimental determination of the tribotechnical characteristics and the following test of the TrS. The use of different methods of surface-strengthening treatment opens up vast possibilities for the control of friction surfaces' contact interaction, independent of the composition and the structure of the main materials of the TrS parts.

Depending on the kind of aggregate of the contacting surface layers of the friction pairs it is possible to divide

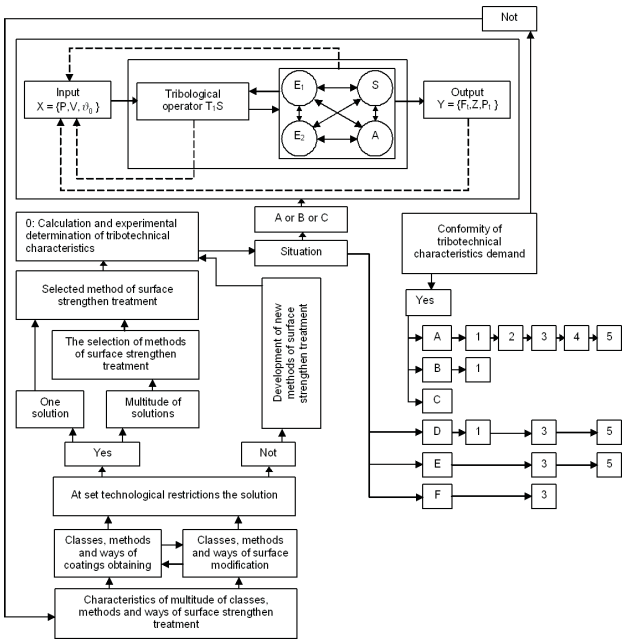


**Figure 2:** Scheme of the selection of the optimum methods of surface-strengthening treatment. Situation: A – the development of a tribological system not having analogues; B – the selection of a new friction pair instead of an out-of-date one; C – the selection of a friction pair for a weak-loaded typical tribological system; D – the improvement of a typical tribological system; E – the replacement of friction pair by a new serial one; F – the determination of an inter-repair cycle. The stages of selection: 0 – the calculation and the experimental determination of the tribotechnical characteristics; 1 – the research test at the determined parameter; 2 – the boundary research test (under extreme conditions); 3 – the model research test; 4 – the defined nature test; and 5 – the exploitation test

**Slika 2:** Shema za izbiro optimalne metode za utrditev površine. Situacija: A – razvoj tribološkega sistema brez analogov; B – izbira novega tornega para namesto opuščenega; C – izbira tornega para za malo obremenjen tribološki sistem; D – izboljšanje tipičnega tribološkega sistema; E – zamenjava tribološkega sistema z novim standardnim; F – določitev vmesnih popravil. Izbira stopnje: 0 – izračun in eksperimentalna določitev triboloških značilnosti; 1 – preizkus pri določenih parametrih; 2 – mejni preizkus (v ekstremnih razmerah); 3 – preizkus modela; 4 – določitev naravnega preizkusa; 5 – preizkus uporabe

them into three classes: 1) the contact of two one-phase surface layers; 2) the contact of a one-phase layer and a composite-structure surface layer; and 3) the contact of two composite-structure surface layers.

Only in the case of the contact of one-phase surface layers is the common number of possible variants of the contacts very high and can be evaluated with the next equation

$$K_{\text{sum}} = 2(n^2 + m^2 + q^2) - 3(n + m + q) + 6 + \\ + 2(nm + nq + mq)$$

where $n$ is the number of simple substances, $m$ is the number of two- and many-component solid solutions, and $q$ is the number of two- and many-component chemical compounds.

These multiplicity of possible variants of the contact in the case of only one-phase surface layers is allowed by the choice of the composition of the surface-layers materials and their structure to control the quality of the physical contact of the friction pairs, in particular the size of real contact area, of the tendency to form desirable secondary structures in the process of friction, the properties of a third (intermediate) substance, and the fatigue-wear resistance, etc.

In reality, the factual variety of the possible contacts of one-phase layers is considerably more, inasmuch as the friction processes depend not only on the chemical composition of the contacted surface layers, but also on their structure and energetic parameters, including the size, shape and character of the mutual orientation of the grains; the structure and strength of the intercrystalline boundaries; the level of the strain hardening; the type of the crystal lattice; the mechanical properties; the surface properties, etc.

The creation on one or both friction surfaces for the layers with a composite structure leads to an essential increasing of the possible variants of the friction surfaces' contacts and to the appearance of some new physico-chemical phenomena in the process of friction. The peculiarities of the contact interaction of such friction pairs are at first connected with the simultaneous presence of the contact aggregate between the friction surfaces. But the description of the friction zone in the contact of such surface layers demands the use of complex or special parameters.

## 5 CONCLUSION

The approach to the development and selection of a surface-strengthening treatment for tribological purposes has to involve methods of system analyses. The tribological system's workpieces' and friction surfaces' functions must be accurately defined in functional, technological, economic, ecological and other respects. The proposed strategy has the potential for simplifying the selection and design of coatings and/or surface layers and the reduction of the development time for new tribological systems and/or the improvement of existing ones. But the subsequent laboratory tests at several levels must also be completed. The development of computer-modelling methods for the selection of surface-engineering processes and expert systems for developing the surface-engineering technology for a particular application is necessary. The system approach could also be useful for the development of new tribological coatings and surface-modification methods. However, a lot has still to be done for the development of a methodology for the selection of optimum methods for surface engineering and their improvement.

## 6 REFERENCES

[1] Holmberg K., Matthews A.: Coatings Tribology. Properties, techniques and applications in surface engineering. – Elsevier Science B. V., Amsterdam, The Netherlands, 1994

[2] Hocking M. G., Vasantasree V., Sidky P. S.: Metallic and ceramic coatings. production, high temperature properties and applications. – Longman Group UK Limited, London. 1989

[3] Jorn Larsen-Basse: Surface engineering and the new millennium. Surface Engineering, 14 (**1998**), 81–83

[4] Budinski K.G.: Surface engineering for wear resistance. – New York, NY, Prentice Hall, 1988

[5] Friedrich C., Berg G., Broszeit E., Berger C. Fundamental economical aspects of functional coatings for tribological applications. Surface and Coatings Technology, 98 (**1998**), 816–822

[6] Stachowiak G. W., Batchelor A. W.: Engineering tribology. Second Edition. – Butterworth-Heinemann, 2001

[7] Bhushan B, Gupta B. K. Handbook of tribology. Materials, coatings, and surface treatments. – McGraw-Hill, 1991

[8] Schiffmann K., Petrik M., Fetzer H. J., Schwarz S., Gemmler A., Griepentrog M., Reiners G. INO-A WWW information system for innovative coatings and surface technology. Surface and Coatings Technology, 153 (**2002**), 217–224

[9] Sedlacek M., Podgornik B., Vizintin J. Tribological properties of DLC coatings and comparison with test results: Development of a database. Materials Characterization, 59 (**2008**) 2, 151–161 doi:10.1016/j.matchar.2006.12.008

UDK 669.1.782
Professional article/Strokovni članek

ISSN 1580-2949
MTAEC9, 44(5)289(2010)

# RECYCLING OF STEEL CHIPS

## RECIKLIRANJE JEKLENIH OSTRUŽKOV

**Matjaž Torkar, Martin Lamut, Agron Millaku**

Institute of Metals and Technology, Lepi pot 11, SI-1000 Ljubljana, Slovenia
matjaz.torkar@imt.si

*Prejem rokopisa – received: 2010-05-17; sprejem za objavo – accepted for publication: 2010-06-20*

The recycling of waste metallic materials and the use of scrap are important for the economic production of a steelworks. Here, we investigate the technology of remelting steel chips. It was confirmed that the main problems with using chips in an electric arc furnace were the chips' large specific surface and the high losses due to the chips' oxidation. To overcome both problems the compaction and remelting of the chips were tested. The investigation revealed that a major problem for the recycling ecology of steel chips was the safe removal of cutting fluids and oils from the chips' surface. The chemical analysis of the remelted chips confirmed that stainless-steel chips can be an acceptable source of the alloying elements chromium, nickel and molybdenum.

Key words: steel chips, magnetic separation, cold compaction, remelting

Recikliranje odpadnih kovinskih materialov in uporaba starega železa sta pomembna za ekonomiko železarne. Tehnologija proizvodnje jekla s pretaljevanjem starega železa v elektro obločni peči je primerna tudi za jeklene ostružke. Preizkušena je bila tehnologija pretaljevanja jeklenih ostružkov. Glavni ugotovljeni problemi pri uporabi ostružkov v elektro obločni peči so velika specifična površina in velike talilne izgube zaradi oksidacije ostružkov. Zato je bilo preizkušeno stiskanje ostružkov in njihovo pretaljevanje. Predstavljeni so rezultati teh preizkusov. Ti so pokazali, da je bila glavna težava pri ekološkem recikliranju jeklenih ostružkov odstranitev rezilne tekočine in olj z njihove površine brez kontaminacije zraka. Kemijska analiza pretaljenih ostružkov je potrdila, da so ostružki nerjavnega jekla koristen vir legirnih elementov, kot so krom, nikelj in molibden.

Ključne besede: jekleni ostružki, magnetno ločevanje, hladno stiskanje, pretaljevanje

## 1 INTRODUCTION

Wastes that were traditionally discarded from industrial production are nowadays recycled.[1] The discarding of waste materials has a negative environmental impact and is a waste of time and money for the manufacturer of steel or machine parts.[2] Steel chips are a by-product of the mechanical working of steel parts in the metal industry and their quantity is considerable. The quantities of steel chips recorded by years in Slovenia are shown in **Table 1**.

**Table 1:** Quantity of steel chips in Slovenia
**Tabela 1:** Količina ostružkov železa v Sloveniji

| Year<br>Leto | Clasification number/Klasifikacijska številka: 120101<br>Quantitiy of filings and turnings of steel/<br>Količina opilkov in ostružkov železa (t) |
|---|---|
| 2002 | 58 120 |
| 2003 | 33 111 |
| 2004 | 48 828 |
| 2005 | 43 991 |
| 2006 | 53 180 |
| 2007 | 93 381 |

Source: Statistical Office of the Republic of Slovenia

Steel production in the Republic of Slovenia is based on the remelting of scrap. From the data in **Table 1** it is evident that steel chips could be an important source of iron and other elements for steel producers.

With the prices of nickel and chromium currently high, and on the rise in recent years, the production of steel is becoming increasingly more expensive, and with the prices rising, the recycling of steel chips is beginning to look more appealing for steel companies.[2,3,4,5] For better productivity during metal working the cutting tools are cooled and lubricated with special cooling liquids consisting of lubrication, cooling and anti-corrosion agents. However, the chips are contaminated with these substances and need to be cleaned before any further processing. It is important to note that discarded coolants from the manufacturing of steel have a more harmful impact on the environment than dry chip processing.[4] This means that the coolants have to be removed in order to obtain more environmentally friendly waste from the chips generated in the processing of the steel. The discarding of metallic chips is harmful to the environment, regardless of whether they are contaminated or not, and these chips should not end up in landfills, thereby losing their potential for reuse. In the near future the recycling of these chips will actually cost less than disposing of them in a landfill.

The first step during the recycling of chips is usually the separation of the cooling liquid and the oil with a centrifuge.[3,4] It is also possible to remove the lubricant by washing them in an organic solvent that dissolves the organic contaminants from the chips' surface. The latter possibility is less acceptable because most organic solvents are carcinogenic and harmful to the environment, and their use and removal are regulated by the law.

Vacuum separation[2] is also used, by heating the chips in a vacuum chamber up to 270 °C. The low pressure in the chamber accelerates the evaporation of volatile components that are pumped out, cooled in a condenser at appropriate temperatures and the oils and water are separated. After regeneration, the oil is reused for machining.

The best quality of regenerated oil is obtained with a treatment involving supercritical $CO_2$ gas at a pressure of 100 bar.[2] However, when compared to other methods, this method is too expensive for the cleaning of chips.

After the chips of structural steel are cleaned they are separated from the chips of stainless steel using magnetic separation.[6]

Steel chips have a high specific volume and a low density that makes the remelting more difficult and with a low yield. For this reason, compacting with a cold press or briquetting, which increase the density of the chips, makes possible a more effective melting process.

The content of chromium in stainless steel is greater than that of nickel, but the price of nickel makes it more costly overall than chromium in the production of stainless steel.

The cost of nickel is so high that the price of stainless steel is directly related to the price of nickel, which has increased six fold from 2002 to 2006.[3] The price of ferrochrome has more than doubled in the past four years (2002 to 2005)[3], but the increase in the chromium price is still lower than the increase in the nickel price. For this reason, any source of chromium and nickel is cost attractive for stainless-steel producers.

For the producer of stainless steel in Slovenia an evaluation of the mixture of chips with respect to the content of chromium, nickel and molybdenum, as a possible additional source of alloying elements, was made.

## 2 EXPERIMENTAL

Magnetic tests showed the chips, declared as stainless-steel chips, were in reality a mixture of carbon steel and stainless steel. After the magnetic separation, however, only the stainless-steel chips were processed further.

Two methods of degreasing the chips were tested: heating in a laboratory furnace up to 400 °C and burning the volatile gases, and washing the chips in a waste organic solvent, trichloroethylene. Using both methods, dry and clean chips were obtained.

The degreased chips were cold pressed into cylindrical compacts, more suitable for remelting because of their higher density and lower volume. For the cold pressing a manually driven screw press was applied. The chips were charged in a hollow, slightly conical tool and repeatedly added and pressed until the tool was full. The pressed chips were then pressed out of the tool from the opposite site.

The compacts were then melted in a 20-kg induction-melting furnace using a premelt of known composition. The compacted chips were added to the primary melt and after remelting a sample of the melt was submitted to chemical analysis and the contents of nickel, chromium and molybdenum in the chips were calculated. The chemical analysis was performed with optical emission spectrometry ARL and controlled with

**Figure 1:** Mixture of steel chips
**Slika 1:** Mešanica jeklenih ostružkov

**Figure 2:** Separated stainles steel chips and compacted, cold pressed chips
**Slika 2:** Ločeni ostružki nerjavnega jekla, hladno stisnjeni ostružki

**Figure 3:** Compacts of stainless steel chips after cold pressing
**Slika 3:** Stisnjeni ostružki nerjavnega jekla po hladnem stiskanju

**Figure 4:** Charging of compact into melt
**Slika 4:** Dodajanje stisnjencev v talino

**Figure 5:** Casting of sample for chemical analysis
**Slika 5:** Ulivanje vzorca za kemijsko analizo

wet chemical analysis. The quantity and composition of the slag were not taken into account.

## 3 RESULTS AND DISCUSSION

The magnetic separation revealed that the investigated sample consisted of a mixture of 1/3 of stainless steel and 2/3 of carbon steels, but for further processing only the chips of stainless steel were used.

Two methods for removal of the cooling fluid were tested. First, degreasing in trichloroethylene, which is an effective solvent for greases and a variety of organic materials. Its use is harmful because it is carcinogenic and it is suitable only for applications in laboratory-controlled conditions, whereas it is not suitable for industrial processing.

The second method was heating the chips to 400 °C in an electric furnace, when the water and oil evaporated, and clean and dry chips were obtained. The heating smoke was burned to $CO_2$ and $H_2O$ by introducing it into a flame.

**Figure 6:** Ingots composed of basic steel and added compacts
**Slika 6:** Ingota, sestavljena iz osnovnega jekla in dodanih stisnjencev

On an industrial level, it is also possible to charge oil-contaminated chips with scrap directly. In this case the organic impurities would be burned out at high temperatures and the formed gases would escape through the filters for furnace exhaust gases. In the case of a too low temperature, the evaporation of oils and their collection in filters may reduce the filters' efficiency.

### *3.1 Compacting the chips*

The direct melting of the chips in the 20-kg induction furnace was not possible. Because of the low density, the chips in the furnace would only be heated to a temperature below the melting point. For the melting it was necessary to prepare chips in a compacted form and for this reason, the chips were cold pressed into a cylindrical form with a pressure of 1765.8 kPa. For comparison the pressing of contaminated and degreased chips was tested. In both cases the product was compacted into a round, cylindrical form with a diameter of 55 mm and length of 120 mm, and with a density of between 3 kg/dm$^3$ and 4 kg/dm$^3$. The pressed forms were of round section and had a diameter of 55 mm and a length of 120 mm. The size of the forms was limited by the dimensions and the height of the pressing-tool cavity.

### *3.2 Remelting the chips*

An induction-melting furnace requires a minimal density of charge, and the density of the compacts was still too low for direct melting in an induction furnace. The compacts were only heated and their temperature did not reach the melting point. To master the melting a primary melt with known composition was prepared and then the compacts were charged into the molten steel. First, 7 kg of mild steel was melted in the 20-kg induction furnace and its chemical composition was determined. The mass of the molten steel was reduced by 765 g to 6 235 g, 13 000 g of compacts added and a total melt mass of 19 235 g was achieved. The slag was

**Table 2:** Chemical composition of primary melt, after the addition of chips and calculated composition of chips. All in mass fractions, *w*/%
**Tabela 2:** Kemijska sestava primarne taline, po dodatku ostružkov in izračunana sestava ostružkov. Vse v mas. deležih, *w*/%

| Chemical composition | | C | Si | Mn | Ni | Cr | Mo | Cu | Fe |
|---|---|---|---|---|---|---|---|---|---|
| Primary melt *w*/% | | 0.14 | 0.25 | 0.19 | 0.04 | 0.03 | 0.05 | 0.11 | 99.30 |
| Weight (g) | 6235 | 8.73 | 15.59 | 11.85 | 2.49 | 1.87 | 3.12 | 6.86 | 6191.36 |
| Mixture *w*/% | | 0.24 | 0.35 | 0.89 | 4.30 | 8.80 | 0.60 | 0.34 | 84.82 |
| Weight (g) | 19235 | 46.16 | 67.32 | 171.19 | 827.11 | 1692.68 | 115.41 | 65.40 | 16315.13 |
| Chips *w*/% | | 0.29 | 0.40 | 1.23 | 6.34 | 13.01 | 0.86 | 0.45 | 77.88 |
| Weight (g) | 13000 | 37.44 | 51.74 | 159.35 | 824.61 | 1690.81 | 112.29 | 58.54 | 10065.23 |

removed from the melt and a sample for chemical analysis was taken. The rest of the melt was cast into ingots with a square cross-section. The weight of the as-cast sample for the chemical analysis and ingots together was 18 150 g. The difference between 1 085 g and 19 235 g is the material loss (slag, drops, remains in the melting furnace).

### *3.3 Determination of the composition of the chips*

The basis for the calculation of the content of elements in the stainless-steel chips was the total mass of 19 235 g. This represents 13 000 g of chips of unknown composition diluted within 6 235 g of mild steel with known composition. A programme was prepared in Excel for the calculation of the chemical composition of the premelt, of the ingots and of the content of the individual elements in the chips. From the chemical composition of the premelt and of the composition of the ingot the content of elements in the chips in **Table 2** was calculated.

## 4 CONCLUSIONS

The recycling of steel chips with remelting in an induction-melting furnace was investigated. Based on the experimental results, the following conclusions can be drawn:

Tests with magnets revealed that the investigated chips were a mixture of 1/3 of non-magnetic fraction (stainless steel) and 2/3 of magnetic fraction (structural steel). Both fractions of chips were successfully separated with magnetic separation and the following composition of the investigated chips was obtained: 13.01 % Cr, 6.34 % Ni, 0.86 % Mo and 0.45 % Cu.

The higher carbon content and the lower chromium content in the chips are probably due to the inaccuracy of magnetic separation method or the incomplete elimination during the burning of the oil contamination.

The investigations confirmed that the compaction of the chips is necessary for a better yield of material in the melting process and that stainless steel is a valuable source of alloying elements.

## 5 REFERENCES

[1] D. Janke, L. Savov, H.-J. Weddige, E. Schulz, Scrap-based steel production and recycling of steel, Materiali in tehnologije 34, (**2000**) 6, 387–399

[2] J. Bongardt, Technical Note: Reduction of waste from fabrication processes. The Journal of The South African Institute of Mining and Metallurgy, March/April 1997, pp 63–67

[3] Sean Dyer, Bao Ngo, Kurt Wivagg, Chip Recycling: Recycling of chips from BZZ conditioning processes, Worcester Polytechnic Institute, A Major Qualifying Project for Degree of Bachelor of Science, www.wpi.edu/Pubs/E-project/Availabel/E-project-04267-151242/unrestricted/YR_SGMQP_05.pdf

[4] V. A. Kurdyukov, A. A. Sergeev and A. A. Reznyakov, Efficient methods of processing metal chips, Metallurgist, 41 (**1997**) 9–11, 331–335

[5] S. I. Stepanov, Some laws on the hot and cold compression of steel chips, Powder Metallurgy and Metal ceramics, 5 (**1966**) 2, 99–102

[6] William J. Bronkala, Magnetic separation, Wiley-VCH Verlag GmbH & Co. KGaA., DOI:10.1002/14356007.b02_19, June 15, 2000